

~~CONFIDENTIAL~~

NASA TECHNICAL  
MEMORANDUM



UB  
NASA TM X-1301

UB  
NASA TM X-1301

NASA LIBRARY  
AMES RESEARCH CENTER  
MOFFETT FIELD, CALIF.  
NOV 15 1966



HYPERSONIC AERODYNAMIC  
CHARACTERISTICS OF THE AMES M-2  
LIFTING ENTRY CONFIGURATION

*by John A. Axelson*  
*Ames Research Center*  
*Moffett Field, Calif.*

Reg # 82563  
~~CONFIDENTIAL~~

~~CONFIDENTIAL~~

NASA TM X-1301

UNCLASSIFIED

HYPERSONIC AERODYNAMIC CHARACTERISTICS OF THE  
AMES M-2 LIFTING ENTRY CONFIGURATION

By John A. Axelson

Ames Research Center  
Moffett Field, Calif.

GROUP 4

Downgraded at 3 year intervals;  
declassified after 12 years

CLASSIFIED DOCUMENT—TITLE UNCLASSIFIED

This material contains information affecting the national defense of the United States within the meaning of the espionage laws, Title 18, U.S.C., Secs. 793 and 794, the transmission or revelation of which in any manner to an unauthorized person is prohibited by law.

NOTICE

This document should not be returned after it has satisfied your requirements. It may be disposed of in accordance with your local security regulations or the appropriate provisions of the Industrial Security Manual for Safe-Guarding Classified Information.

NATIONAL AERONAUTICS AND SPACE ADMINISTRATION

~~CONFIDENTIAL~~

~~CONFIDENTIAL~~

# HYPERSONIC AERODYNAMIC CHARACTERISTICS OF THE AMES M-2 LIFTING ENTRY CONFIGURATION\*

By John A. Axelson  
Ames Research Center

## SUMMARY

The hypersonic aerodynamic characteristics of the M-2 lifting entry configuration have been measured in the Ames 3.5-foot hypersonic wind tunnel at Mach numbers in air of 5.2, 7.4, and 10.4 and in the 14-inch helium wind tunnel at Mach numbers of 10.4, 17.3, and 21.0. The corresponding test Reynolds numbers varied from 0.8 million to 2.4 million in air and from 1.7 million to 4.3 million in helium. Aerodynamic force and static stability characteristics are presented for angles of attack from zero lift attitude (near  $-5^\circ$ ) to that for maximum lift (approximately  $45^\circ$ ).

The results indicate that the variation of Mach number had relatively little effect on the hypersonic aerodynamic characteristics. The maximum trimmed lift-drag ratio was approximately 1.2 for both the air and helium measurements, and occurred near  $10^\circ$  angle of attack and 0.2 lift coefficient. The maximum lift coefficient was about 0.45 and occurred near  $45^\circ$  angle of attack. The models could be trimmed with approximately 5-percent static margin over the range from maximum lift down to zero lift by progressively increasing the pitch-flap deflection from  $0^\circ$  to  $60^\circ$ .

The models with rudders undeflected exhibited insufficient static directional stability at low angles of attack. The incorporation of  $25^\circ$  rudder flare resulted in favorable directional stability characteristics. It is surmised that an M-2 vehicle's rolling and yawing motion can be controlled with the rudders as a result of the coupling between rudder-produced sideslip and the rolling moment produced by the inherent lateral stability of the configuration.

## INTRODUCTION

Research is being conducted by the National Aeronautics and Space Administration to develop a maneuverable, lifting-entry vehicle capable of a horizontal landing on the ground. The advantages to be derived from the application of the lifting-body concept to entry vehicles are well documented in references 1 and 2. Noteworthy among the advantages are reduced heating rates and reduced decelerations during entry, and significantly increased operational flexibility gained from the enlarged entry corridors and from the increased glide range for reaching accessible landing sites.

---

\*Title, Unclassified.

Earlier studies to develop the configuration identified as the M-2 are reported in references 3 through 8. One of the objectives of this program is to provide the entry vehicle with a lateral-range capability of 1000 nautical miles, which approximates the orbit-transfer distance or spacing between consecutive orbits for the latitudes of the United States. Depending upon the particulars of the orbit, this range would permit launch and landing after one orbit within the confines of this country. It was shown in reference 3 that this could be achieved with a vehicle that developed a hypersonic lift-drag ratio near 1.3.

The purpose of the present investigation was to evaluate the hypersonic aerodynamic characteristics of the M-2 and to develop suitable stabilizing and control surfaces. A concurrent study of the aerodynamic loadings on the same model at hypersonic and at subsonic speeds is reported in reference 9. The models for these hypersonic studies differed from those of the earlier investigations in that the outboard elevons and side-mounted yaw flaps were eliminated, and rudders were added to provide hypersonic directional stability and to function as a combined lateral-directional control at all flight speeds. Because of the scarcity of hypersonic control data, results for a variety of aerodynamic controls are included. Aerodynamic parameters pertinent to future mission studies and to flight-simulator investigations are discussed and compared with theory.

#### NOTATION

b	model span
$C_D$	drag coefficient, $\frac{\text{drag}}{qS}$
$C_L$	lift coefficient, $\frac{\text{lift}}{qS}$
$C_l$	rolling-moment coefficient, $\frac{\text{rolling moment}}{qSb}$
$C_{l_p}$	damping-in-roll coefficient, $\frac{\partial C_l}{\partial (pb/2V)}$
$C_{l_\beta}$	lateral-stability parameter, $\frac{\partial C_l}{\partial \beta}$
$C_m$	pitching-moment coefficient, $\frac{\text{pitching moment}}{qSl}$
$C_n$	yawing-moment coefficient, $\frac{\text{yawing moment}}{qSb}$
$C_{n_\beta}$	directional-stability parameter, $\frac{\partial C_n}{\partial \beta}$

~~CONFIDENTIAL~~

$C_Y$	side-force coefficient, $\frac{\text{side force}}{qS}$
$c$	control chord
$\frac{L}{D}$	lift-to-drag-ratio
$l$	model length
$M$	Mach number
$p$	rolling velocity
$q$	dynamic pressure
$R$	Reynolds number (based on model length)
$S$	planform area
$t$	thickness
$V$	flight velocity
$\alpha$	angle of attack
$\beta$	sideslip angle
$\delta$	control deflection angle

#### Subscripts

min	minimum
p	pitch flaps
s	moments referred to stability axes (fig. 4)
t	anhedral tails

#### EXPERIMENT

##### Wind Tunnels

The hypersonic tests in air were conducted in the Ames 3.5-foot hypersonic wind tunnel, a blowdown type in which compressed air is heated during passage through a pebble-bed heater and is then accelerated in one of the available, interchangeable nozzles leading to the 3.5-foot-diameter test section. A sketch of the facility is shown in figure 1. For the present tests the air was compressed and heated to provide a nominal total temperature of 2000° R at

~~CONFIDENTIAL~~

~~CONFIDENTIAL~~

pressures up to 1020 psi. The model support system was servo-controlled and hydraulically operated through an angle-of-attack range from  $-5^{\circ}$  to  $+15^{\circ}$ . The model forces and moments were measured with conventional strain-gage balances (a 1.5-inch balance thermally insulated from the models by a double-walled, evacuated steel jacket, or a 1-inch balance maintained at room temperature by a water jacket).

The hypersonic tests in helium were conducted in the Ames 14-inch helium wind tunnel, which operates at ambient room temperature and at pressures up to 2000 psi. The model support system was operable over angles between  $\pm 14^{\circ}$ . The model forces and moments were measured with a 5/8-inch-diameter strain-gage balance with no additional thermal protection device. Further details on the 14-inch helium wind tunnel may be found in reference 10.

### Models and Configuration

Six models differing in size and mounting arrangement were used in the present air and helium wind-tunnel experiments. These models are shown outside of the test section of the 3.5-foot hypersonic wind tunnel in the photograph of figure 2. The model support strut and the tapered sting are visible through the door opening. (The small cone mounted at the front of the sting was not a part of the present study.) The three models appearing in the upper left-hand portion of figure 2(a) were used in the air tests in the 3.5-foot wind tunnel. The three smaller models appearing in the lower right-hand portion of the photograph were used in the helium tests and were also the models used for the study reported in reference 8. The models were 24, 12, 6, and 3.5 inches long, and there was a pair of models for each of the two shorter lengths.

The 24-inch and 12-inch models used for the air tests were machined from Inconel castings and the controls and canopy were made of 347 stainless steel. The three small models used in the helium tests were made of aluminum. One of the 6-inch models was cast of copper-beryllium alloy and was used for shadowgraph tests in the 3.5-foot wind tunnel.

As shown in figure 2, the models were mounted with the sting and balance entering the model either through the base or through the top leeward surface of the model. The former mounting was used for low angles of attack, while the latter mounting was used for high angles of attack. The 12-inch model initially tested at high angles of attack had a 3.12-inch-diameter housing (fig. 2(a)) covering the 1.5-inch-diameter balance and its vacuum jacket. This model was later modified to eliminate the housing and to fit the smaller 1.0-inch balance and its 1.25-inch-diameter water jacket. Both types of model mounting were incorporated into this model, as shown in figures 2(b) and 2(c), so that tests could be made over the angle-of-attack range from  $-15^{\circ}$  to  $+45^{\circ}$ .

Except for the differences in mounting, the models were geometrically similar. Reference dimensions of the 12-inch model are shown in figure 3(a). The dimensions of the other models were in proportion to their lengths. The canopy was the same as that used in earlier M-2 studies and is considered a

~~CONFIDENTIAL~~

representative but not optimum design. The body nose bluntness also corresponded to that of the earlier models.

The dimensions of the two basic controls, the rudders and the lower pitch flaps, are included on figure 3(a) (25° rudder flare is considered the standard configuration for the present study). All of the various controls and components investigated are shown in figure 3(b). Additional details of the nose flaps and outboard elevons tested only on the 3.5-inch model are shown in figure 3(c). Also included in figure 3(c) are details of the anhedral tail surfaces which were tested on the two larger models in air and on the 6-inch model in helium. These surfaces were conceived primarily for augmenting static stability at transonic speeds, but were evaluated hypersonically as part of the present study.

Most of the tests in air were conducted with the canopy removed. The canopies were not removable from the small models, however, so all helium results are with the canopies on the models.

### Tests

The nominal test conditions for the present investigation are summarized as follows:

Mach number	Model length, in.	Angles of attack, deg	Angles of sideslip, deg	Reynolds numbers, million
<u>Air</u>				
5.2	24.0	5 to 25	-6 to 5 at $\alpha = 10$	0.8
	12.0	25 to 45		
7.4	24.0	-7 to 25	-6 to 5 at $\alpha = 10$	1.0, 2.4
	12.0	25 to 65	-15 to 5 at $\alpha = 40$	1.2
10.4	24.0	5 to 25	-6 to 5 at $\alpha = 10$	1.0, 2.0
	12.0	-15 to 42	-10 to 5 at $\alpha = 30$	1.0
<u>Helium</u>				
10.4	6.0	0 to 45	-14 to 14 at $\alpha = 14, 28$	1.7
17.3	3.5	-14 to 64	-14 to 14 at $\alpha = 36$	1.0
	6.0	0 to 14		3.1
21.0	6.0	-8 to 14	-8 to 8 at $\alpha = 0$	4.3

Six-component balance measurements were taken during the pitch and sideslip tests in both tunnels. The availability of bent stings in the two facilities and the model mounting arrangements determined the angles of attack at which the sideslip tests were performed. Yawing moments were not measured for one sideslip run of the 2-foot model because of a temporary system change to permit monitoring of the instantaneous load during tunnel shutdown.

Rudder flares of 0° and 25° (the presently established standard) were tested at all Mach numbers in both air and helium. Additional rudder flares

~~CONFIDENTIAL~~

of  $15^\circ$  and  $35^\circ$  and several differential rudder deflections were tested at 7.4 Mach number. Pitch-flap settings were  $0^\circ$ ,  $15^\circ$ ,  $35^\circ$ , and  $45^\circ$  in air and  $0^\circ$ ,  $35^\circ$ ,  $45^\circ$ , and  $60^\circ$  in helium.

### Precision

The test Mach numbers and the dimensionless aerodynamic coefficients presented in this report are considered to be accurate within the following limits:

Mach number	Accuracy of aerodynamic coefficients, percent
<u>Air</u>	
5.20 $\pm$ 0.03	$\pm 2$
7.40 $\pm$ 0.05	$\pm 3$
10.40 $\pm$ 0.05	$\pm 3$
<u>Helium</u>	
10.40 $\pm$ 0.10	$\pm 3$
17.30 $\pm$ 0.10	$\pm 2$
21.00 $\pm$ 0.10	$\pm 2$

The angles of attack and sideslip are considered to be accurate within  $\pm 0.2^\circ$ . The deflection angles of the controls are accurate within  $\pm 0.3^\circ$ . The accuracies of the coefficients allow for the  $0.2^\circ$  uncertainty in stream angularity.

Sting-interference effects were likely to have affected the measured pitching moments under some test conditions (e.g., when the sting became inclined and exposed to the free stream). A sting inclined at an angle exceeding the Mach angle in a hypersonic flow tends to develop a shock wave along its windward side because of the presence of a supersonic cross flow. Such shocks develop at fairly small inclination angles, since the Mach angles at hypersonic speeds are also small. For example, the Mach angles at Mach numbers of 5.2, 10.4, and 21.0 are  $11^\circ$ ,  $5.5^\circ$ , and  $2.7^\circ$ , respectively. In the present tests, except at  $M = 10.4$  in helium, the models at high angles of attack were mounted with the stings attached to the top leeward surfaces behind the canopy location. Sting-interference effects tended to be small with this mounting arrangement, because the stings were partially shielded from the oncoming flow, and because the inclination angles of the stings relative to the free stream never exceeded  $15^\circ$ .

### PRESENTATION OF RESULTS

The model configuration used as the reference for comparing the experimental results in air is the body-fin combination with rudders flared  $25^\circ$  and with the canopy removed. The effects of adding various combinations of deflected controls and model components to this standard configuration are shown in the figures. For the helium results the reference model configuration is the body-fin combination plus canopy and  $25^\circ$  rudder flare.

~~CONFIDENTIAL~~

All longitudinal aerodynamic characteristics are referred to the wind axes. The lateral and directional characteristics in helium are referred to the body axes, and those in air are shown for both the body axes and the stability axes. The orientation of these axes systems and the directions of the positive forces and moments are shown in figure 4.

#### Measurements in Air

The longitudinal aerodynamic characteristics for the three test Mach numbers of 5.2, 7.4, and 10.4 in air are presented in figures 5, 6, and 7, respectively, for the body-fin configuration (pitch flaps retracted and canopy removed) with  $0^\circ$  and  $25^\circ$  rudder flares. Also shown in figures 5 and 6 are results for the models with  $25^\circ$  rudder flare in combination with the anhedral tails (a set of auxiliary surfaces included in the present study). The longitudinal results for the model with  $25^\circ$  rudder flare and with  $35^\circ$  pitch flaps are shown in figure 8 for the three Mach numbers, and similar results for several pitch-flap deflections are shown in figure 9 for a Mach number of 7.4. The effects of adding the canopy are shown in figure 10.

The lateral-directional moment characteristics (yawing-moment and rolling-moment coefficients) are presented as functions of sideslip angle in figures 11, 12, and 13 for a model angle of attack of  $10^\circ$ , in figure 14 for  $40^\circ$  angle of attack, and in figure 15 for  $30^\circ$  angle of attack. The lateral-directional characteristics in sideslip for the model with several different rudder settings are shown in figure 16. In figures 11 through 16, the coefficients referred to the body axes are shown on the left, and those referred to the stability axes are plotted at the right. Additional rudder characteristics for the model at  $0^\circ$  sideslip angle for an angle-of-attack range from  $-5^\circ$  to  $+45^\circ$  at  $M = 7.4$  are shown in figure 17. The variations of side-force coefficient with sideslip angle are shown in figure 18 for an angle of attack of  $10^\circ$  and in figure 19 for angles of attack of  $40^\circ$  and  $30^\circ$ .

#### Measurements in Helium

The longitudinal aerodynamic characteristics for the three test Mach numbers of 10.4, 17.3, and 21.0 in helium are presented in figures 20, 21, and 22, respectively. The lateral-directional moment characteristics are shown in figures 23, 24, and 25 for the various control arrangements investigated (fig. 3). The side-force coefficients are shown in figures 26, 27, and 28.

#### Summary and Comparisons

A summary of the longitudinal aerodynamic characteristics from the helium and air tests is presented in figure 29. More detailed comparisons of the air and helium results appear in figure 30. Shadowgraph and schlieren photographs of the same model at the same test Mach number in air and in helium are shown in figures 31 and 32, respectively. Two additional schlieren photographs of the model with and without a canopy modification are shown in figure 33 for  $M = 21.0$  in helium.

## DISCUSSION

## Longitudinal-Force Characteristics

The longitudinal-force characteristics of primary interest in trajectory and simulator studies are: the lift coefficient at maximum lift-drag ratio; the lift-curve slope; the maximum lift coefficient; the minimum drag coefficient and drag-rise (or drag-due-to-lift) parameter; and the maximum lift-drag ratio. These parameters are discussed next, and simplified expressions for use in the aforementioned studies are presented where appropriate.

Lift.-- Varying the hypersonic test Mach number produced relatively little change in the lift characteristics (fig. 29). Interpolation of the results indicates that the lift coefficient for trimmed maximum lift-drag ratio was near 0.2 (figs. 8, 9(b)) and occurred near  $\alpha = 10^\circ$ . The lift curves exhibit reduced slopes near  $\alpha = 0^\circ$  and above  $\alpha = 30^\circ$  (figs. 6(b), 9(b), 20(b)). Between  $5^\circ$  and  $30^\circ$  the lift curves at trim can be approximated within 4 percent by the straight-line relationship:

$$C_L = 0.11 + \frac{0.32}{25} (\alpha - 5) \quad (5 \leq \alpha \leq 30)$$

The slopes of the linear portions of the lift curves are plotted in figure 29(b) and were typically close to 0.012 per degree (about half the subsonic value). The maximum lift coefficient (trimmed) was close to 0.44 in air (figs. 5(b), 6(b), 7(b)) and in helium (figs. 20(b), 21(b)), and occurred between  $40^\circ$  and  $50^\circ$  angle of attack.

Drag.-- Drag parameters of general interest are the minimum drag coefficient and the increase of drag coefficient with increasing lift coefficient. The minimum drag coefficients occurred between  $0^\circ$  and  $-5^\circ$  angle of attack and varied with model configuration and test conditions as follows:

Mach number	Reynolds number, million	Canopy	Rudder flare, deg	Pitch flaps, deg	$C_{D_{min}}$
<u>Air</u>					
5.2	0.8	off	25	35	0.085
7.4	1.0	off	0	0	.068
	1.0	off	25	0	.074
	1.0	off	25	35	.078
	1.0	off	25	45	.079
	1.0	on	0	0	.074
10.4	1.1	off	0	0	.066
	1.1	off	25	0	.077
	1.1	off	25	35	.077
	1.1	on	25	35	.081
	1.1	on	25	45	.084
	1.1	on	25	0	.080
<u>Helium</u>					
10.4	1.7	on	25	0	.074
	1.7	on	25	45	.076
17.3	3.1	on	25	0	.066
	3.1	on	25	45	.070
21.0	4.3	on	25	0	.066
	4.3	on	0	45	.061
	4.3	on	25	45	.068

CONFIDENTIAL

The addition of the canopy and the incorporation of  $25^\circ$  rudder flare each increased  $C_{D_{min}}$  0.006 at  $M = 7.4$  in air. At  $M = 10.4$  the addition of the canopy produced an incremental drag coefficient of only 0.003, while the  $25^\circ$  rudder flare added an incremental drag coefficient of 0.011. At  $M = 21.0$  in helium, the  $25^\circ$  rudder flare added an incremental drag coefficient of 0.007. Deflecting the pitch flaps  $45^\circ$  caused small additional increases in  $C_{D_{min}}$ , the increment decreasing from 0.005 at  $M = 7.4$  in air to 0.002 at  $M = 21.0$  in helium.

The increase in drag coefficient with increasing lift coefficient was approximately parabolic for angles of attack below  $30^\circ$  (figs. 6(d), 30(d)). The relationship between drag coefficient and the square of the lift coefficient was almost linear as shown in figure 30(e) for  $M = 10.4$  in air and in helium. The rise in  $C_D$  with increasing  $C_L^2$  was slightly greater in air than in helium. The estimate for air using modified Newtonian theory (skin friction neglected) also indicated a nearly parabolic functional relationship between lift and drag coefficients, and the drag rise factor was very close to those measured in air and in helium. The parabolic functional relationship and the measured and computed values are:

$$\begin{aligned} C_D &= C_{D_{L=0}} + \frac{\partial C_D}{\partial C_L^2} C_L^2 \quad (0^\circ \leq \alpha \leq 30^\circ) \\ &= 0.074 + 2.40 C_L^2 \quad (M = 10.4, \text{ air}) \\ &= 0.074 + 2.32 C_L^2 \quad (M = 10.4, \text{ helium}) \\ &= 0.045 + 2.30 C_L^2 \quad (\text{impact theory, inviscid air}) \end{aligned}$$

Lift-drag ratio.— The M-2 development study in reference 3 indicated that an atmosphere-entry vehicle could achieve a 1000-nautical-mile lateral range corresponding to the distance between consecutive orbits over the United States, if the vehicle developed a hypersonic lift-drag ratio near 1.3. The trimmed maximum lift-drag ratio measured with the present models in air and in helium was 1.2 or greater (figs. 8(c), 20(c)).

Since the variation of drag with lift was essentially parabolic, with minimum drag occurring near zero lift, the hypersonic maximum lift-drag ratio for the M-2 can be expressed as

$$\left(\frac{L}{D}\right)_{\max} = \frac{1}{2} \sqrt{\frac{1}{(\partial C_D / \partial C_L^2) C_{D_{min}}}}$$

For entry studies, primary interest is in the angle-of-attack range between maximum lift-drag ratio and maximum lift coefficient. The present data in the range between  $15^\circ$  and  $45^\circ$  indicate that the trimmed lift-drag ratios may be

CONFIDENTIAL

CONFIDENTIAL

approximated within 3 percent by a linear function of angle of attack:

$$\frac{L}{D} = 0.60 + 0.02 (45 - \alpha) \quad (15^\circ \leq \alpha \leq 45^\circ)$$

### Longitudinal Stability and Control

The original  $13^\circ$  half-cone with no boattailing from which the M-2 evolved (ref. 3) trimmed at a low angle of attack near that for maximum lift-drag ratio. To trim the simple half-cone to high angle of attack near maximum lift would have required controls that would produce a nose-up moment while maintaining stability. There were obvious disadvantages to this scheme. If the trimming controls were located forward on the body to produce nose-up moment, they would adversely affect static stability, as will be shown in the case of the nose flaps which caused directional instability. Controls mounted on the upper aft surface, on the other hand, could produce a nose-up moment at low angles of attack by exerting a download near the tail. This location of controls, however, results in their passage into the "shadow" or leeward side of the vehicle and rapid loss in control effectiveness as angle of attack is increased. Another significant disadvantage to the half-cone was the large base area and the associated base drag which penalizes low-speed performance. Boattailing not only improves lift-drag ratio at low speeds but also reduces the moment required for trim at high angles.

Static longitudinal stability.— The present experimental results (figs. 5, 6, 7, 9, 20, 21) show that the M-2 with pitch flaps retracted trimmed at angles of attack near  $45^\circ$ , corresponding to maximum lift coefficient. With increasing pitch-flap deflection, trim occurred at progressively lower angles of attack down to zero lift. The static margin was at least 5 percent of the body length over this angle-of-attack range. The reference moment center for the present results is the same as that used in the earlier referenced studies and is shown in figure 3(a).

Pitch flaps.— The pitch-flap deflection required for trim at the attitude for maximum lift-drag ratio (fig. 8) was approximately  $35^\circ$  ( $0^\circ$  pitch flap corresponds to flaps retracted). The flaps had the effect of partially restoring the lower afterbody intentionally removed from the original half-cone by boattailing to achieve the high-angle trim capability. It is indicated in figures 9(a) and 30(a) that trim at zero angle of attack would require about  $50^\circ$  deflection of the pitch flaps.

The pitch flaps maintained effectiveness throughout the wide angle-of-attack range investigated because of their windward exposure. The effectiveness was dependent upon model angle of attack, however, and was nonlinear with respect to flap deflection. Deflecting the flaps increased the lift coefficients slightly because of the positive lift contribution of the flaps (figs. 9(b), 20(b)), but flap deflections up to  $45^\circ$  caused little or no change in lift-drag ratio (figs. 9(c), 20(c)). Deflecting the flaps produced a small increase in static directional stability (figs. 16, 23), but produced no other observable effects on hypersonic aerodynamic characteristics.

Canopy.- A representative canopy included in the earlier studies was tested in the present air and helium investigations. The addition of the canopy at  $M = 7.4$  in air produced a nose-down pitching moment which almost resulted in a second trim point around  $\alpha = -5^\circ$  with zero pitch flaps (fig. 10(a)). The tendency toward this low-angle trim was considerably reduced at the higher Mach numbers in air and in helium (figs. 20(a), 21(a), 22(a), 30(a)). This low-angle trim is to be avoided, because it would require an additional hypersonic control that produced nose-up pitching moments. The complications associated with such a control have already been discussed. It should be noted that future canopy designs must be checked for their effects on trim conditions near zero lift. The addition of the canopy produced no discernible effects on the lateral-directional characteristics.

Visual evidence that the bluntness of the canopy may have influenced the flow separation from the body nose is presented in the schlieren photographs of figure 33 for a Mach number of 21.0 in helium. A small splitter plate added forward of the canopy appears to have lessened the flow separation (fig. 33(b)) compared to that of the unmodified canopy (fig. 33(a)). The flow separation is clearly indicated for Mach numbers of 10.4 and 21.0 in the helium schlieren pictures of figures 32 and 33, but is not apparent in the less sensitive shadowgraph of the model at  $M = 10.4$  in air (fig. 31). The extent to which separation might differ in helium and in air, and might be influenced by the model temperature relative to the temperature of the test medium is not yet known.

Nose flaps.- The nose flaps were investigated briefly at  $M = 17.3$  in helium to determine their effectiveness in increasing the trim angle at the high angles of attack. They increased the trim angle by only  $7^\circ$  (fig. 21(a)) but, as expected, they seriously reduced the static directional stability (fig. 24(a)).

Elevons.- The elevons which were tested in earlier M-2 studies and which exhibited adverse lateral-control characteristics (high adverse yaw) were tested briefly at high angles of attack in helium at  $M = 17.3$ . Both elevons were set at the negative  $40^\circ$  incidence selected in reference 8 for the high angle-of-attack trim condition. As shown in figure 21, the elevons exerted no significant effect on the aerodynamics or on the static margin of the model near trim.

Anhedral tails.- These surfaces were considered as possible means for augmenting the static longitudinal and directional stability, particularly at transonic speeds. An earlier test of the M-2 with elevons removed had indicated neutral stability (see fig. 14(c) of ref. 6) at  $M = 0.9$ . The anhedral tails (fig. 4) favorably increased the hypersonic longitudinal and directional stability (figs. 12, 13, 14, 15), decreased the lateral stability (dihedral effect) at high angles of attack (figs. 14(b), 15(b)), and reduced the high-trim angle of attack with pitch flaps retracted (figs. 5(a), 6(a), 7(a)).

~~CONFIDENTIAL~~

## Lateral-Directional Characteristics

Yawing-moment and rolling-moment coefficients are shown in figures 11 through 16 for sideslip tests in air at angles of attack of  $10^\circ$ ,  $30^\circ$ , and  $40^\circ$  ( $10^\circ$  is near maximum lift-drag ratio and  $40^\circ$  is near maximum lift). At the higher angles of attack, all model configurations tested exhibited favorable directional stability about the stability axes, as evidenced by the stable variations of  $C_{n\beta}$  with sideslip angle (figs. 14(b), 15(b)). (The relationship between body and stability axes is shown in fig. 4.) At the lower angle of attack, the model with the rudders undeflected exhibited almost neutral static directional stability (figs. 11(b), 12(b), 13(b)) in air and in helium (figs. 23, 25).

Rudder flare.— Airfoils exhibit nonlinear lift curves at hypersonic speeds, as explained in detail in reference 11. Stabilizing surfaces would be expected to perform in a like manner, with low lift-curve slope or effectiveness through zero angle of inclination to the hypersonic stream. Adding rudder flare to the present model permitted the rudders to act at larger angles of attack where increased lift-curve slope and greater effectiveness occurred. In addition, the flared rudders tended to emerge from the engulfing boundary layer passing from the more forward body and fins. As shown in figures 12 through 16 and in figures 23 through 25, rudder flare significantly increased the static directional stability as expected from the foregoing reasoning. Rudder flare had little effect on the rolling-moment characteristics referred to the body axes, while it decreased the lateral stability (dihedral effect) referred to the stability axes at high angle of attack (figs. 14(b), 15(b), 16(b)). The increased directional stability and reduced lateral stability produced by the rudder flare lessen the likelihood of the occurrence of Dutch roll. (A tendency toward Dutch-roll instability was observed with an earlier M-2 model during subsonic free-flight tests reported in ref. 4.) Because satisfactory lateral-directional characteristics resulted with  $25^\circ$  rudder flare, longitudinal aerodynamic characteristics were also measured with this flare. Rudder flare thus provided an effective control over the level of the static directional stability and also over the ratio of directional to lateral stability over a wide test range of angles of attack.

Typical values for the hypersonic static stability and side-force derivatives for the model with  $25^\circ$  rudder flare have been evaluated for simulator and trajectory studies. The following averaged values are generally accurate within  $\pm 12$  percent.

	$0^\circ \leq \alpha \leq 10^\circ$	$30^\circ \leq \alpha \leq 40^\circ$
$C_{n\beta}$	0.0025	0.0021
$C_{l\beta}$	-.0024	-.0030
$C_{Y\beta}$	-.0160	-.0180
$C_{n s \beta}$	.0025	.0033
$C_{l s \beta}$	-.0024	-.0014

Rudder lateral-directional control.— The concept of using differential rudder deflection for controlling roll of the M-2 is based on advantageously using the coupling between the inherent lateral stability of the configuration and rudder-induced sideslip. A concurrent simulator study published in reference 12 supported the practicability of this type of lateral control. The present results (figs. 16, 17, 24) show that differential rudder was effective in producing yawing moments over a wide range of angles of attack and sideslip and, consequently, would cause sideslip motion and attendant rolling motion to a vehicle in flight.

The yawing moments produced by  $20^\circ$  differential rudder (fig. 17(a)) varied considerably over the test range of angles of attack from  $-5^\circ$  to  $+45^\circ$ . The minimum yawing moments around  $6^\circ$  angle of attack are considered to indicate that at this  $\alpha$ , the rudders were subjected to the maximum submergence in the boundary layer from the body. The body boundary layer passed below the rudder for  $\alpha < 6^\circ$  or tended to pass inside the fins for  $\alpha > 6^\circ$ . The rolling-moment results in figure 17(b) show that  $20^\circ$  differential rudder produced a favorable or augmenting rolling moment ( $C_{l_s}$  between 0.002 and 0.004) about the stability axes over the range of angles of attack of practical interest ( $15^\circ \leq \alpha \leq 45^\circ$ ). This augmenting rolling moment would add to the body rolling moment produced by the coupling between sideslip and lateral stability.

A maximum roll response may be estimated from the results shown in figure 16(b) and assuming a typical damping-in-roll coefficient of  $-0.3$ . The data indicate that  $35^\circ$  differential rudder would produce about  $3^\circ$  of sideslip to the stability axis and a corresponding rolling-moment coefficient  $C_{l_s}$  near 0.012. For a flight speed of 10,000 feet per second and a vehicle of 10-foot span, the resulting rolling velocity about the stability axis would be 80 radians per second. This is, of course, excessive, and much smaller rudder deflections would suffice. Rolling velocities for other flight speeds and other vehicle sizes may be estimated from the roll helix angle ( $pb/2V = \Delta C_l / C_{l_p}$ ). The present results indicate that adequate roll response would result from the use of rudders for lateral control at hypersonic speeds.

No effect of lower pitch-flap deflection on rudder characteristics was noted, but a slight increase in directional stability at the higher angles of attack accompanied deflection of the flaps, as noted earlier (fig. 16).

#### Comparison of Air and Helium Results

The flight Mach number during atmosphere entry and return to earth decreases from about 30 to the subsonic value ( $\sim 0.3$ ) corresponding to landing. In the interest of obtaining aerodynamic measurements at increasingly higher Mach numbers, the tests up to a Mach number of 21 in helium were added to the tests to  $M = 10.4$  in air. Some confidence that the measurements in helium provide a good qualitative and possibly a quantitative guide for extrapolating the air results to higher Mach numbers can be gained from inspection of the present measurements at  $M = 10.4$  both in helium and in air (fig. 30).

[REDACTED]

Theoretical studies reported in references 11 and 13 identified the effects of varying the gas specific-heat ratio ( $7/5$  for air and  $5/3$  for helium) on the flow properties through normal and oblique shock waves and on the inviscid aerodynamic characteristics of blunt and sharp wedges and cones. The principal findings were that increasing the gas specific-heat ratio decreased the pressure coefficients for the strong-shock solutions and increased those for the weak-shock solutions. Consequently, the loadings were lower on the blunt nose portions of the bodies, but higher on the aftersurfaces as the gas specific-heat ratio was increased. Associated with the higher gas specific-heat ratio were significantly increased lift coefficients and slightly increased lift-drag ratios and inviscid drag coefficients. These effects decreased with increasing amounts of bluntness and were much smaller for cones than for wedges. Comparisons of the experimental results for cones in air and in helium presented in references 14 and 15 indicate higher lift-drag ratios, slightly higher lift coefficients, and slightly lower drag coefficients for the sharp cones in helium. There were no significant differences between the aerodynamic coefficients for the blunted,  $10^\circ$  half-angle cones in air and helium.

The present results (fig. 30) indicate close agreement between the helium and air results. The only significant difference occurred in the pitching-moment coefficients with  $0^\circ$  pitch flaps (fig. 30(a)). This difference can be attributed to the greater sting interference during the helium test wherein the model was base-mounted over the entire angle-of-attack range, whereas the model was top-mounted for the tests in air above  $15^\circ$  angle of attack. Note that the sting interference was practically eliminated and excellent agreement resulted when the pitch flaps were deflected  $45^\circ$  and the sting became effectively shielded (fig. 32).

#### Reynolds Number Effects

As previously mentioned under Experiment, the variation in test Reynolds number was obtained by varying the total pressure for consecutive runs of the 24-inch model. No discernible effects of Reynolds number variation on the measured model characteristics were found. The concurrent study of hypersonic pressure distributions reported in reference 9 also indicated no significant effect of a variation in test Reynolds number.

#### CONCLUSIONS

The more significant conclusions drawn from the hypersonic aerodynamic characteristics measured for the M-2 lifting entry configuration during air and helium wind-tunnel tests over a Mach number range from 5.2 through 21.0 are:

1. Variation in hypersonic test Mach number produced no large effects on the measured aerodynamic characteristics.

~~CONFIDENTIAL~~

2. The lower pitch flaps were effective in trimming the model over the angle-of-attack range from zero lift through maximum lift with an attendant static margin of approximately 5-percent model length aft of the moment center at 55 percent of the body length.

3. The model with retracted rudders exhibited neutral static directional stability. The addition of rudder flare, however, produced favorable directional stability and control characteristics and the directional stability increased with increasing rudder flare.

4. The rudders were effective for both directional and lateral control. The lateral-control capability derives from the coupling between rudder-induced sideslip and the inherent lateral stability of the configuration.

5. The maximum trimmed lift-drag ratio was approximately 1.2 and occurred near  $10^\circ$  angle of attack and a lift coefficient of 0.2.

6. The maximum lift coefficient was approximately 0.45 and occurred near  $45^\circ$  angle of attack where the corresponding lift-drag ratio was 0.6.

Ames Research Center

National Aeronautics and Space Administration

Moffett Field, Calif., July 13, 1966

124-07-02-10

#### REFERENCES

1. Eggers, Alfred J., Jr.: The Possibility of a Safe Landing. In: Space Technology, Howard S. Seifert, ed., John Wiley and Sons, Inc., 1959, pp. 13-01 to 13-53.
2. Chapman, Dean R.: An Approximate Analytical Method for Studying Entry Into Planetary Atmospheres. NASA TR R-11, 1959.
3. Rakich, John V.: Supersonic Aerodynamic Performance and Static-Stability Characteristics of Two Blunt-Nosed, Modified  $13^\circ$  Half-Cone Configurations. NASA TM X-375, 1960.
4. Hassell, James L., Jr.; and Ware, George M.: Investigation of the Low-Subsonic Stability and Control Characteristics of a 0.34-Scale Free-Flying Model of a Modified Half-Cone Reentry Vehicle. NASA TM X-665, 1962.
5. Kenyon, George C.; and Edwards, George G.: A Preliminary Investigation of Modified Blunt  $13^\circ$  Half-Cone Re-entry Configurations at Subsonic Speeds. NASA TM X-501, 1961.

~~CONFIDENTIAL~~

6. Kenyon, George C.; and Sutton, Fred B.: The Longitudinal Aerodynamic Characteristics of a Re-entry Configuration Based on a Blunt  $13^\circ$  Half-Cone at Mach Numbers to 0.92. NASA TM X-571, 1961.
7. Kenyon, George C.: The Lateral and Directional Aerodynamic Characteristics of a Re-entry Configuration Based on a Blunt  $13^\circ$  Half Cone at Mach Numbers to 0.90. NASA TM X-583, 1961.
8. Rakich, John V.: Aerodynamic Performance and Static-Stability Characteristics of a Blunt-Nosed, Boattailed,  $13^\circ$  Half-Cone at Mach Numbers From 0.6 to 5.0. NASA TM X-570, 1961.
9. Axelsson, John A.: Pressure Distributions for the M-2 Lifting Entry Vehicle at Mach Numbers of 0.23, 5.2, 7.4, and 10.4. NASA TM X-997, 1964.
10. McDevitt, John B.; and Mellenthin, Jack A.: Characteristics of a Blunt Half-Cone Entry Configuration at Mach Numbers From 10.9 to 21.2 in Helium. NASA TM X-655, 1962.
11. Cleary, Joseph W.; and Axelsson, John A.: Theoretical Aerodynamic Characteristics of Sharp and Circularly Blunt-Wedge Airfoils. NASA TR R-202, 1964.
12. Taylor, Lawrence W.; Samuels, James L.; and Smith, John W.: Simulator Investigation of the Control Requirements of a Typical Hypersonic Glider. NASA TM X-635, 1962.
13. Cleary, Joseph W.: An Experimental and Theoretical Investigation of the Pressure Distribution and Flow Fields of Blunted Cones at Hypersonic Mach Numbers. NASA TN D-2969, 1965.
14. Ladson, Charles L.; and Blackstock, Thomas A.: Air-Helium Simulation of the Aerodynamic Force Coefficients of Cones at Hypersonic Speeds. NASA TN D-1473, 1962.
15. Harris, Julius E.: Force-Coefficient and Moment-Coefficient Correlations and Air-Helium Simulation for Spherically Blunted Cones. NASA TN D-2184, 1964.

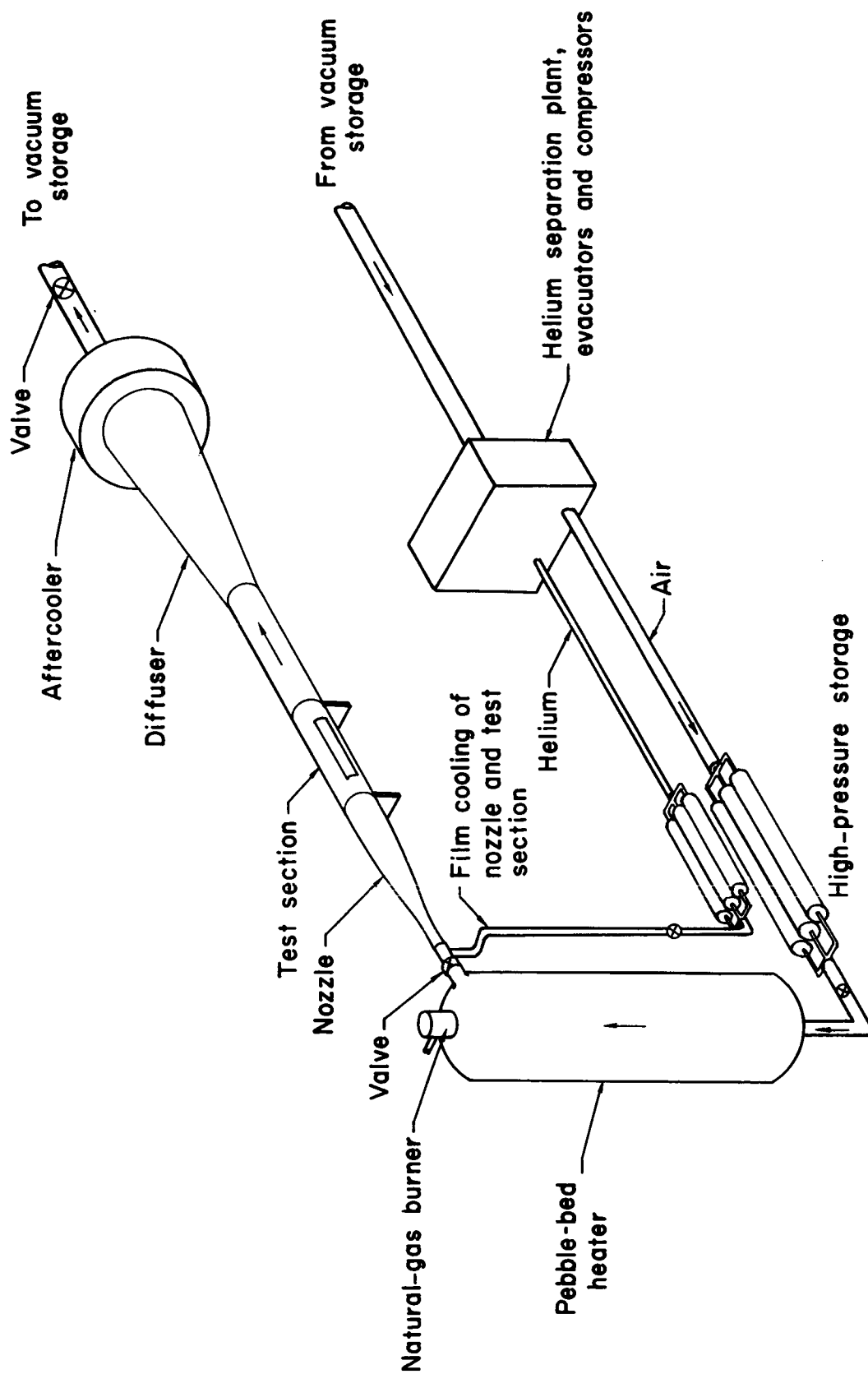
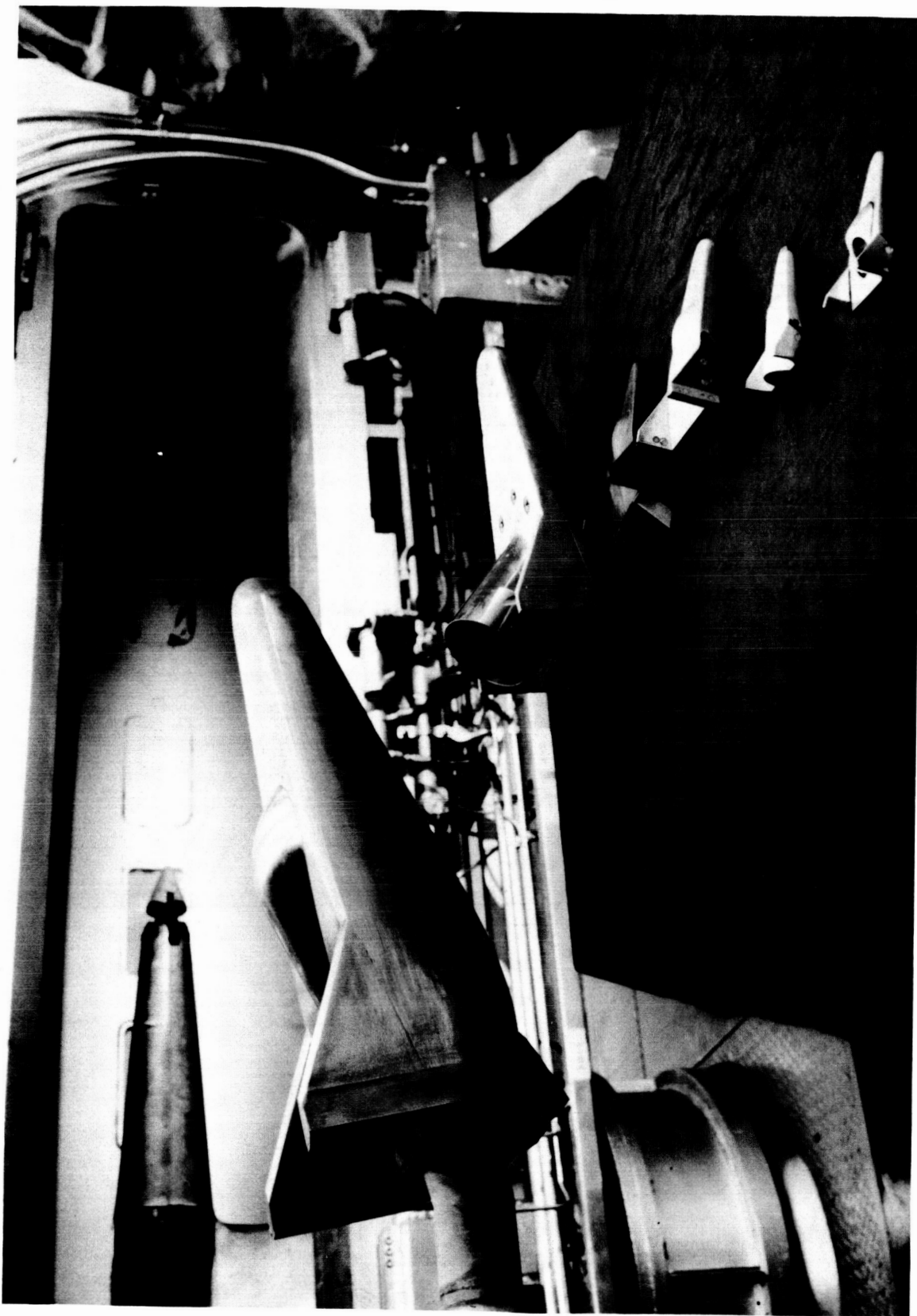


Figure 1.- Schematic drawing of the Ames 3.5-foot hypersonic wind tunnel.

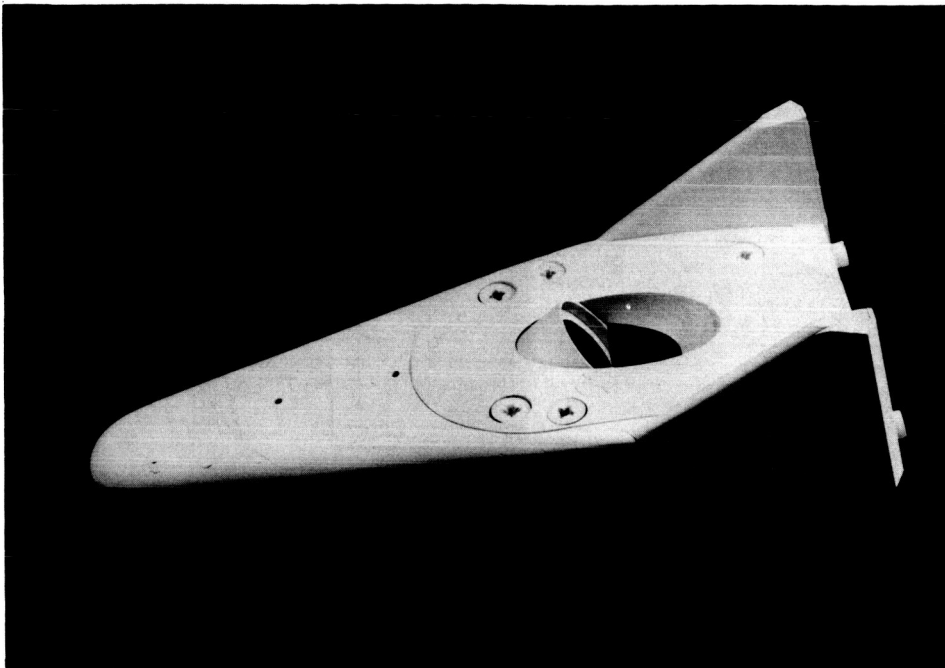


A-30990

(a) 3.5, 6.0, 12.0, and 24.0 inch models.

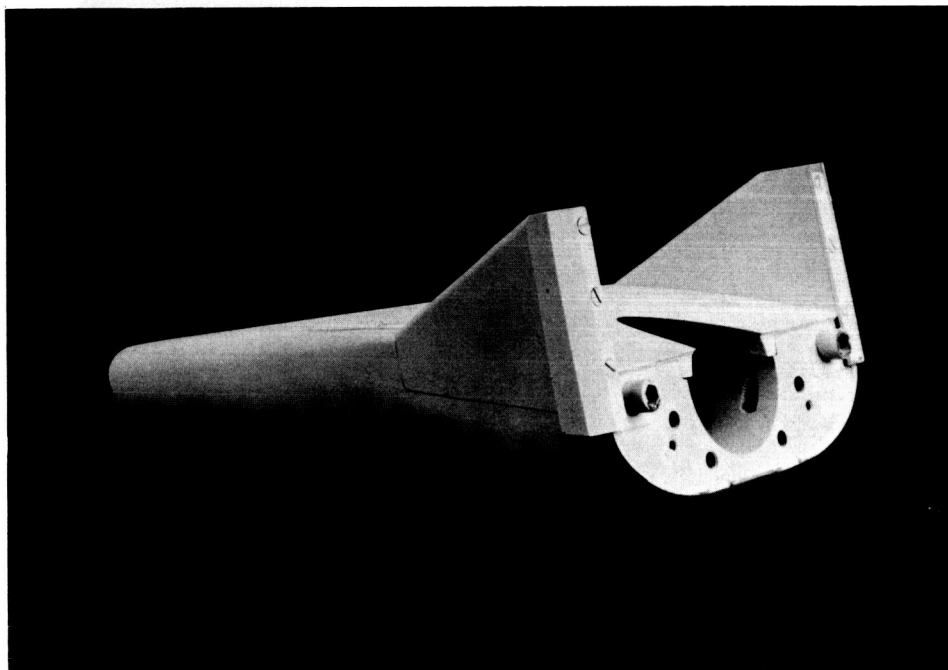
Figure 2.-- Photographs of M-2 models used in the hypersonic wind-tunnel investigation.

~~CONFIDENTIAL~~



A-36840

(b) Modified 12.0 inch model, 30° top mount.



A-36838

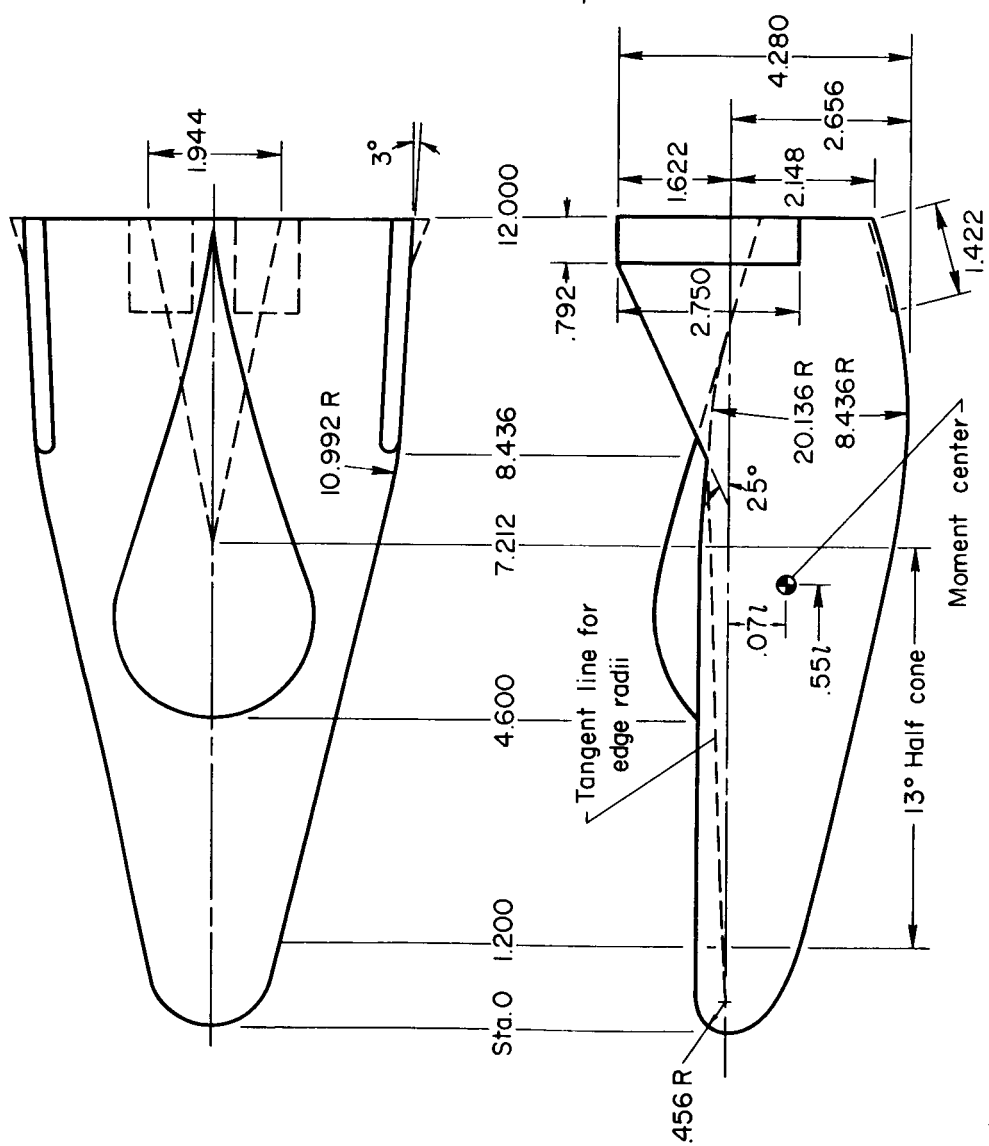
(c) Modified 12.0 inch model, base mount.

Figure 2.- Concluded.

~~CONFIDENTIAL~~

NOSE COORDINATES BELOW  
CONE CENTER LINE

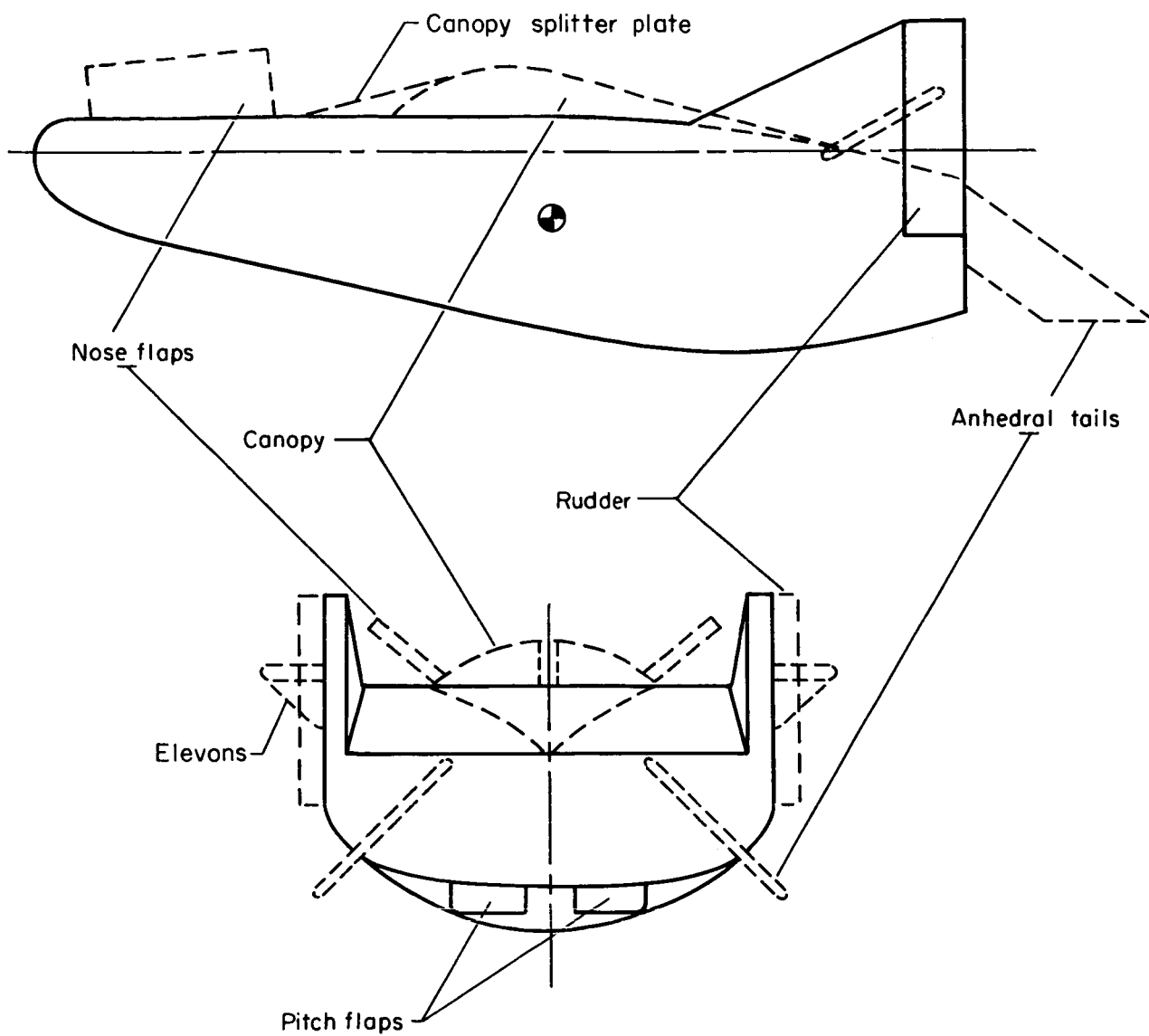
STATION	RADIUS
0.120	0.443
.240	.607
.360	.720
.480	.803
.600	.867
.720	.918
.840	.958
.960	.993
1.080	1.023
1.200	1.051



Note: All dimensions in inches.

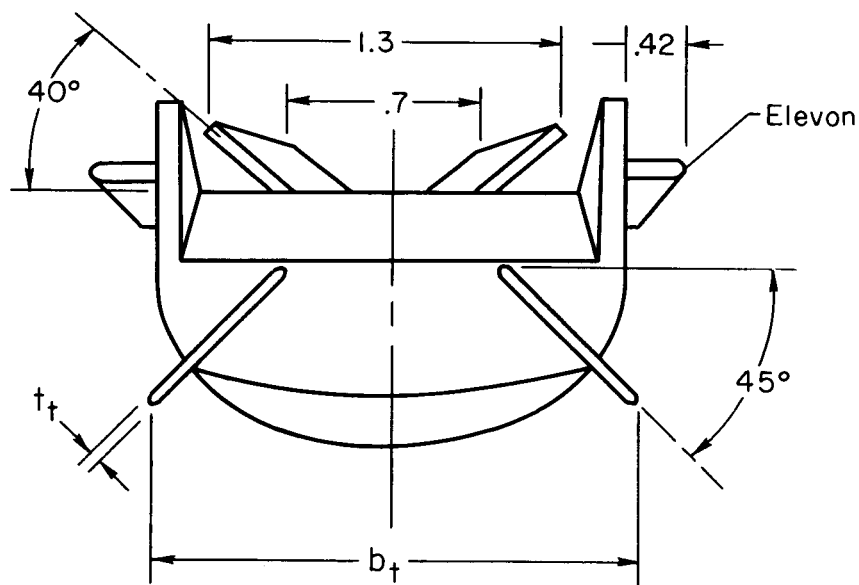
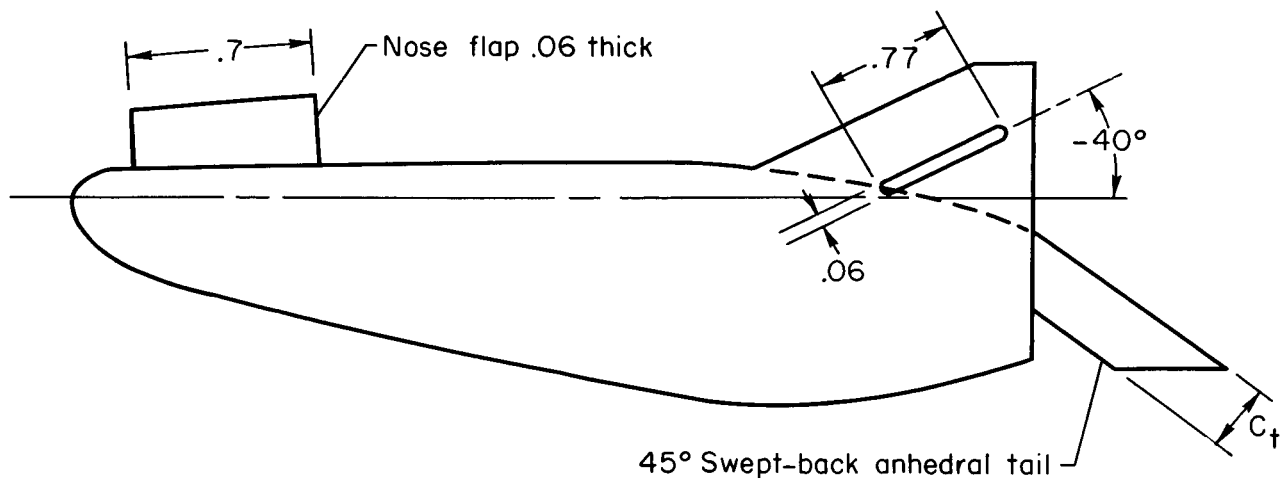
(a) Dimensions of the 12-inch model.

Figure 3.- Details of the M-2 models.



(b) Sketch of the model controls and components.

Figure 3.- Continued.



Nose flap and elevon dimensions for 3.5-inch model.  
Anhedral tail dimensions for other models.

Model, in.	$c_t$	$b_t$	$t_t$
6	0.5	3.25	0.10
12	1.0	6.00	.09
24	2.0	12.00	.18

(c) Details of extra controls.

Figure 3.- Concluded.

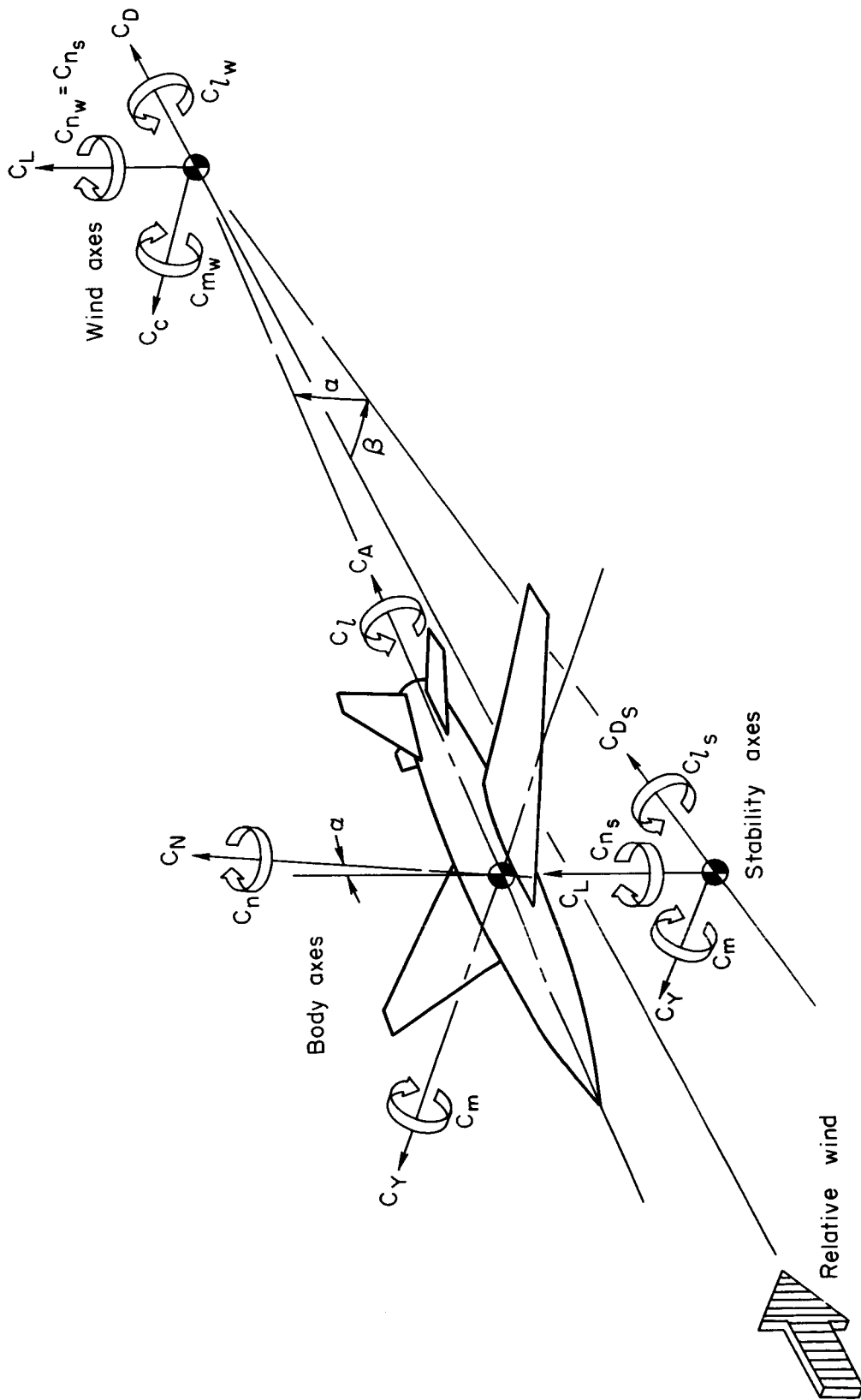
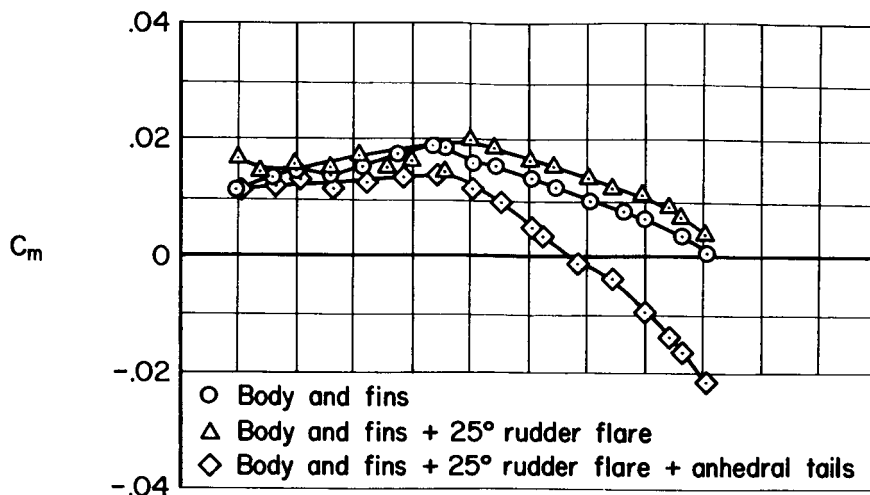
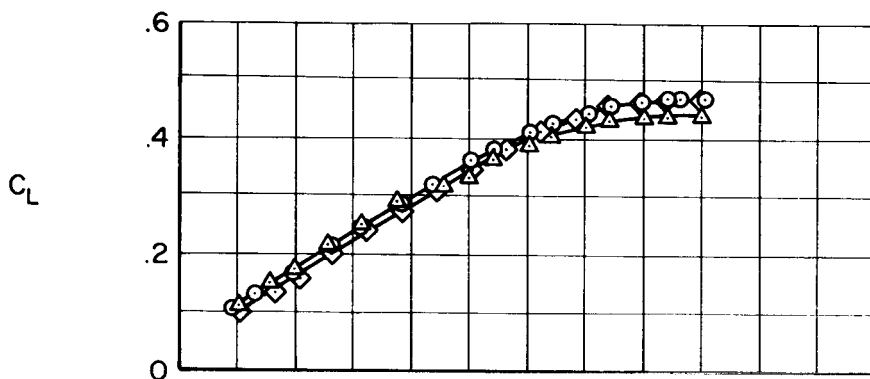


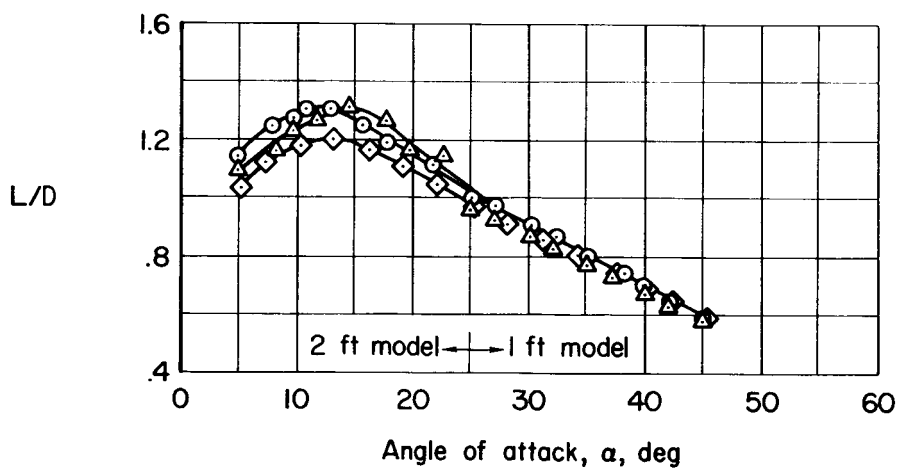
Figure 4.- Orientation of force and moment coefficients about body, wind, and stability axes.



(a) Pitching-moment coefficient.

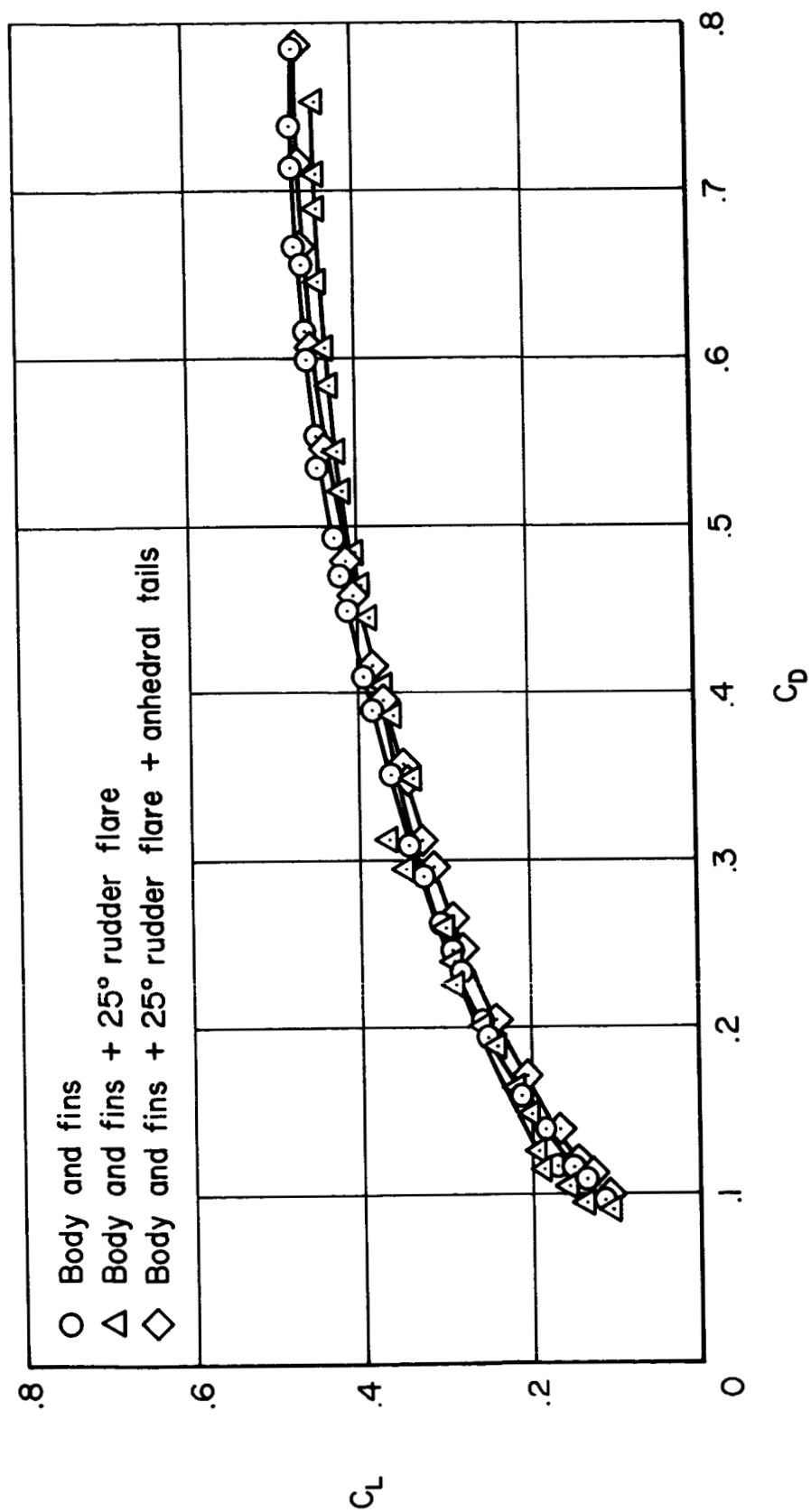


(b) Lift coefficient.



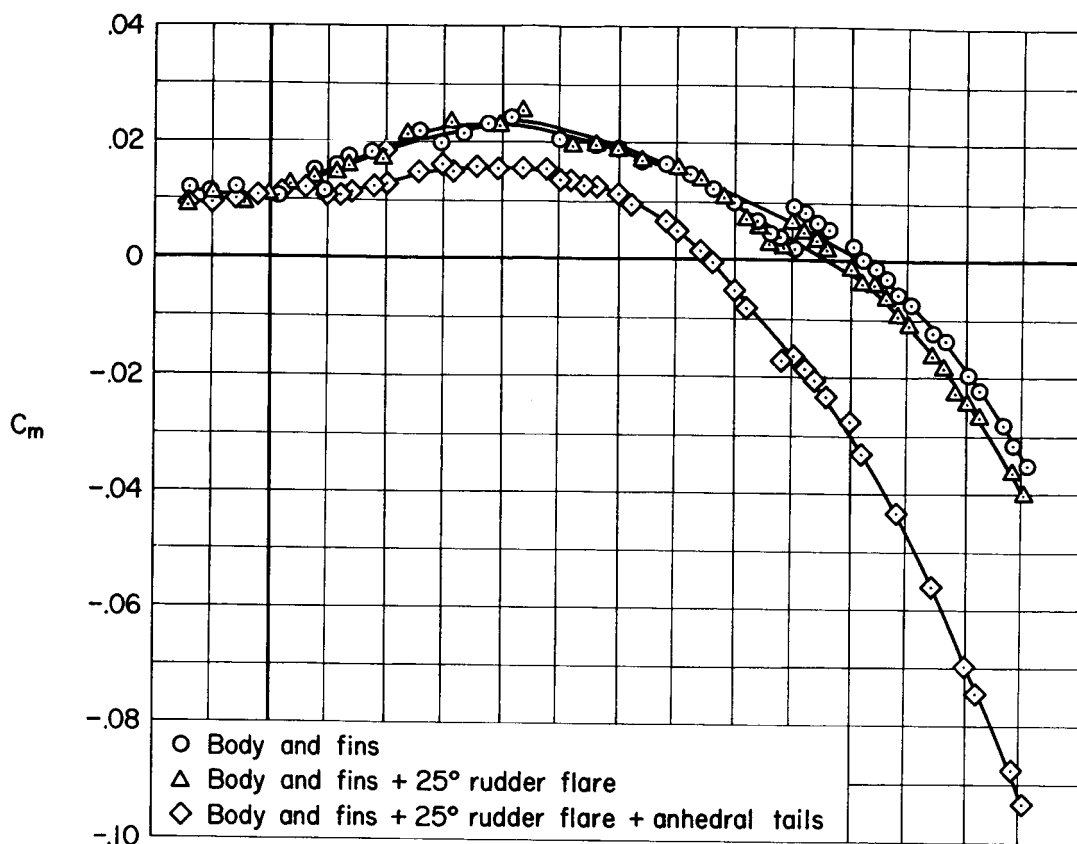
(c) Lift-drag ratio.

Figure 5.- Longitudinal aerodynamic characteristics;  $M = 5.2$ , air.

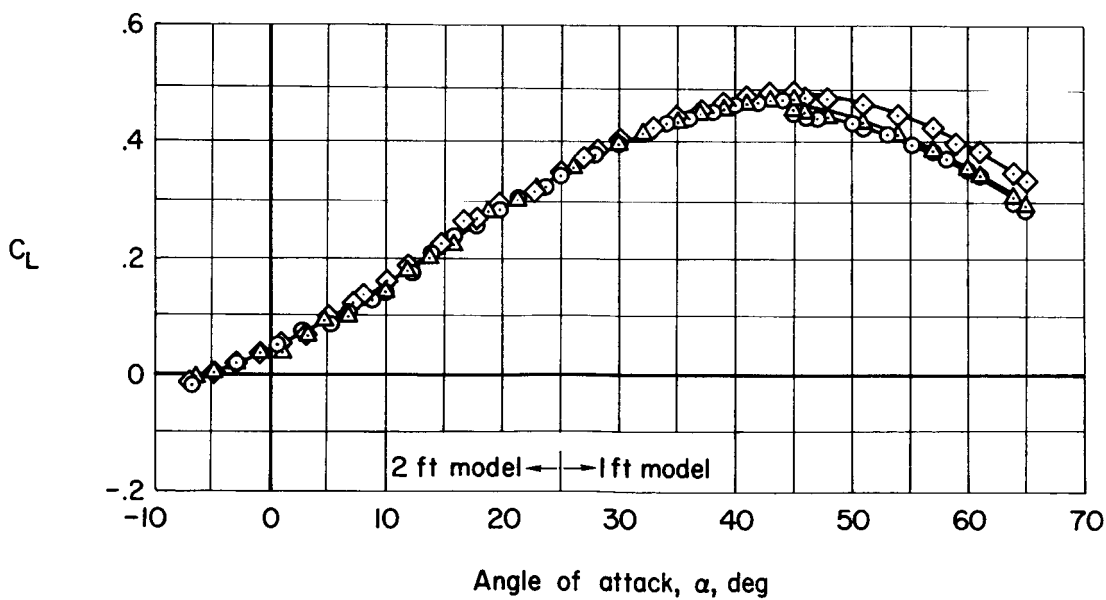


(a) Lift-drag polar.

Figure 5.- Concluded.

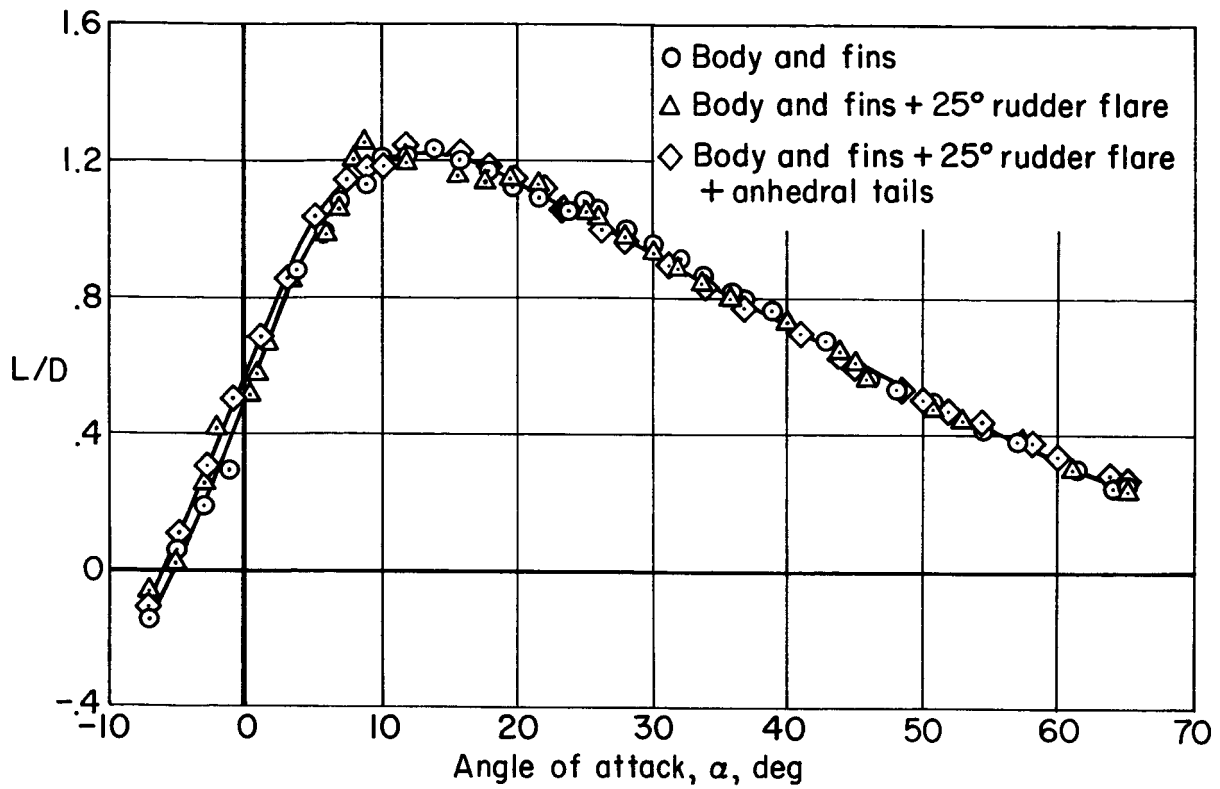


(a) Pitching-moment coefficient.

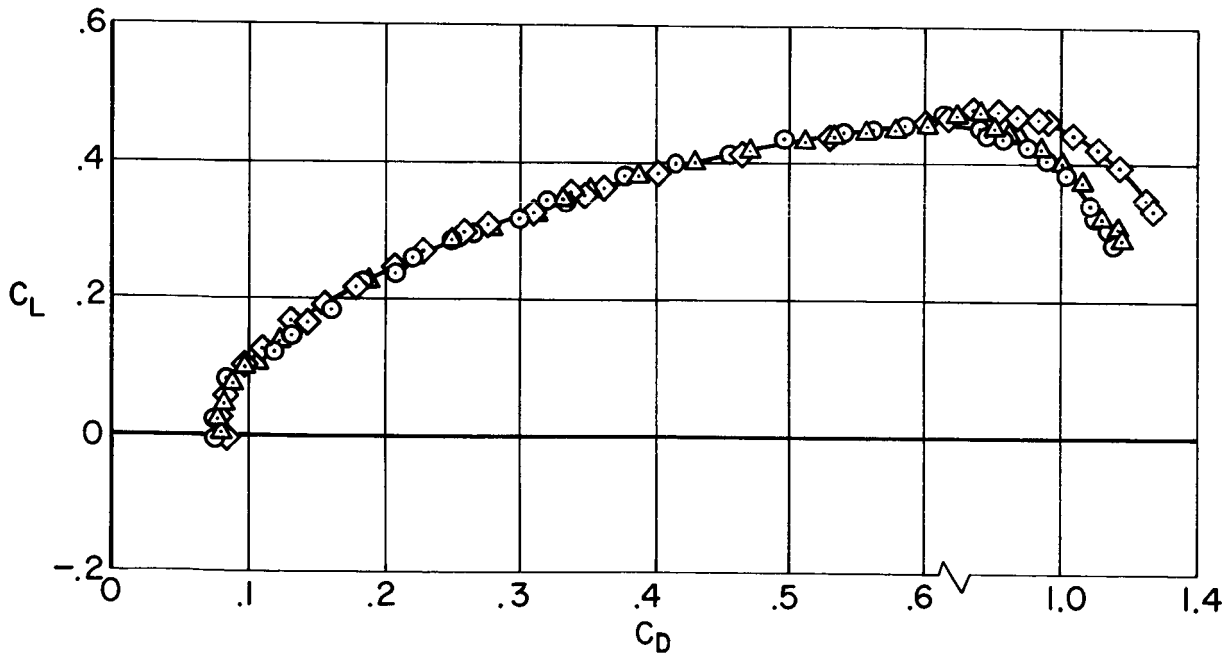


(b) Lift coefficient.

Figure 6.- Longitudinal aerodynamic characteristics;  $M = 7.4$ , air.

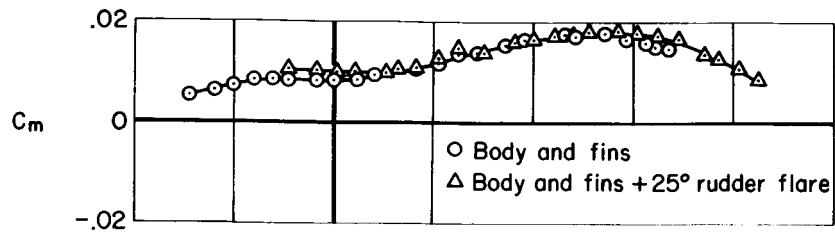


(c) Lift-drag ratio.

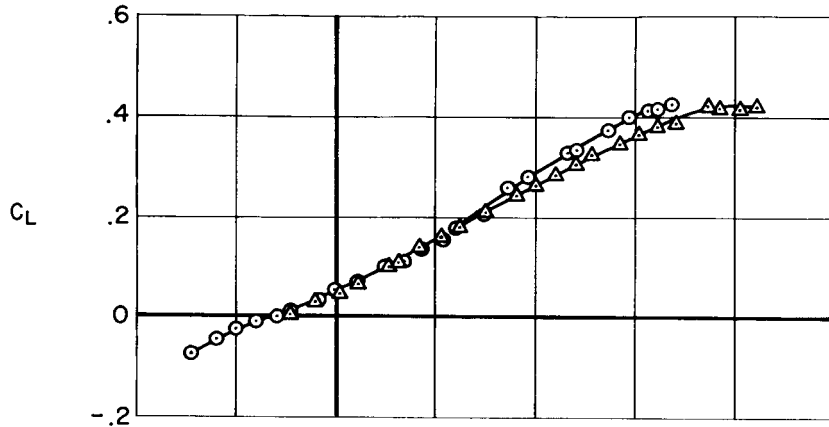


(d) Lift-drag polar.

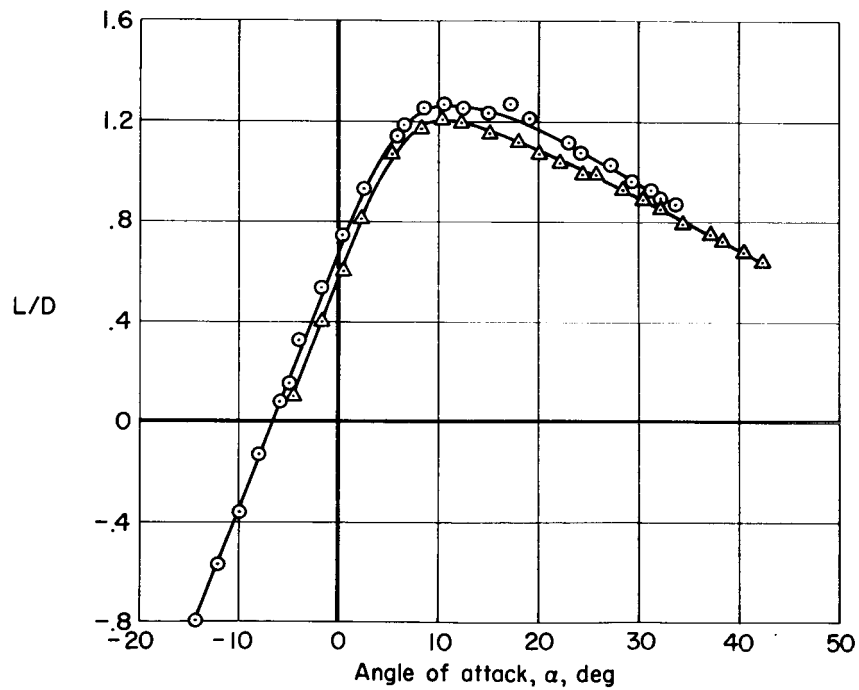
Figure 6.- Concluded.



(a) Pitching-moment coefficient.

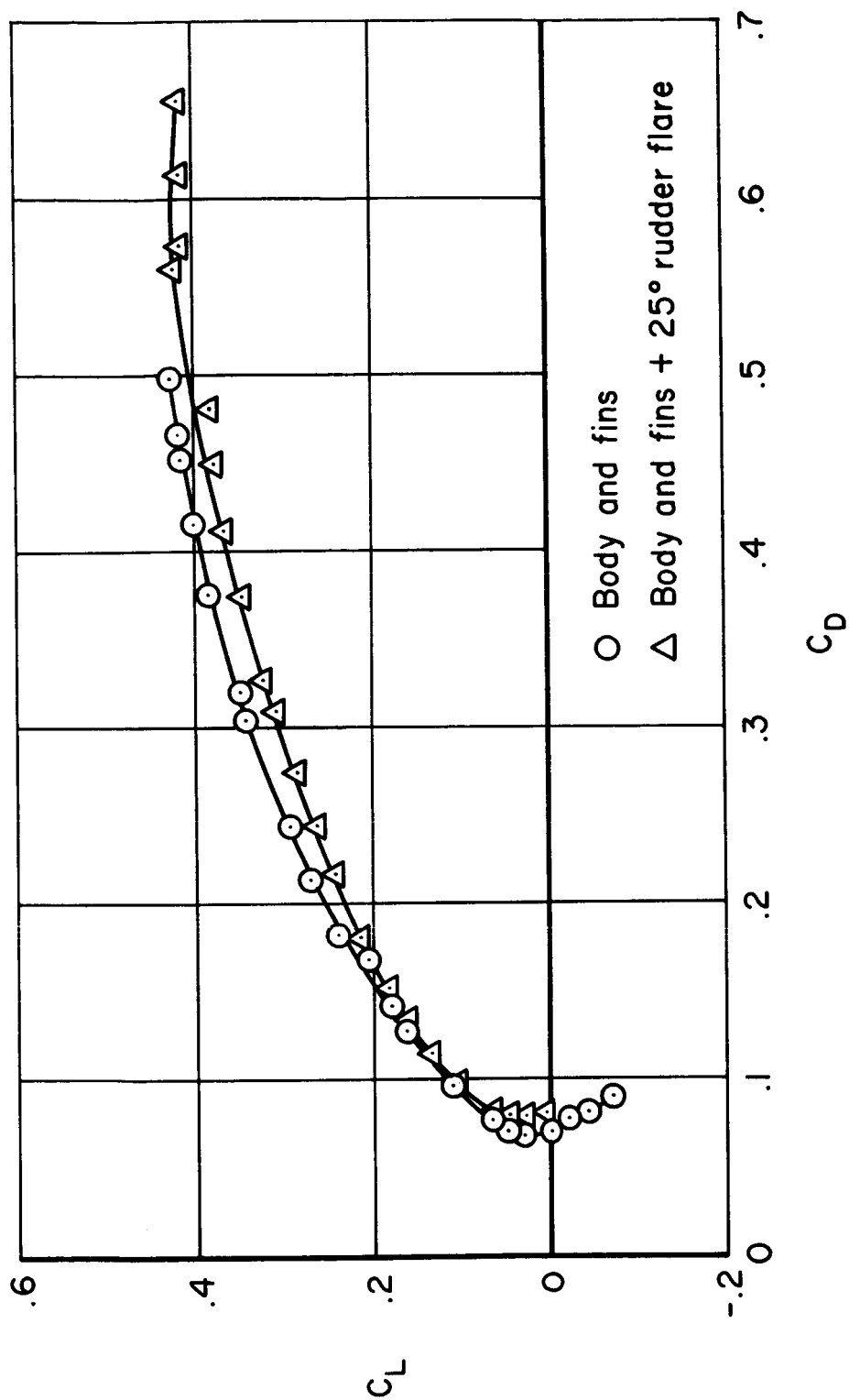


(b) Lift coefficient.



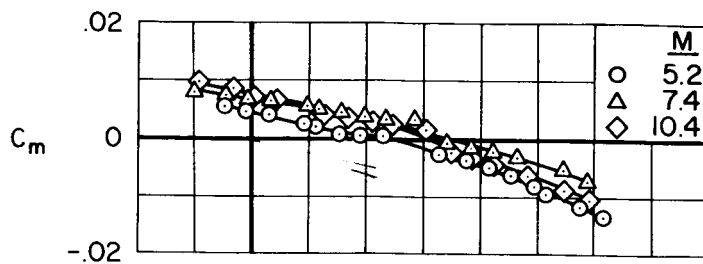
(c) Lift-drag ratio.

Figure 7.- Longitudinal aerodynamic characteristics;  $M = 10.4$ , air.

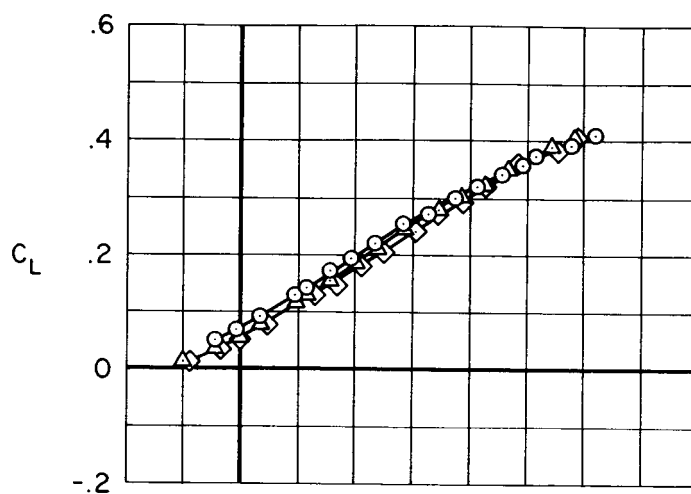


(d) Lift-drag polar.

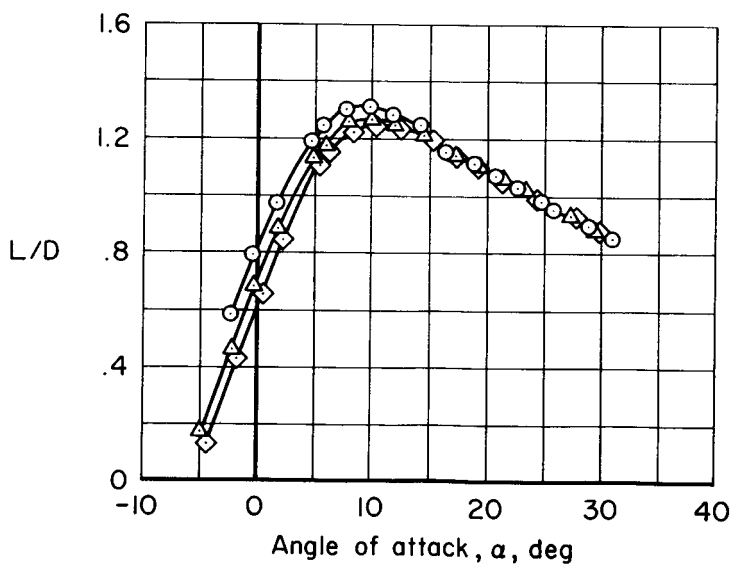
Figure 7.- Concluded.



(a) Pitching-moment coefficient.

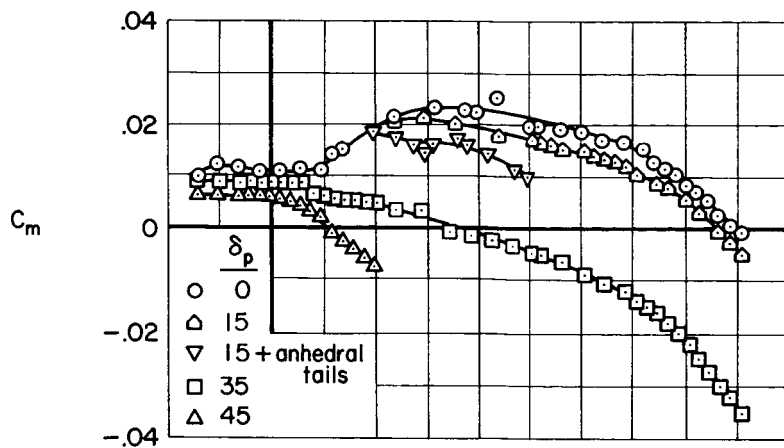


(b) Lift coefficient.

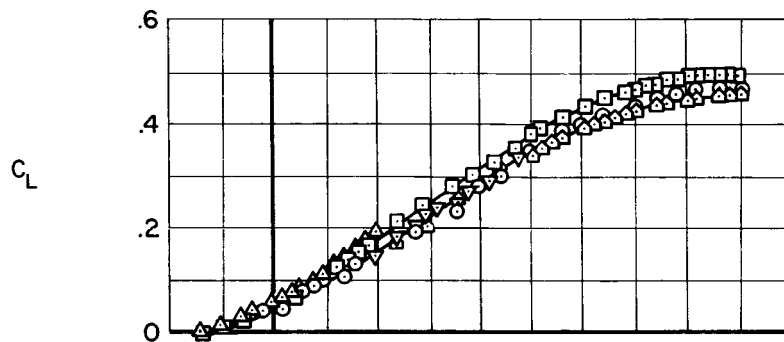


(c) Lift-drag ratio.

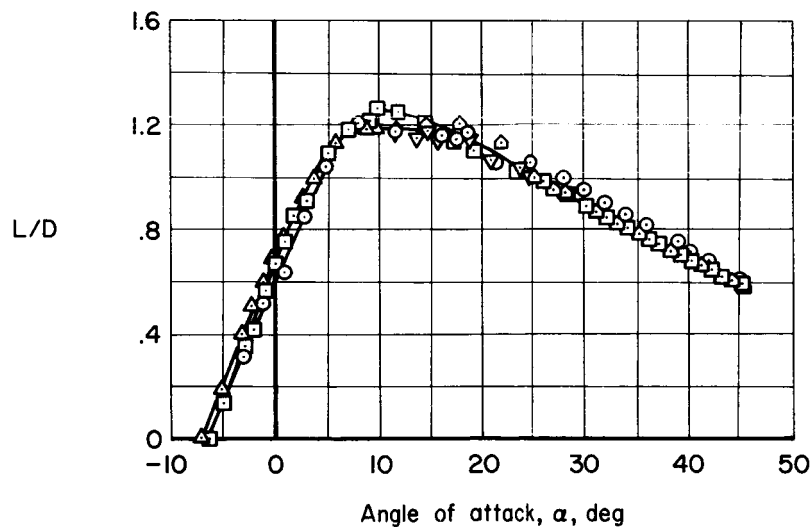
Figure 8.- Effects of Mach number on the longitudinal aerodynamic characteristics;  $25^\circ$  rudder flare,  $\delta_p = 35^\circ$ , air.



(a) Pitching-moment coefficient.

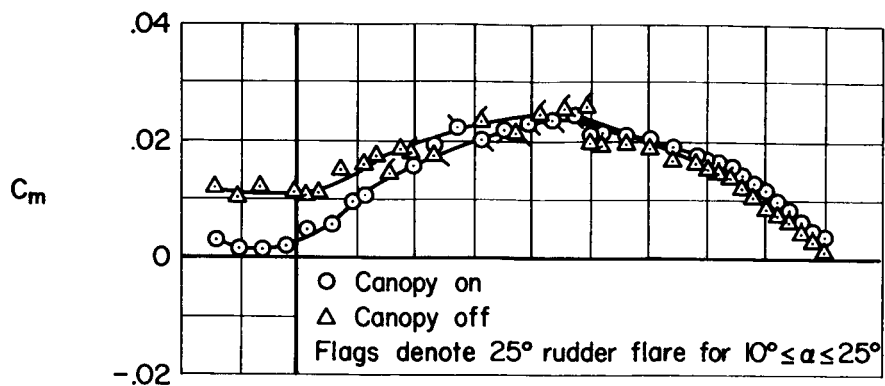


(b) Lift coefficient.

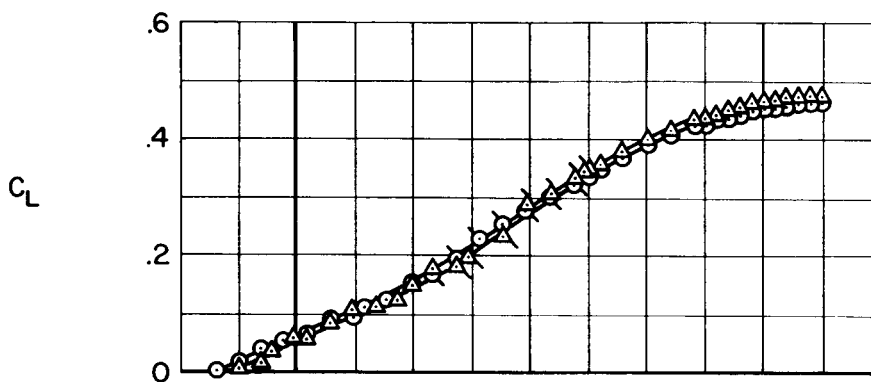


(c) Lift-drag ratio.

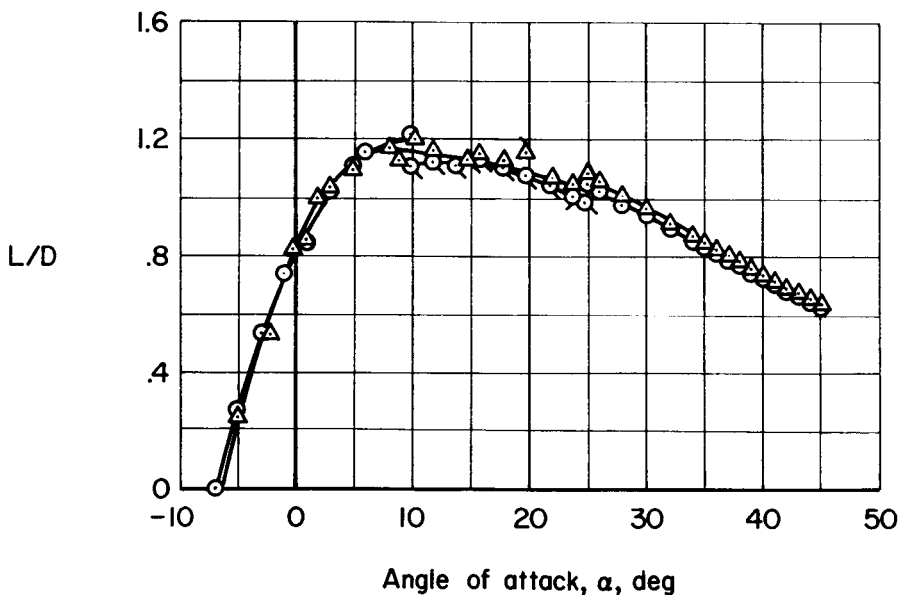
Figure 9.- Effects of pitch-flap deflection on longitudinal aerodynamic characteristics; 25° rudder flare,  $M = 7.4$ , air.



(a) Pitching-moment coefficient.

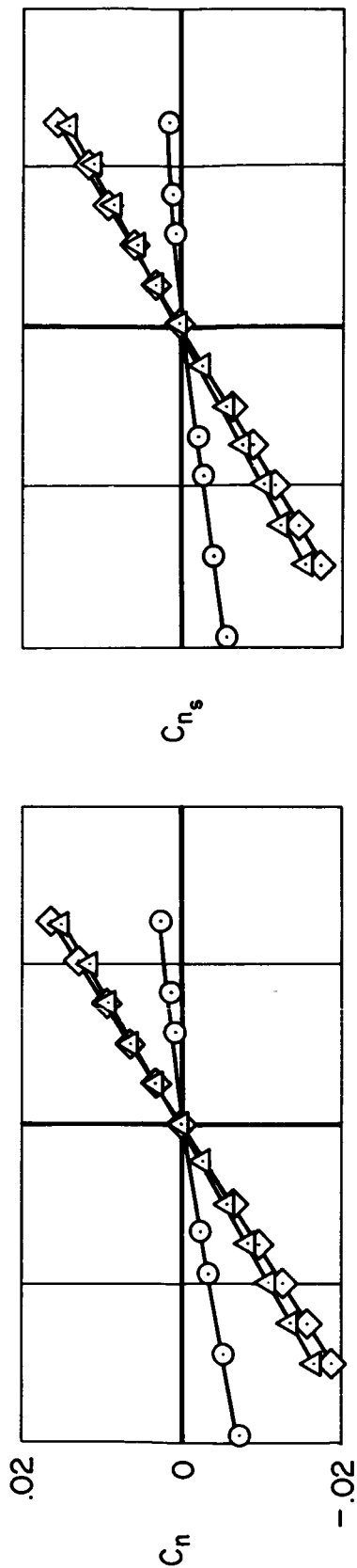


(b) Lift coefficient.

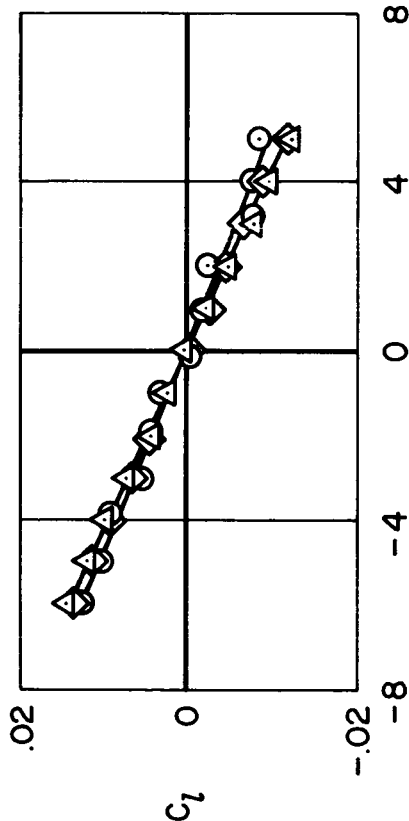


(c) Lift-drag ratio.

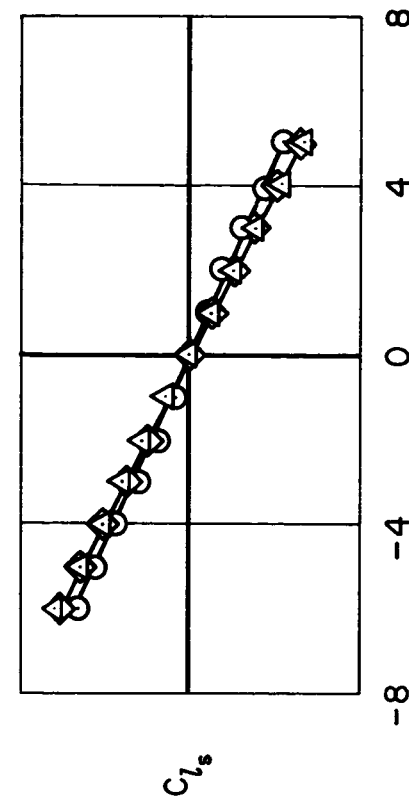
Figure 10.- Effects of adding the canopy on the longitudinal aerodynamic characteristics;  $M = 7.4$ , air.



- Body and fins
- △ Body and fins + 25° rudder flare
- ◇ Body and fins + 25° rudder flare + anhedral tails

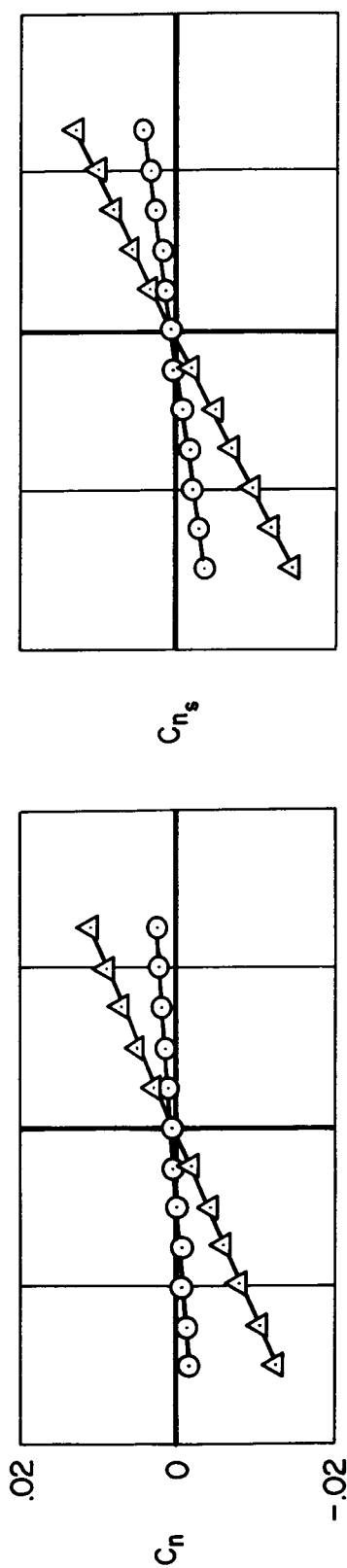


(a) Body axes.

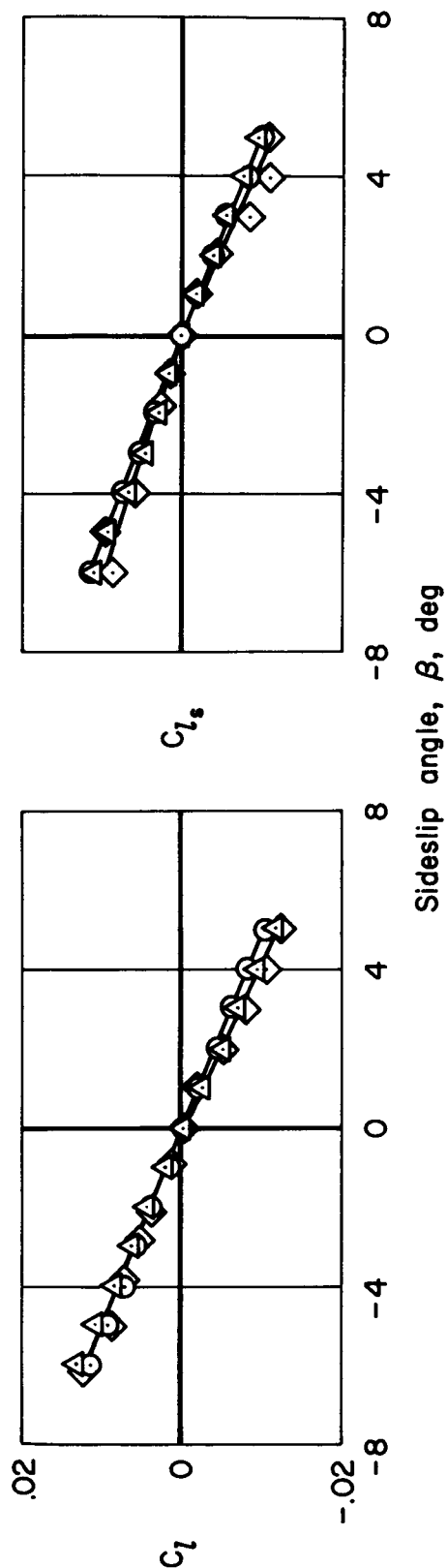


(b) Stability axes.

Figure 11.- Lateral-directional moment characteristics;  $\alpha = 10^\circ$ ,  $M = 5.2$ , air.



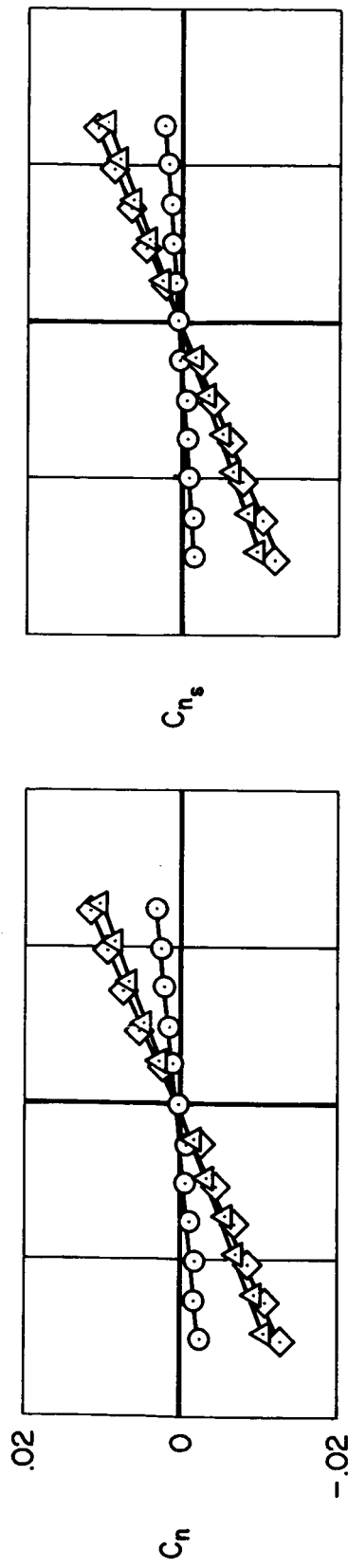
- Body and fins, with and without canopy
- △ Body and fins + 25° rudder flare
- ◇ Body and fins + 25° rudder flare + anhedral tails



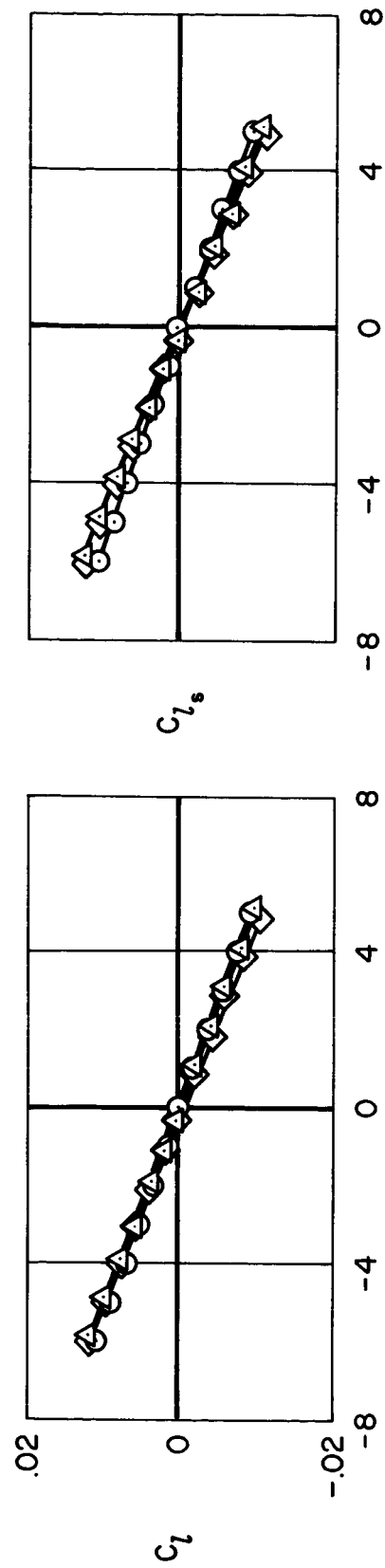
(a) Body axes.

(b) Stability axes.

Figure 12.- Lateral-directional moment characteristics;  $\alpha = 10^\circ$ ,  $M = 7.4$ , air.



- Body and fins
- △ Body and fins + 25° rudder flare
- ◇ Body and fins + 25° rudder flare + anhedral tails

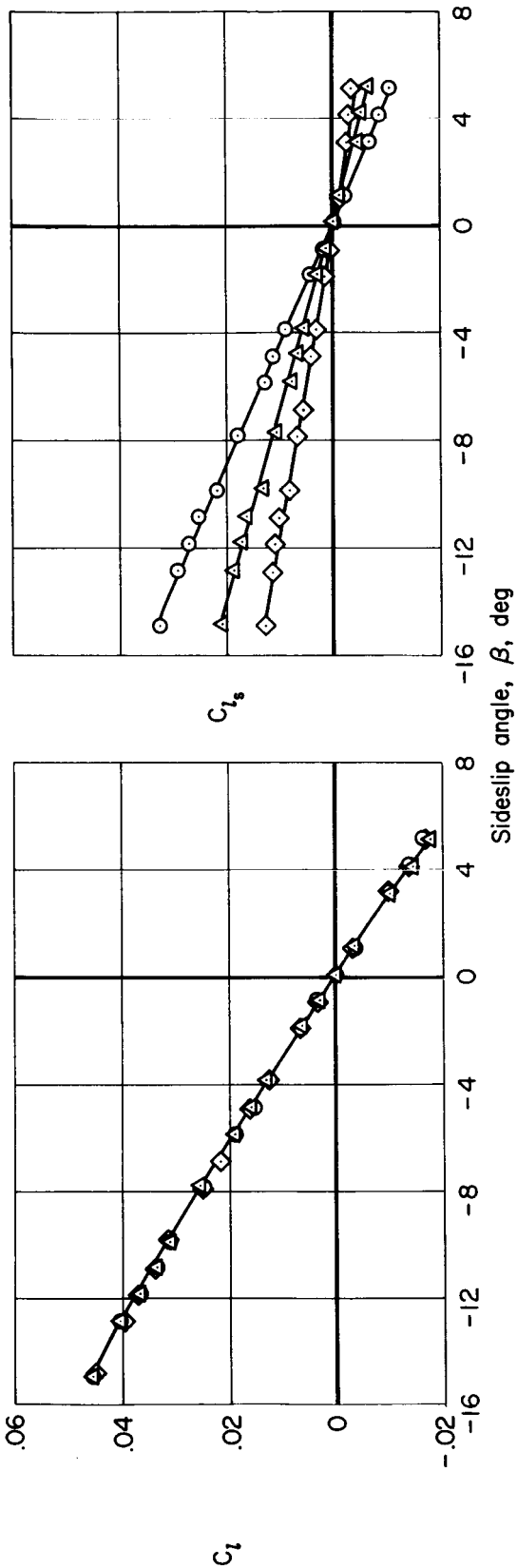
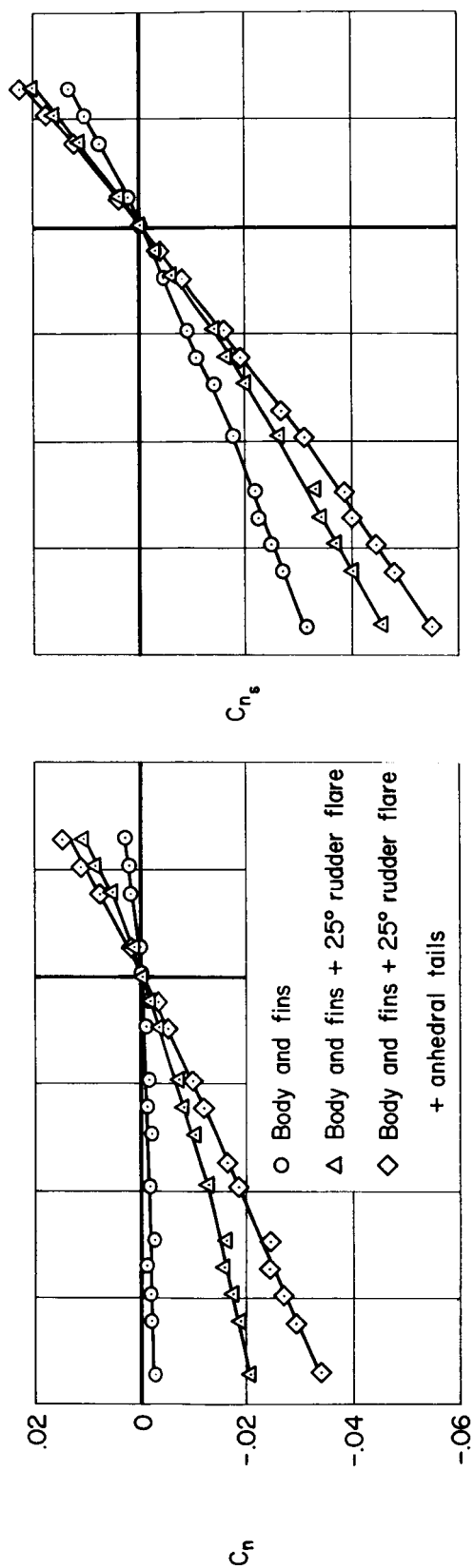


Sideslip angle,  $\beta$ , deg

(b) Stability axes.

(a) Body axes.

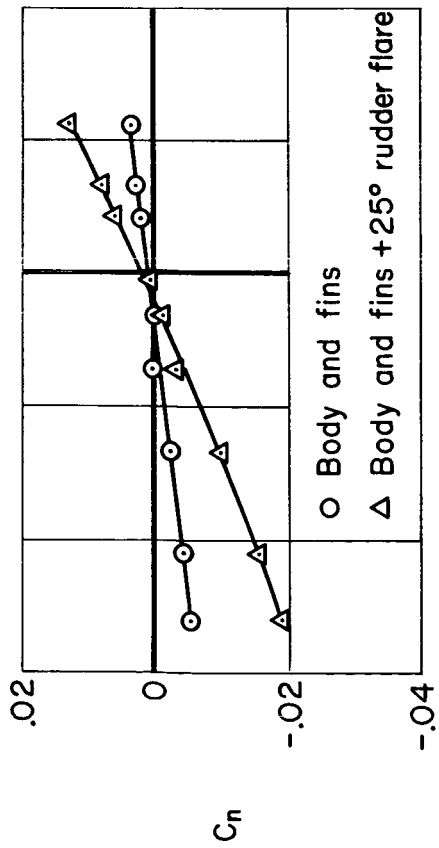
Figure 13.- Lateral-directional moment characteristics;  $\alpha = 10^\circ$ ,  $M = 10.4$ , air.



(a) Body axes.

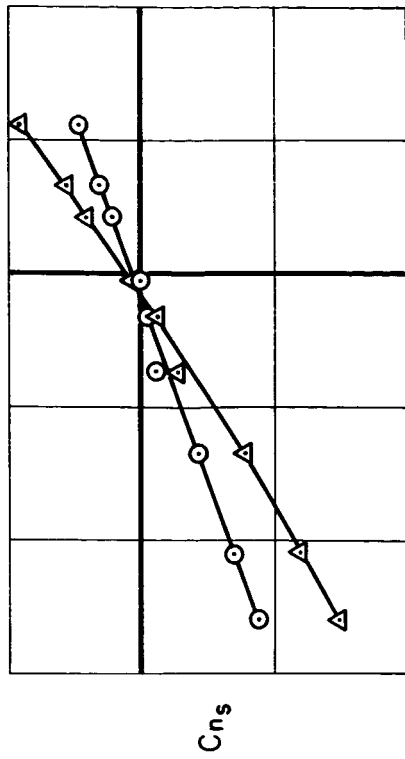
(b) Stability axes.

Figure 14.- Lateral-directional moment characteristics;  $\alpha = 40^\circ$ ,  $M = 7.4$ , air.

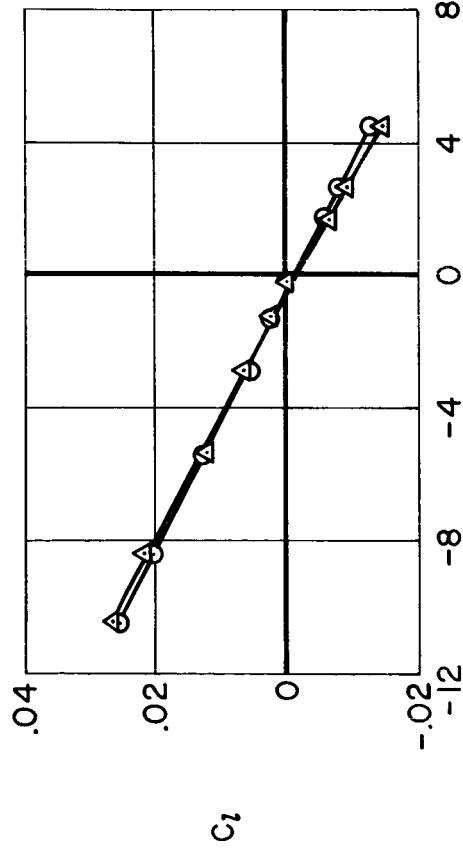


○ Body and fins  
 △ Body and fins + 25° rudder flare

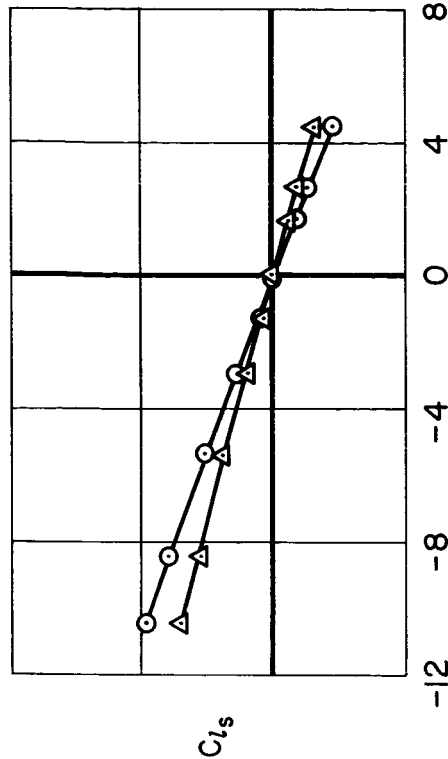
(a) Body axes.



(b) Stability axes.

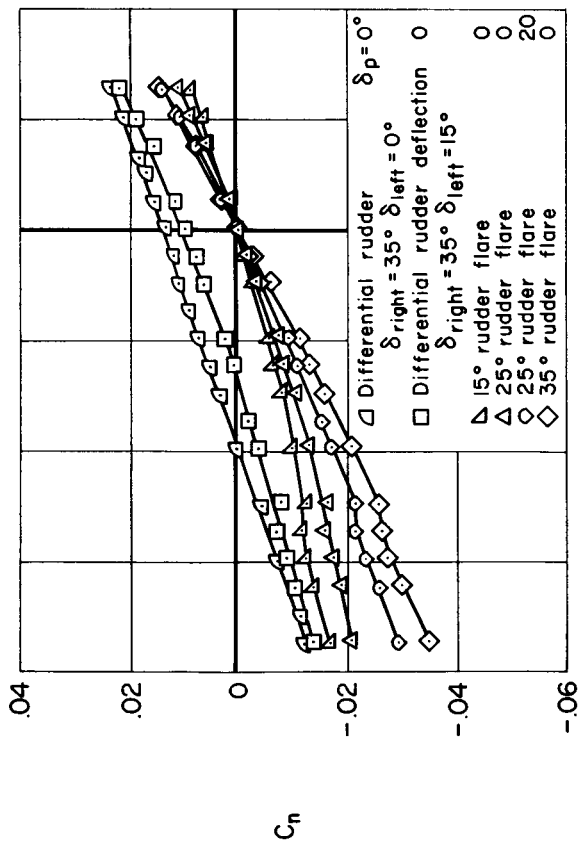


(a) Body axes.

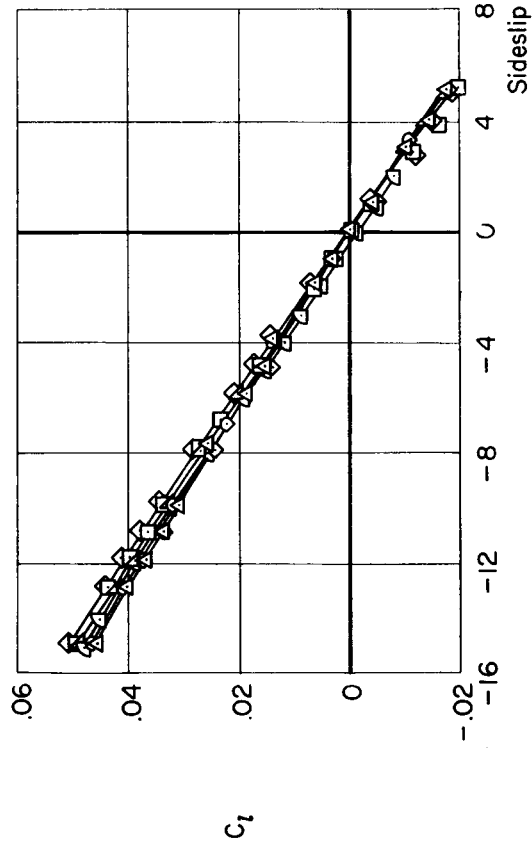


(b) Stability axes.

Figure 15.- Lateral-directional moment characteristics;  $\alpha = 30^\circ$ ,  $M = 10.4$ , air.

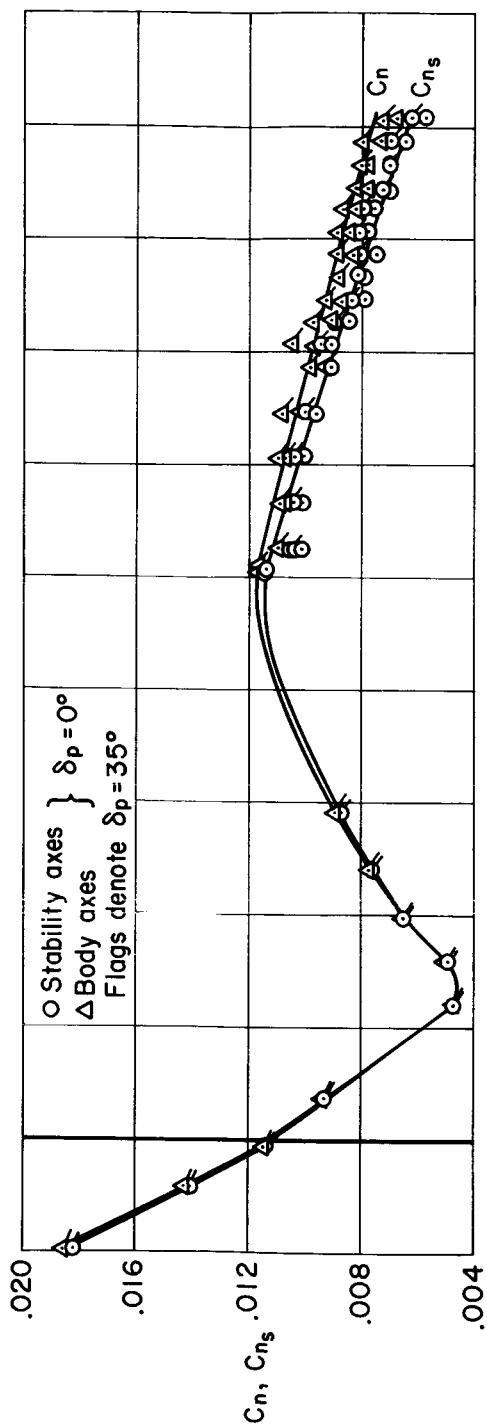


(a) Body axes.

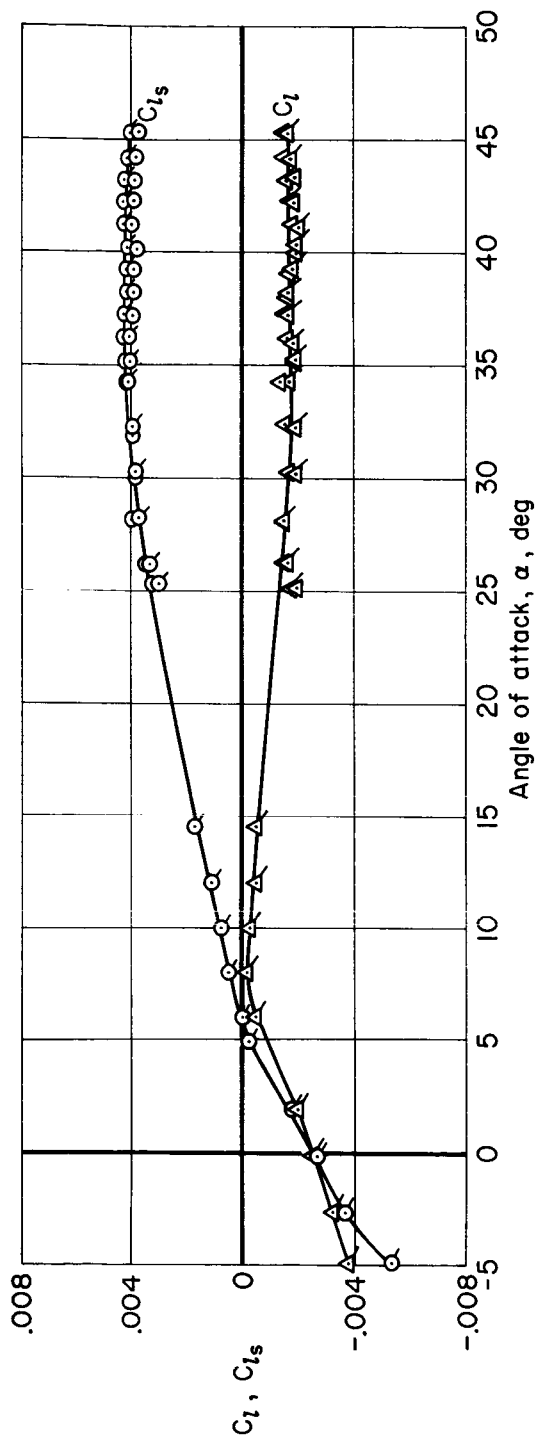


(b) Stability axes.

Figure 16.- Effects of rudder deflection on lateral-directional moment characteristics;  $\alpha = 40^\circ$ ,  $M = 7.4$ , air.

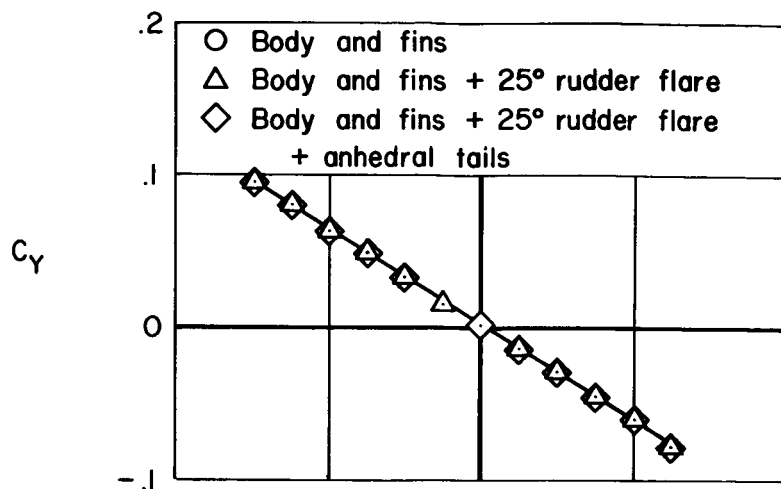


(a) Yawing-moment coefficient.

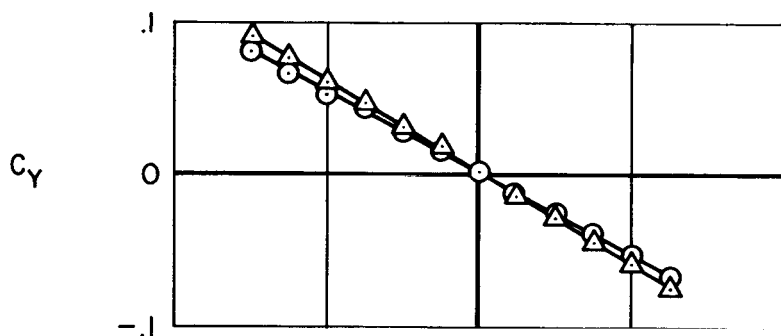


(b) Rolling-moment coefficient.

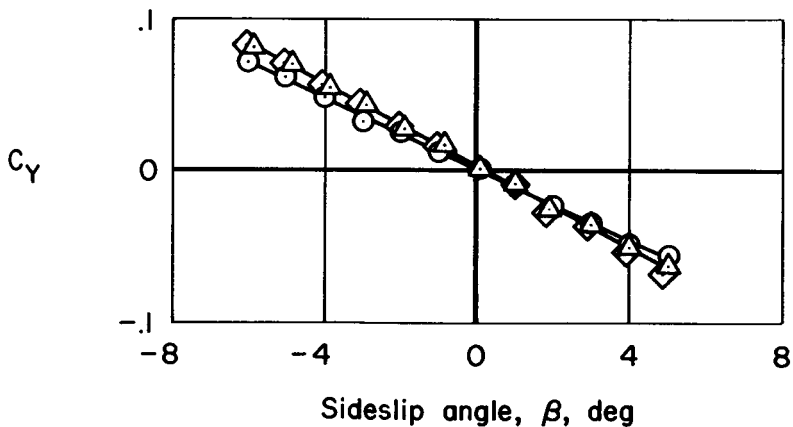
Figure 17.- Variation of rudder control characteristics with angle of attack;  
 $\delta_{\text{right}} = 35^\circ$ ,  $\delta_{\text{left}} = 15^\circ$ ,  $\beta = 0^\circ$ ,  $M = 7.4$ , air.



(a)  $M = 5.2$



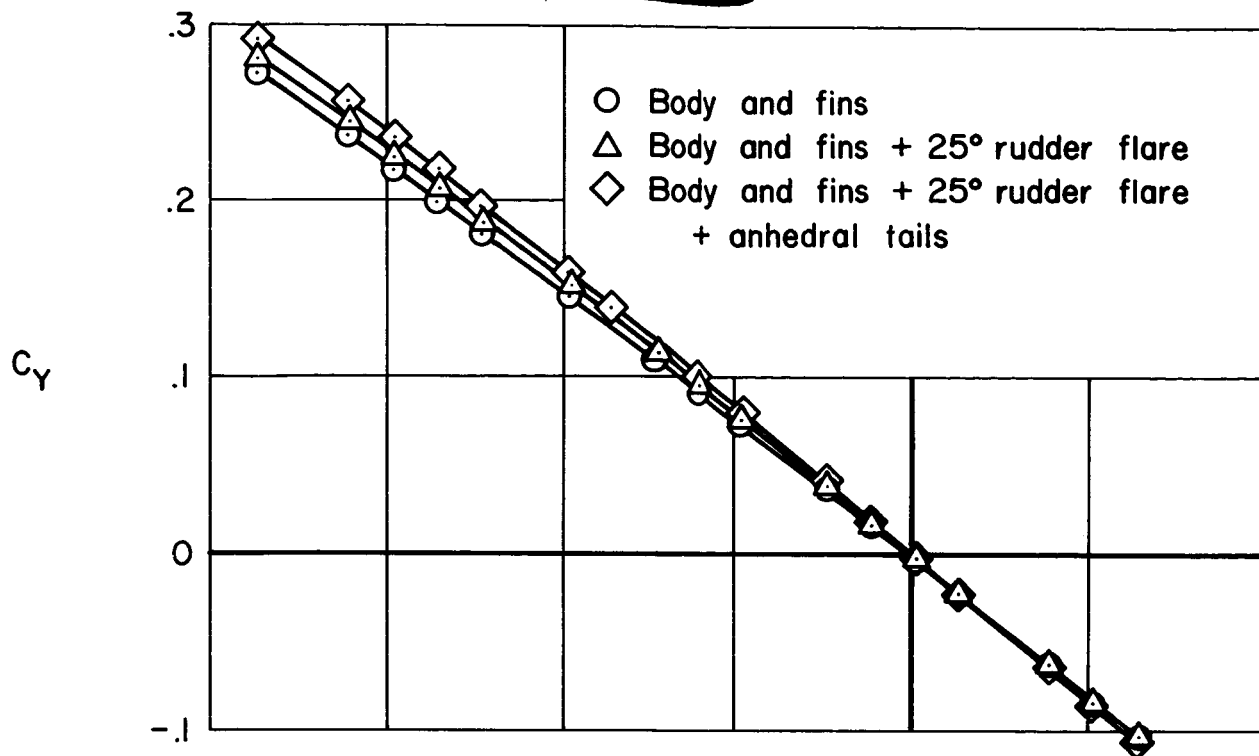
(b)  $M = 7.4$



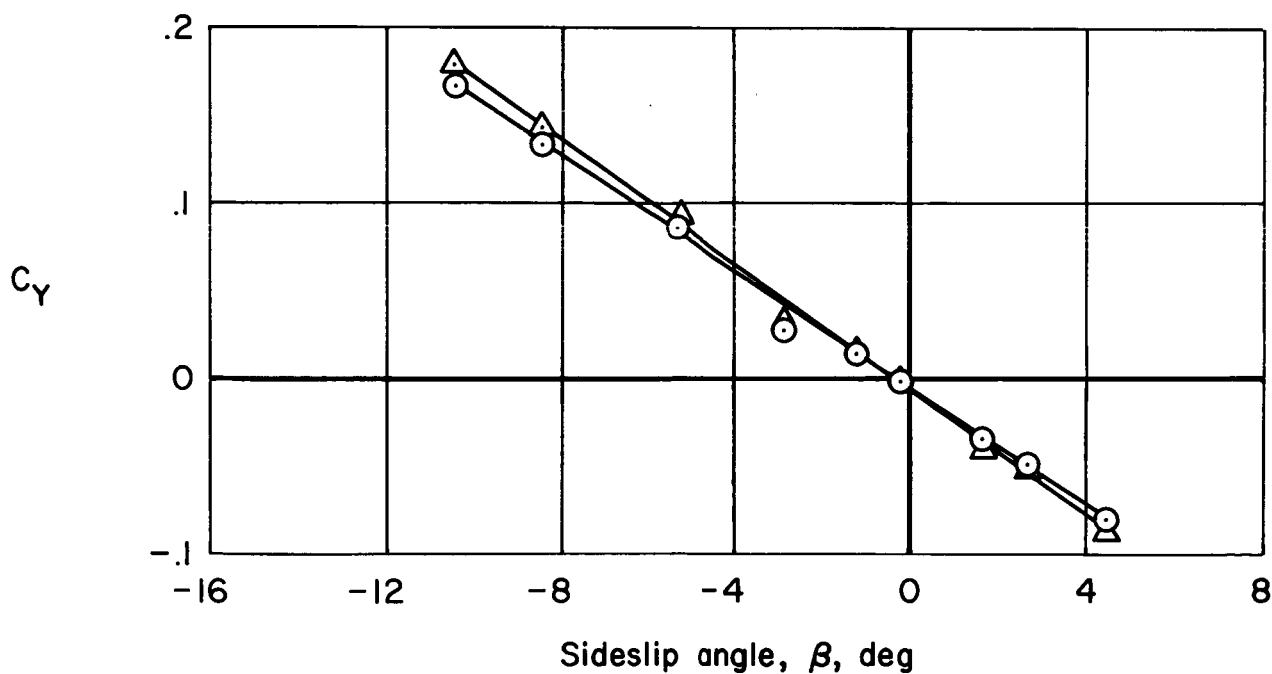
(c)  $M = 10.4$

Figure 18.- Variation of side-force coefficient with sideslip angle;  
 $\alpha = 10^\circ$ , air.

~~CONFIDENTIAL~~



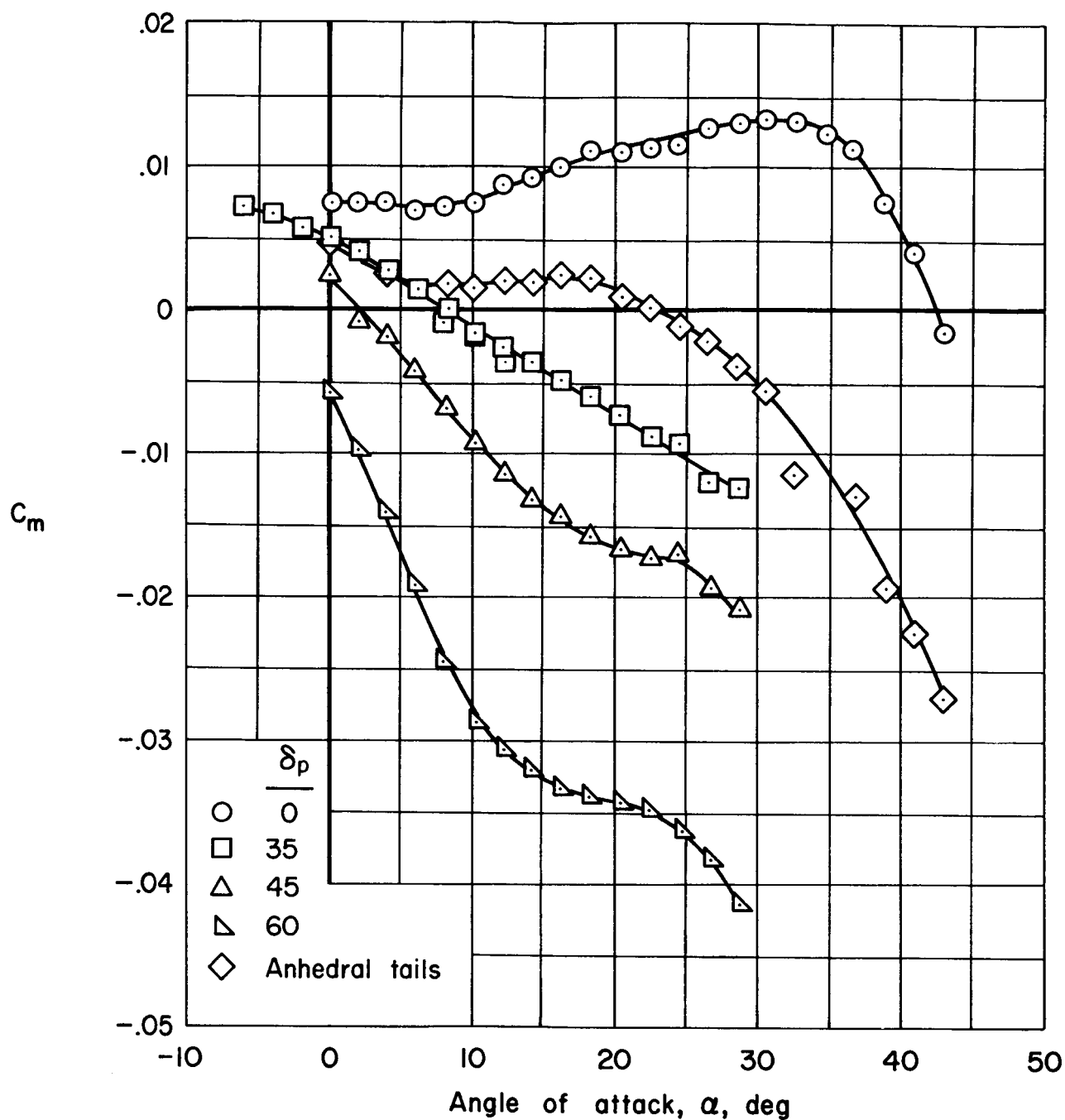
(a)  $M = 7.4$ ,  $\alpha = 40^\circ$ .



(b)  $M = 10.4$ ,  $\alpha = 30^\circ$ .

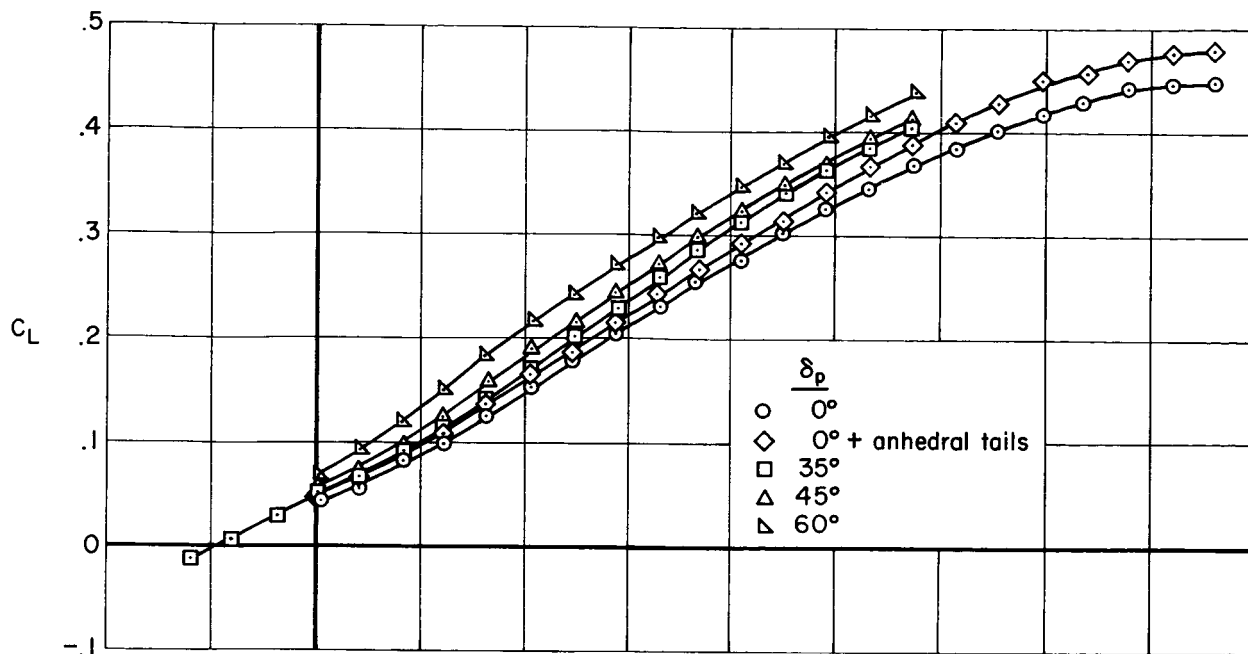
Figure 19.- Variation of side-force coefficient with sideslip angle:  
air.

~~CONFIDENTIAL~~

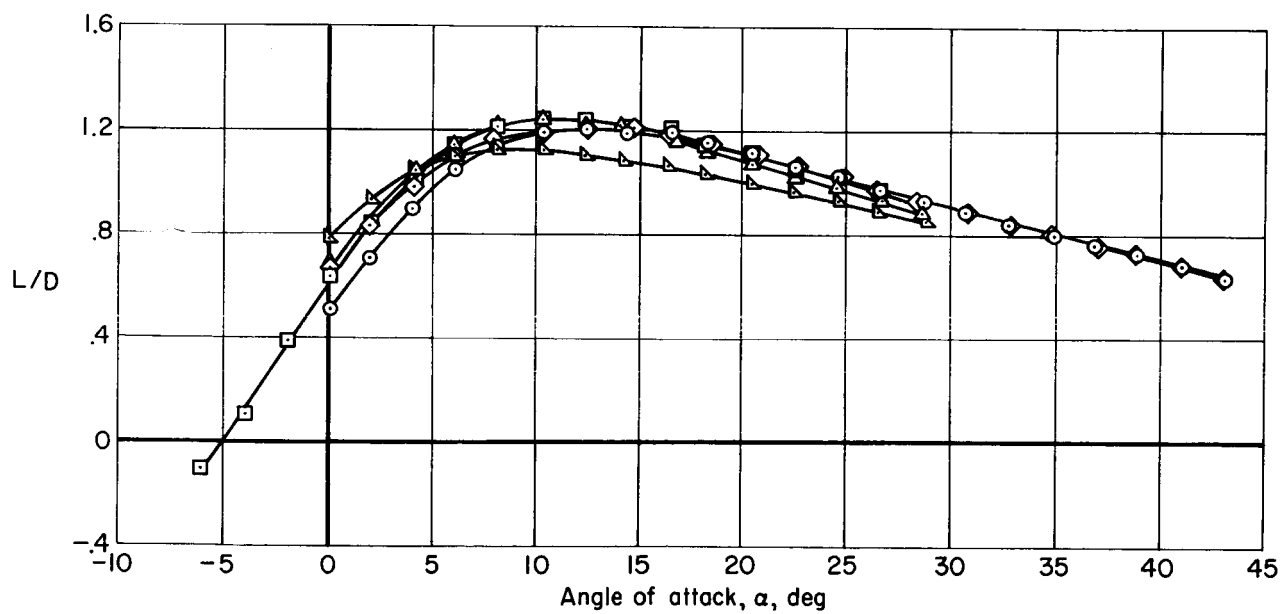


(a) Pitching-moment coefficient.

Figure 20.- Effects of pitch-flap deflection and of anhedral tails on the longitudinal aerodynamic characteristics;  $25^\circ$  rudder flare, canopy on,  $M = 10.4$ , helium.

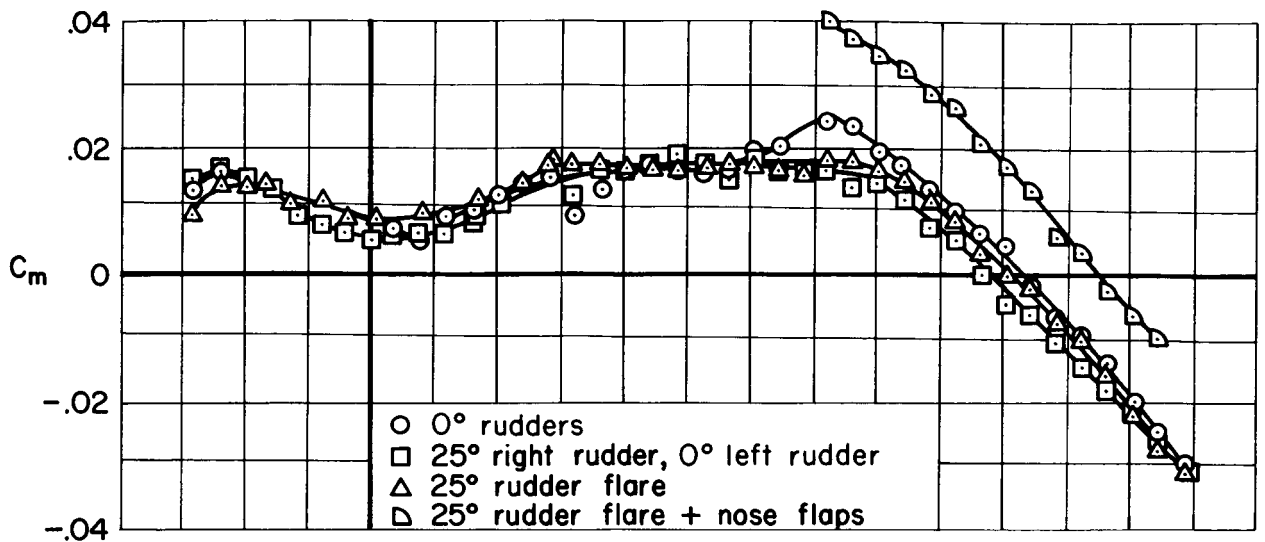


(b) Lift coefficient.

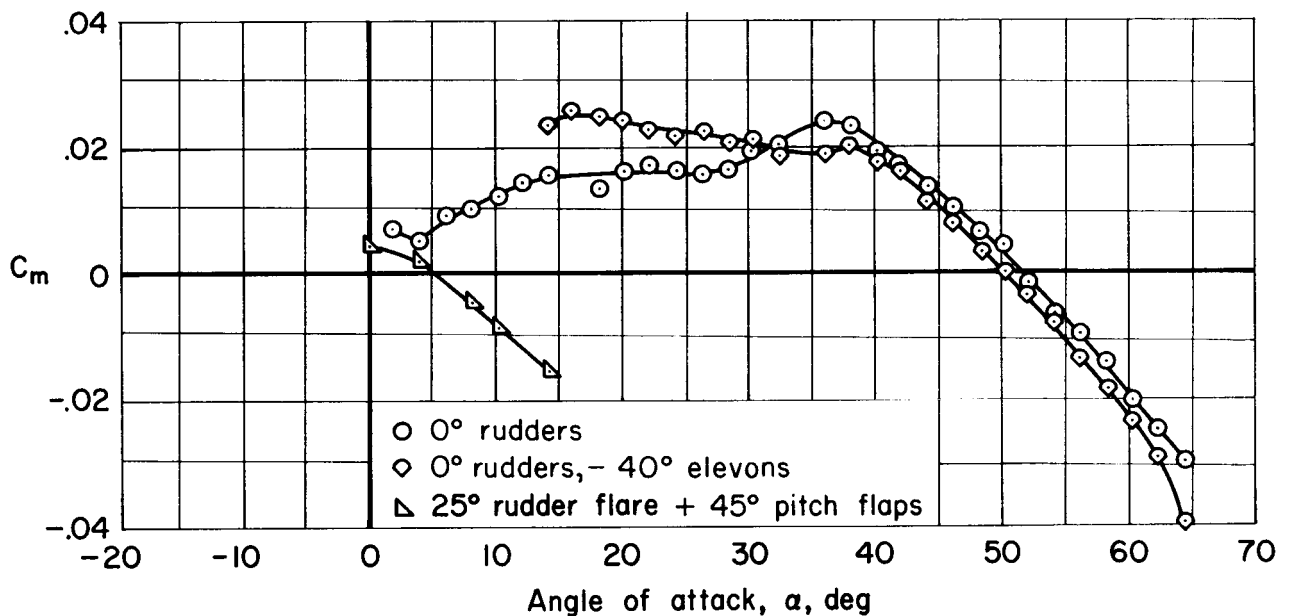


(c) Lift-drag ratio.

Figure 20.- Concluded.

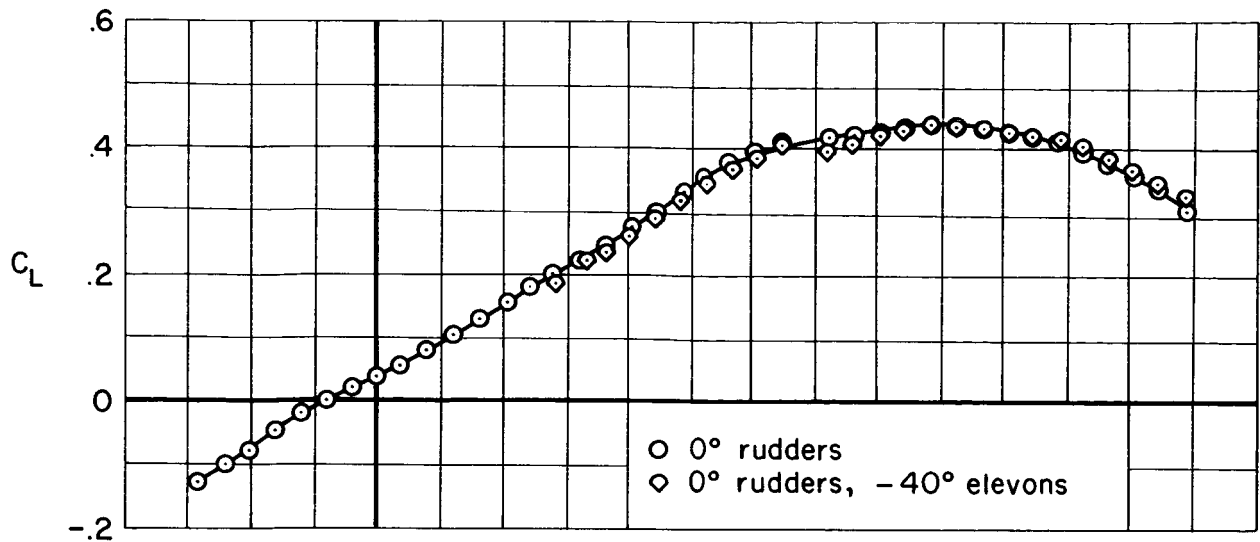


(a) Effects of rudder deflection and of nose flaps on pitching-moment coefficient.

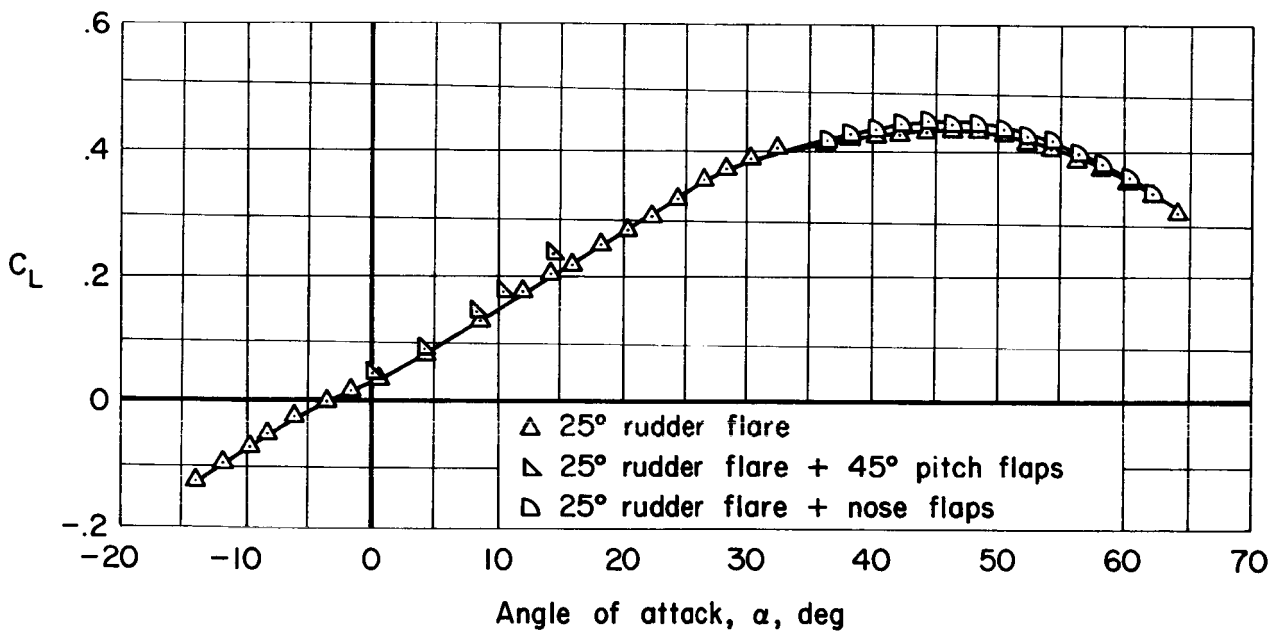


(b) Effects of  $-40^\circ$  elevons and of  $45^\circ$  pitch flaps on pitching-moment coefficient.

Figure 21.- Effects of various control arrangements on the longitudinal aerodynamic characteristics; canopy on,  $M = 17.4$ , helium.

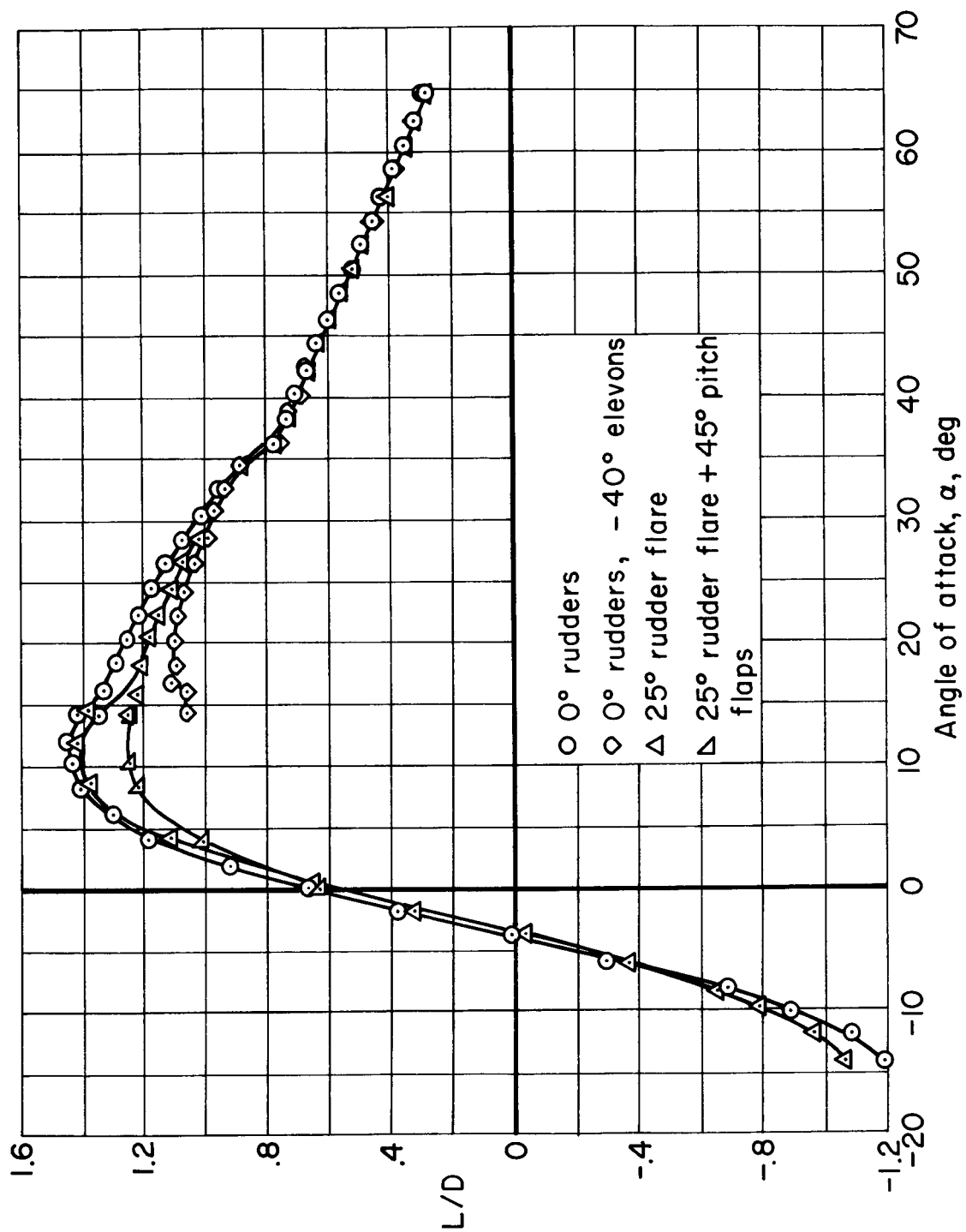


(c) Effect of -40° elevons on lift coefficient.



(d) Effects of pitch flaps and of nose flaps on lift coefficient.

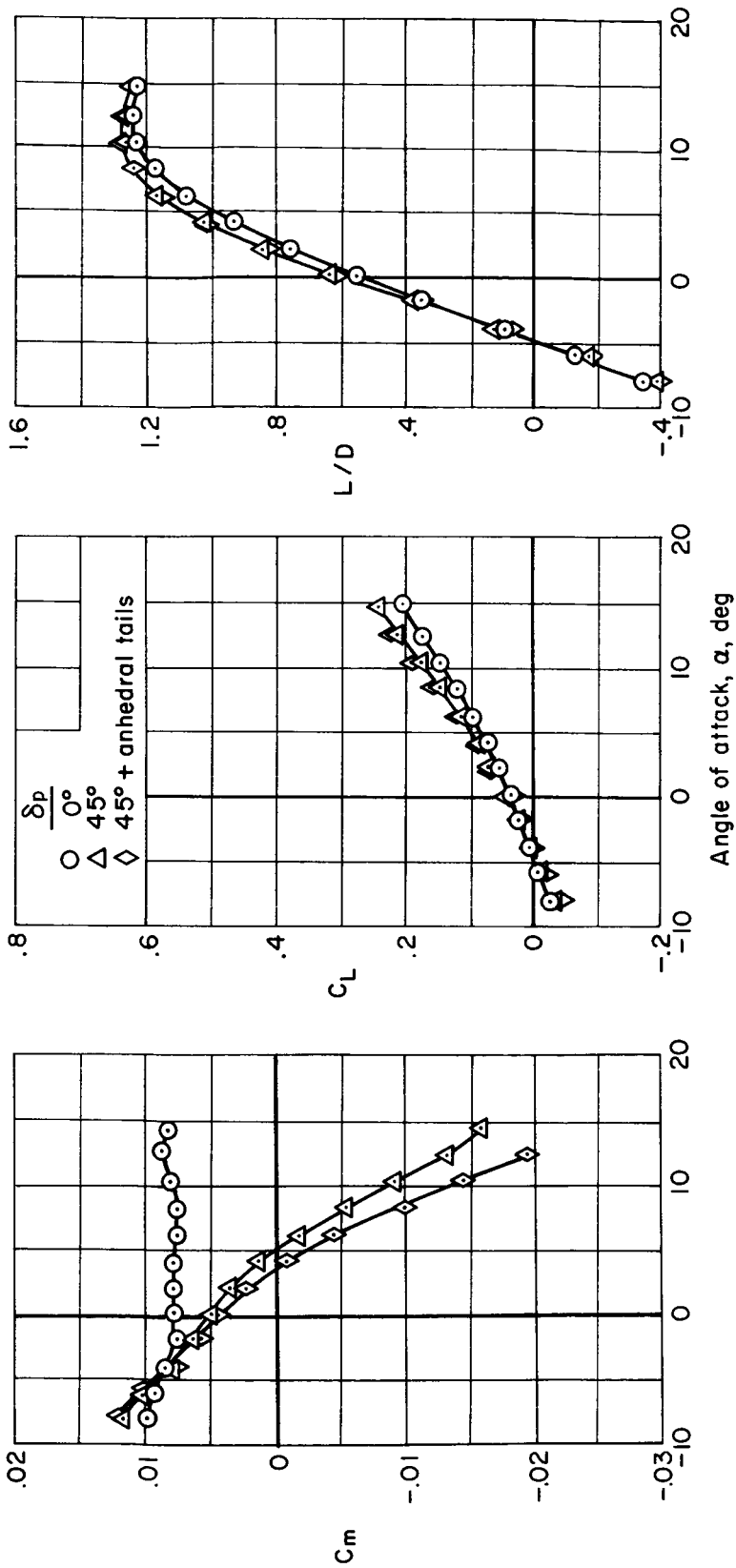
Figure 21.- Continued.



(e) Lift-drag ratio.

Figure 21.- Concluded.

CONFIDENTIAL



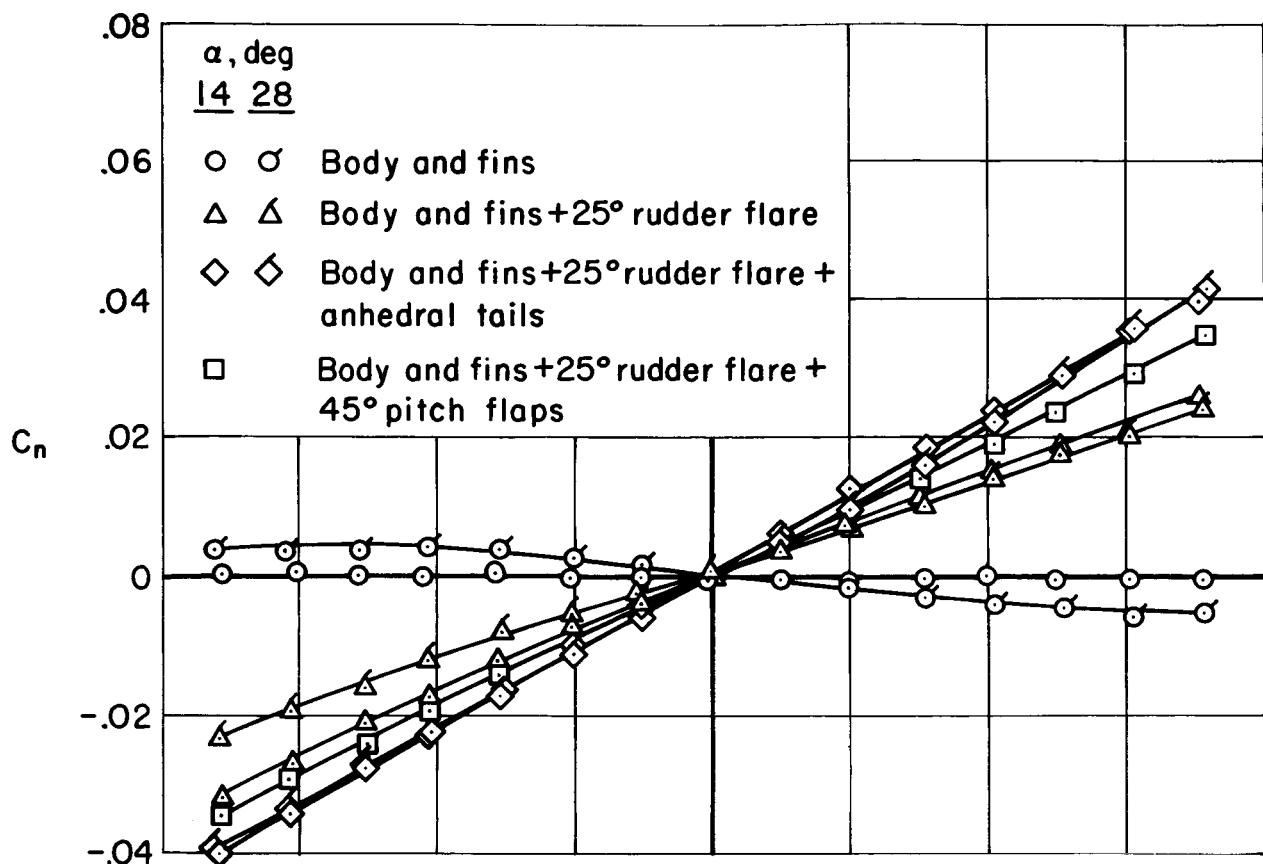
(a) Pitching-moment coefficient.

(b) Lift coefficient.

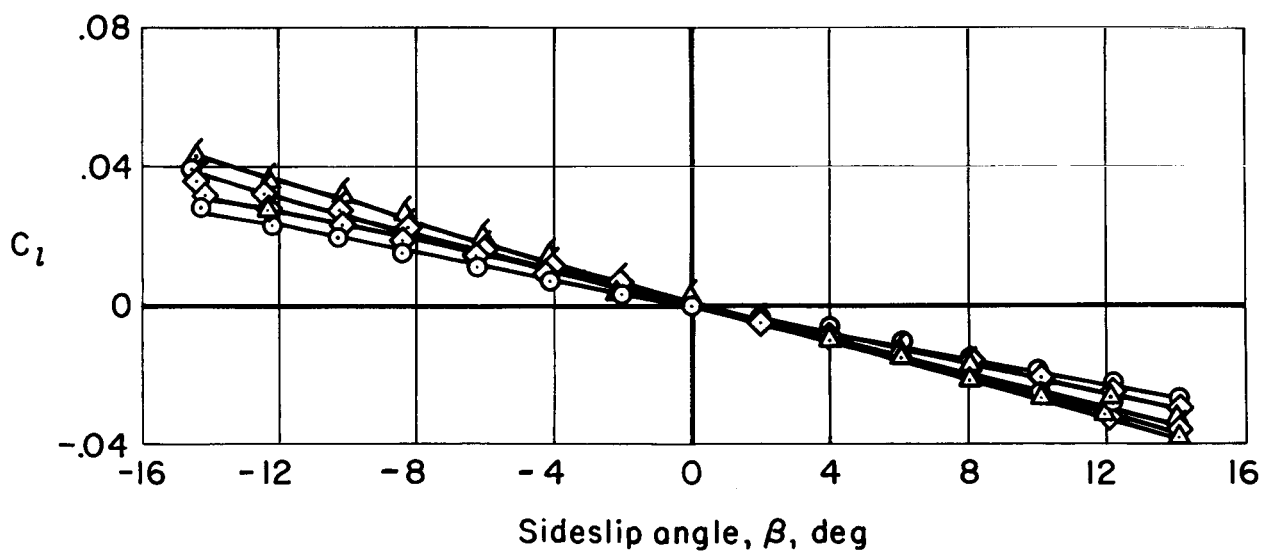
(c) Lift-drag ratio.

Figure 22.- Effects of pitch flaps and of anhedral tails on longitudinal aerodynamic characteristics; canopy on,  $25^\circ$  rudder flare,  $M = 21.0$ , helium.

CONFIDENTIAL

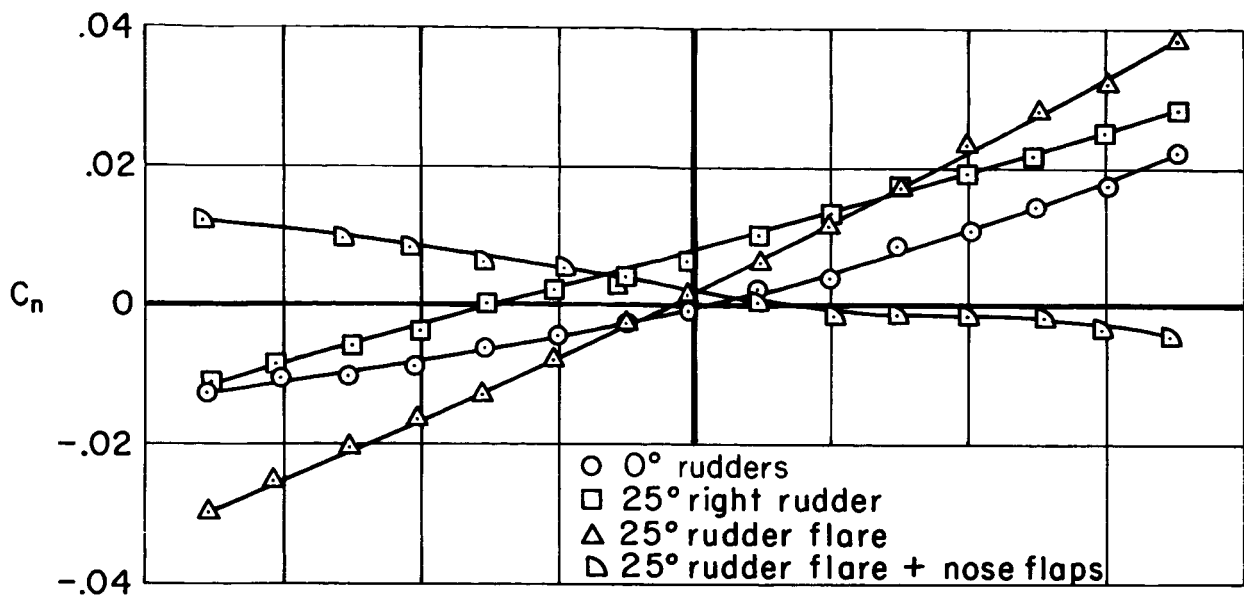


(a) Yawing-moment coefficient.

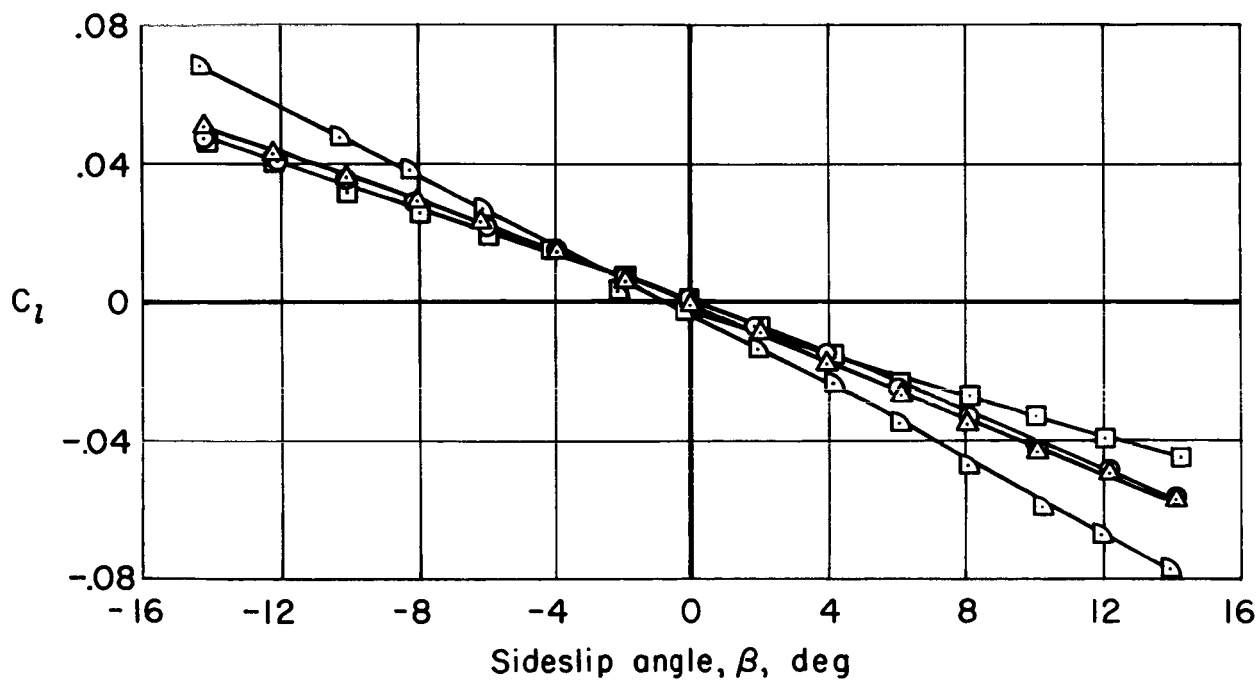


(b) Rolling-moment coefficient.

Figure 23.- Lateral-directional moment characteristics; canopy on,  $M = 10.4$ , helium.

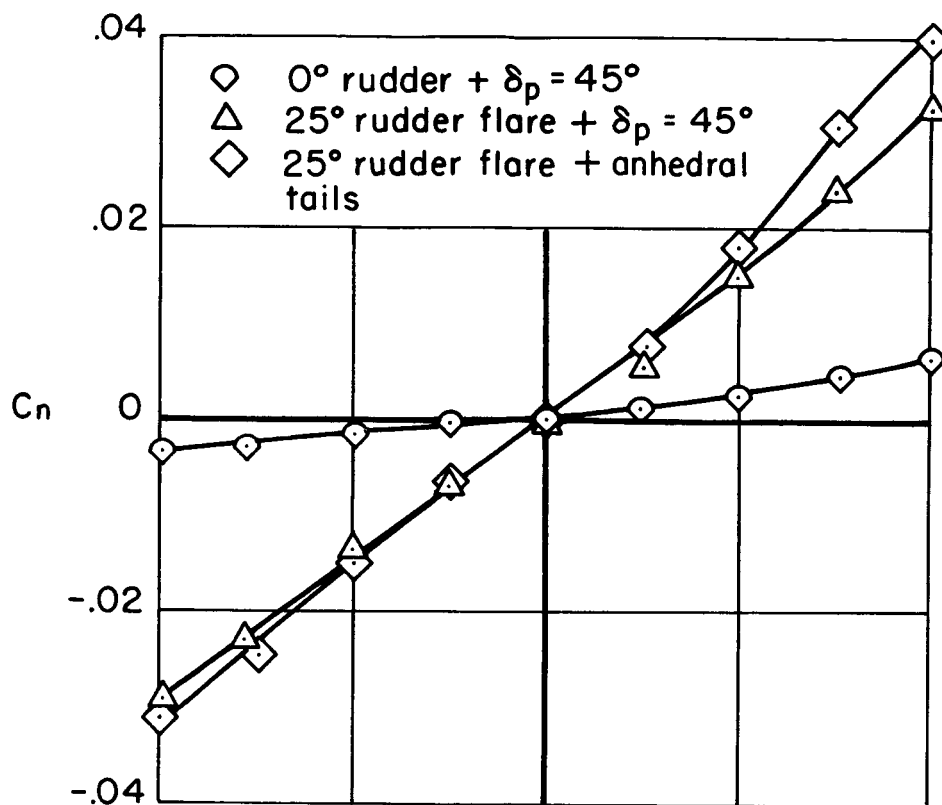


(a) Yawing-moment coefficient.

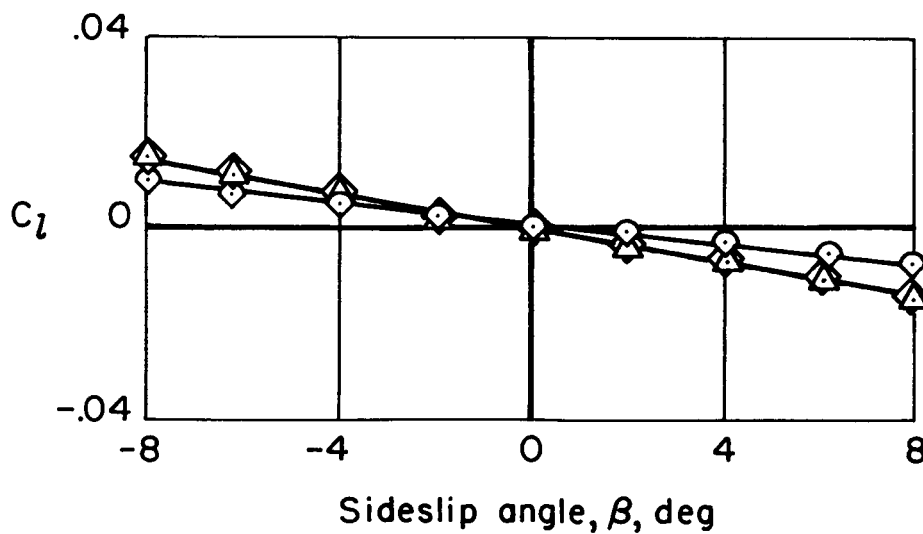


(b) Rolling-moment coefficient.

Figure 24.- Lateral-directional moment characteristics; canopy on,  $M = 17.3$ , helium,  $\alpha = 36^\circ$ .

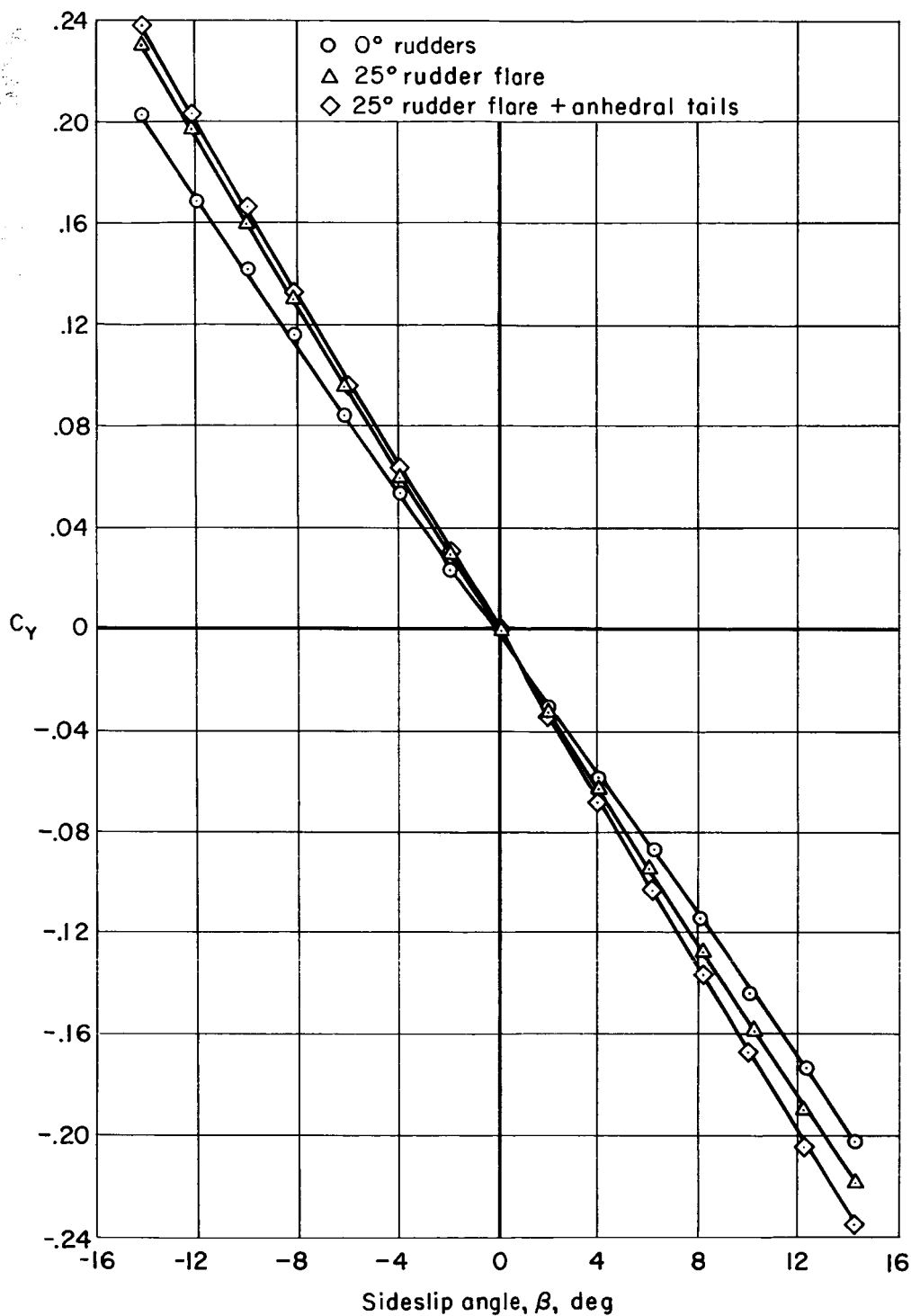


(a) Yawing-moment coefficient.



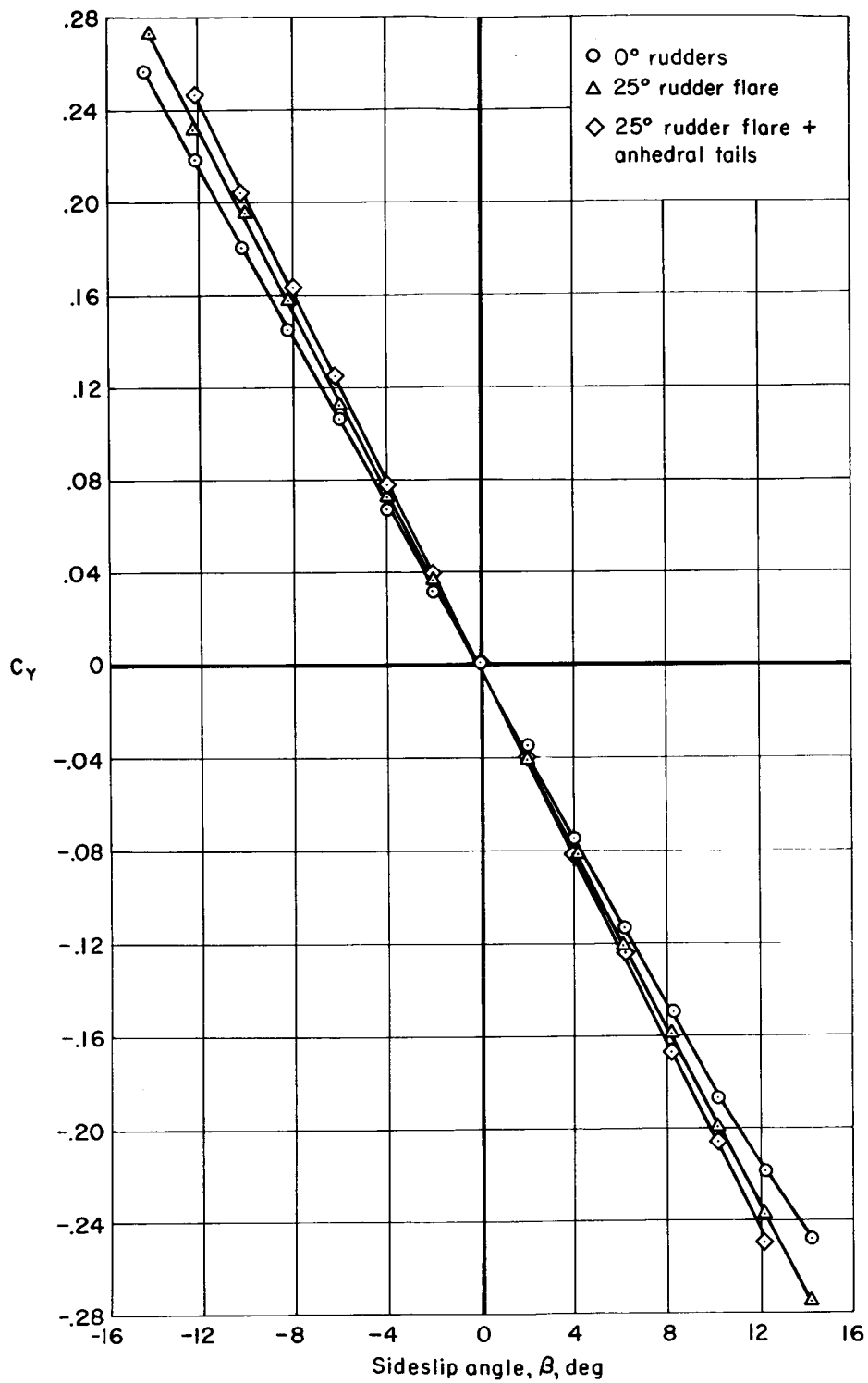
(b) Rolling-moment coefficient.

Figure 25.- Lateral-directional moment characteristics; canopy on,  $M = 21.0$ , helium,  $\alpha = 0^\circ$ .



(a)  $\alpha = 14^\circ$

Figure 26.- Variation of side-force coefficient with sideslip angle; canopy on,  $M = 10.4$ , helium.



(b)  $\alpha = 28^\circ$

Figure 26.- Concluded.

CONFIDENTIAL

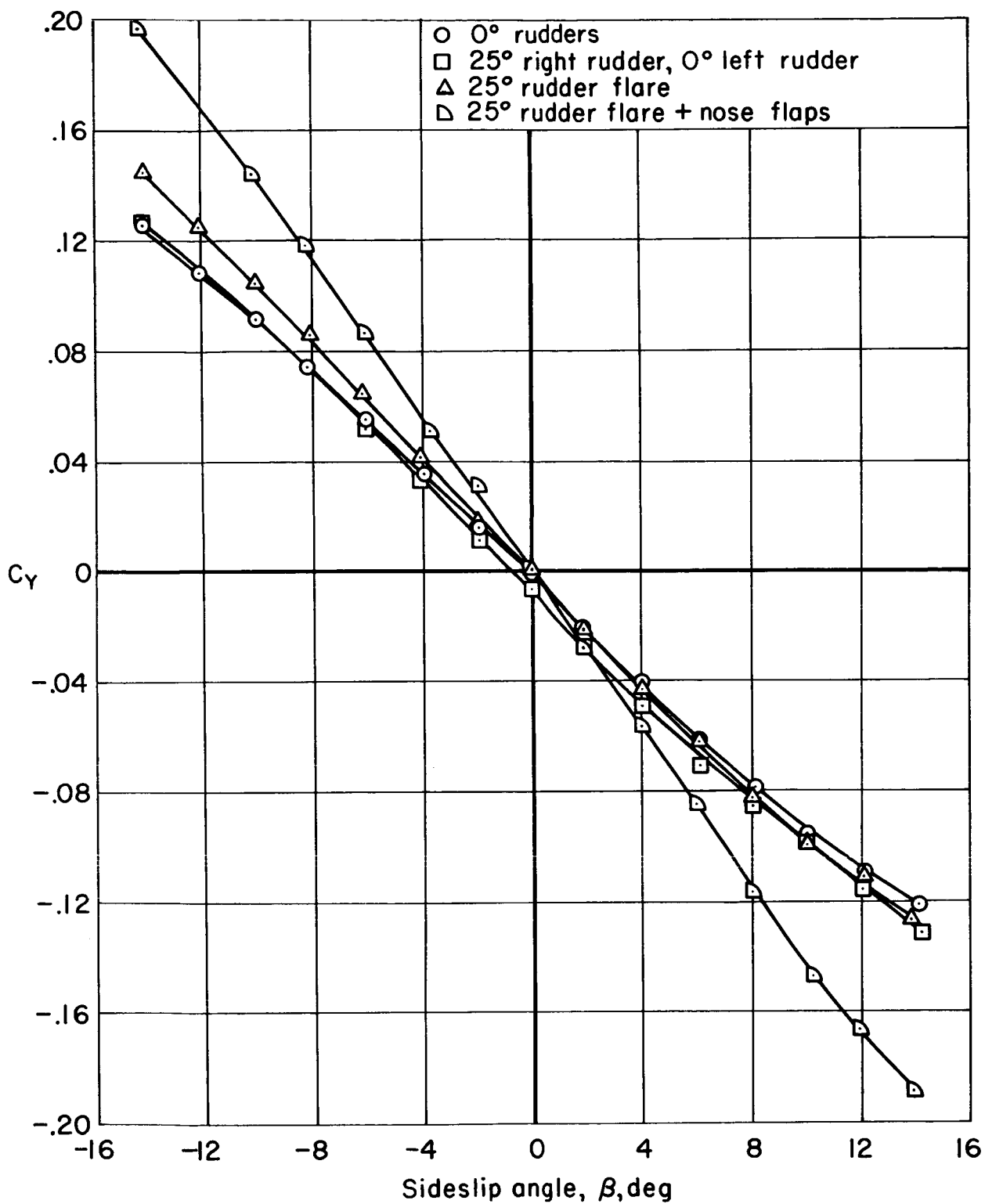


Figure 27.- Variation of side-force coefficient with sideslip angle; canopy on,  $\alpha = 36^\circ$ ,  $M = 17.3$ , helium.

CONFIDENTIAL

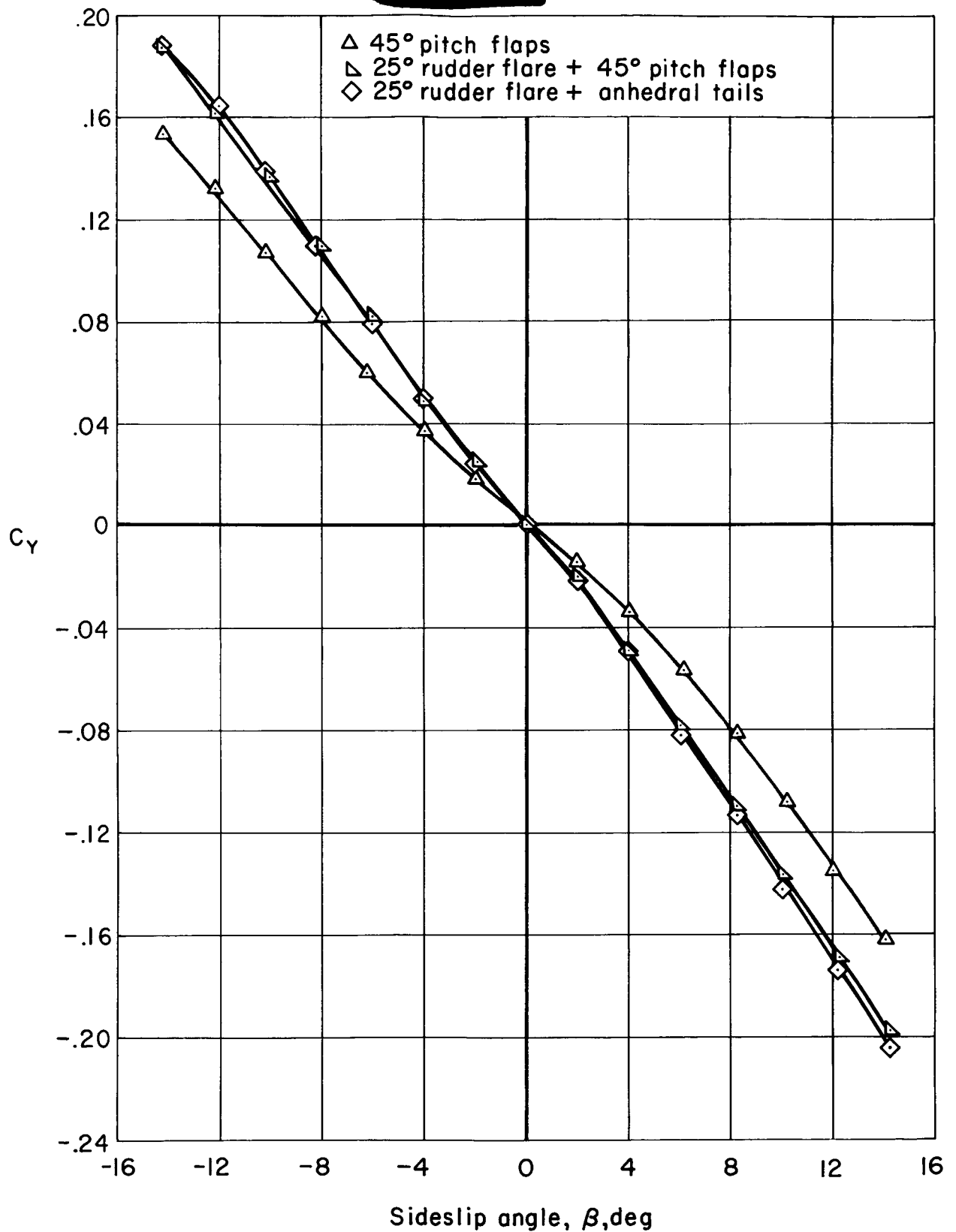
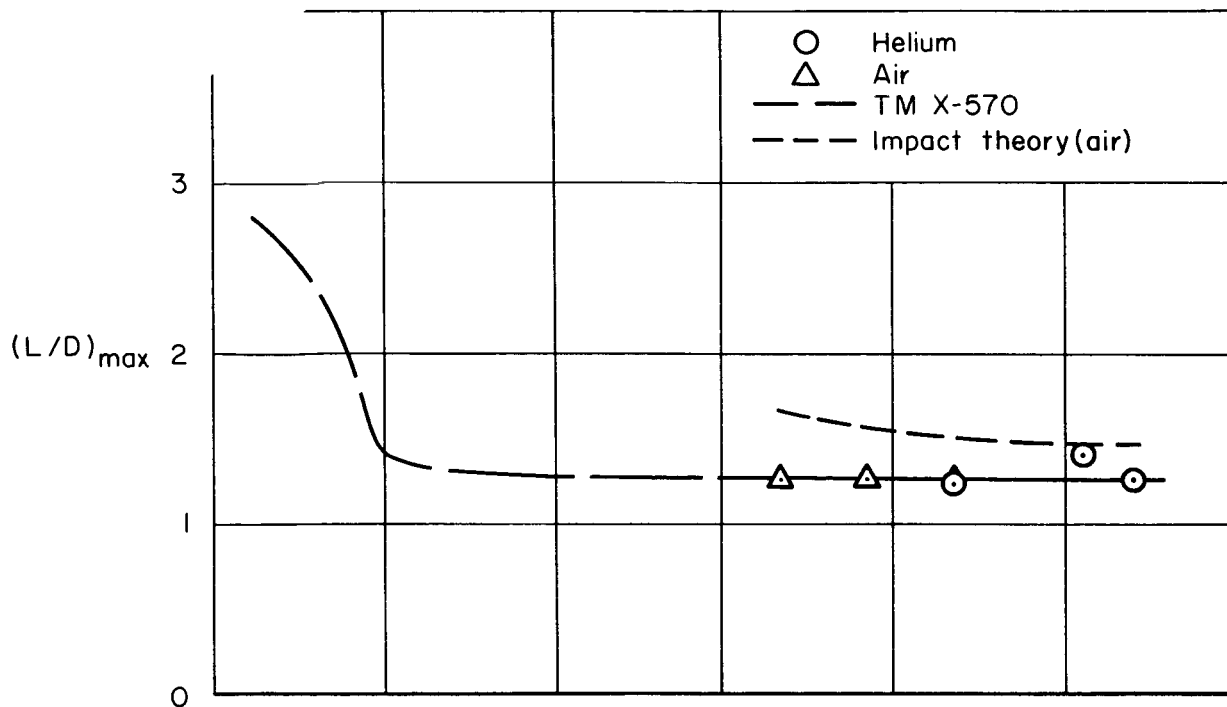
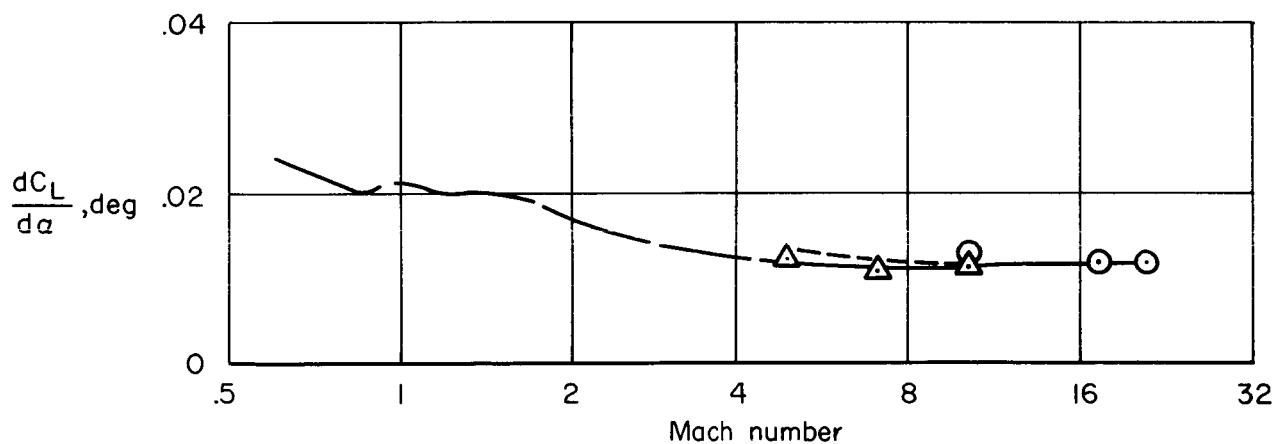


Figure 28.- Variation of side-force coefficient with sideslip angle; canopy on,  $\alpha = 0^\circ$ ,  $M = 21.0$ , helium.

~~CONFIDENTIAL~~



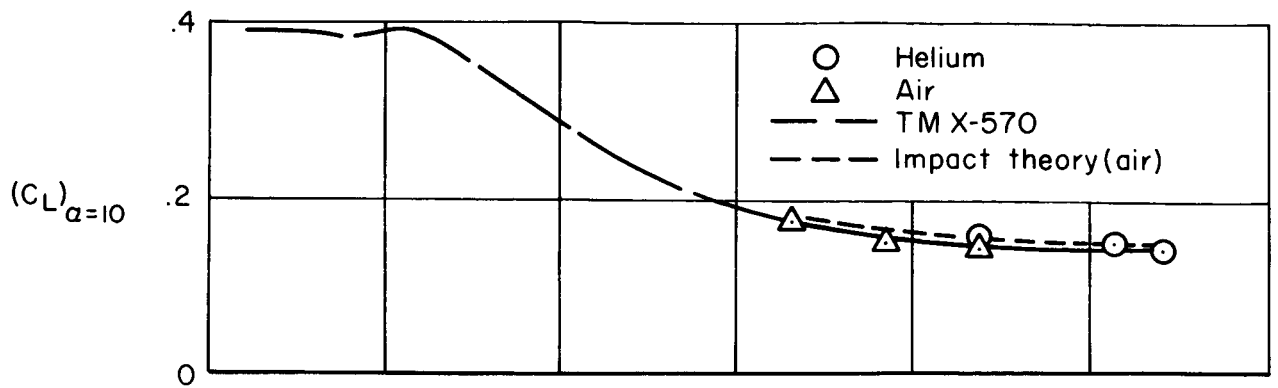
(a) Maximum lift-drag ratio.



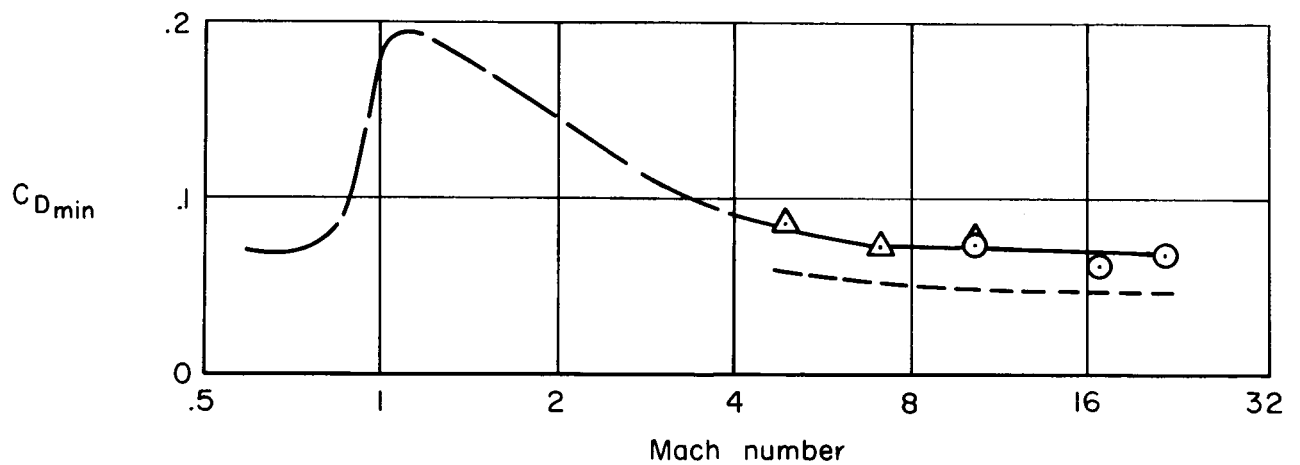
(b) Lift-curve slope;  $\alpha = 10^\circ$ .

Figure 29.- Summary of longitudinal aerodynamic parameters;  $25^\circ$  rudder flare for  $M \geq 5$ .

~~CONFIDENTIAL~~



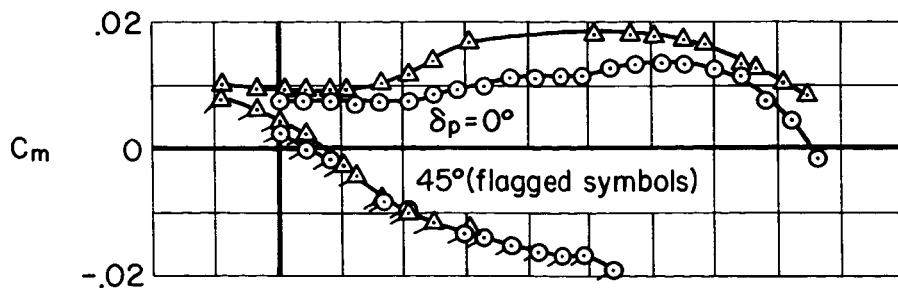
(c) Lift coefficient at  $\alpha = 10^\circ$ .



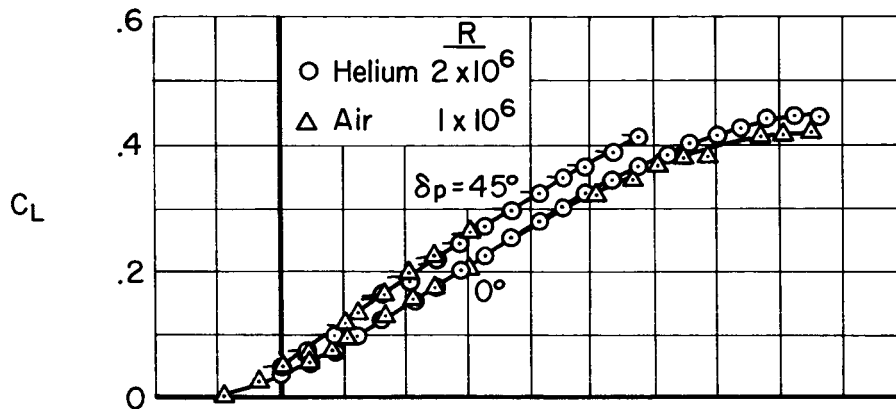
(d) Minimum-drag coefficient.

Figure 29.- Concluded.

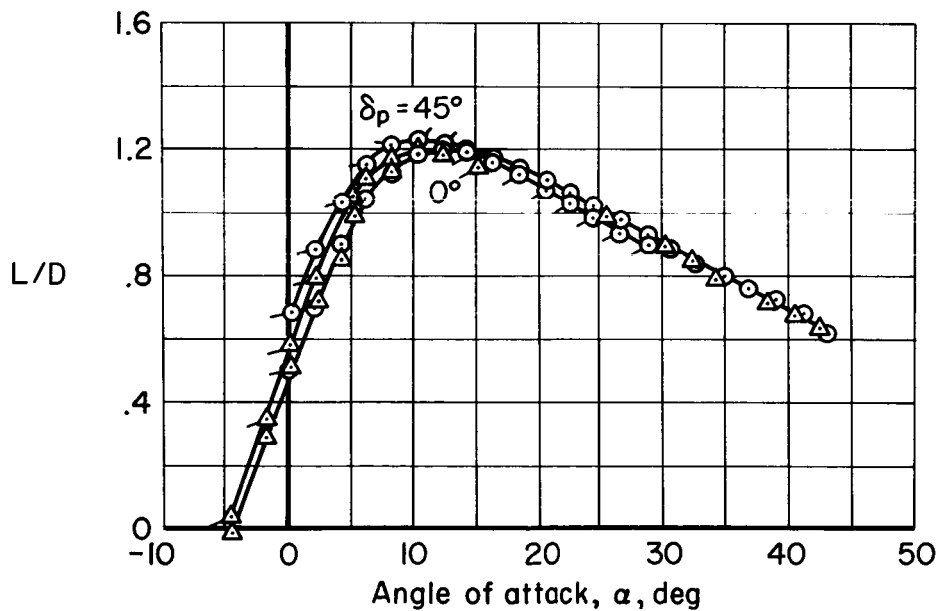
~~CONFIDENTIAL~~



(a) Pitching-moment coefficient.



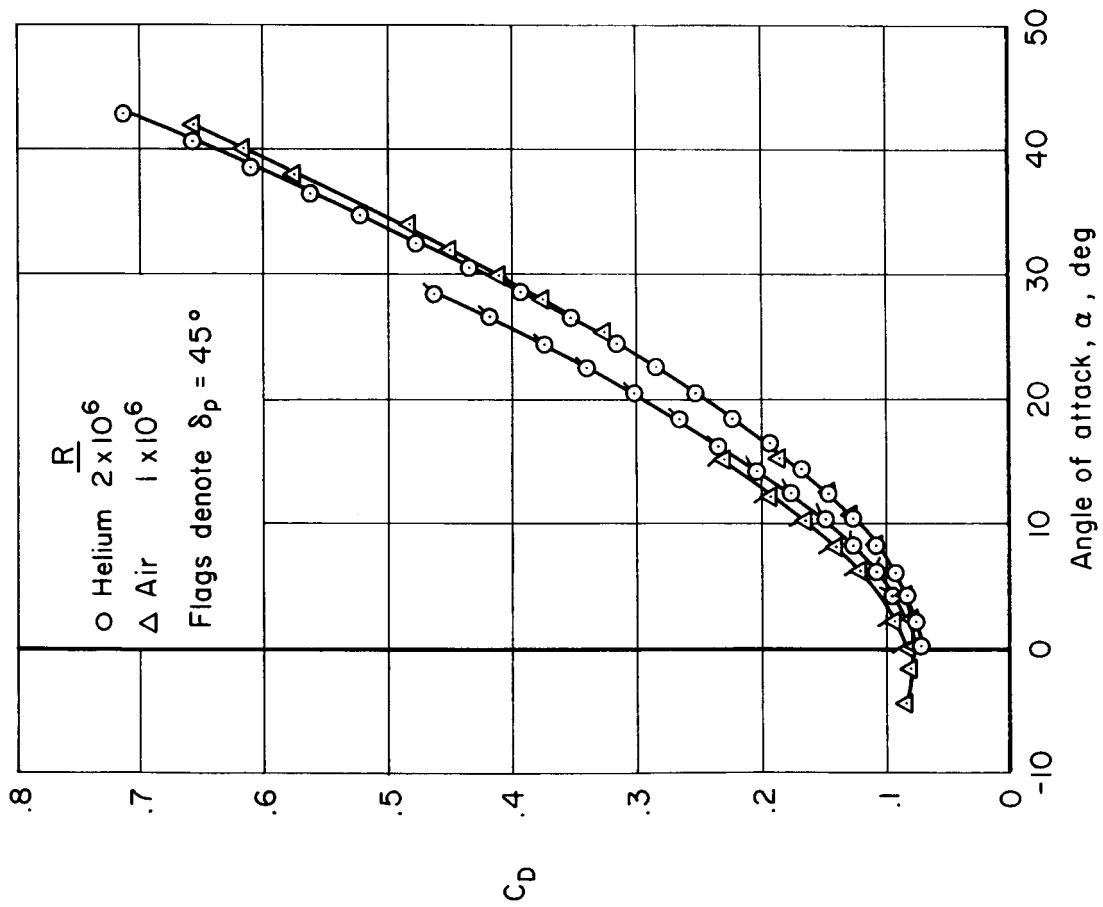
(b) Lift coefficient.



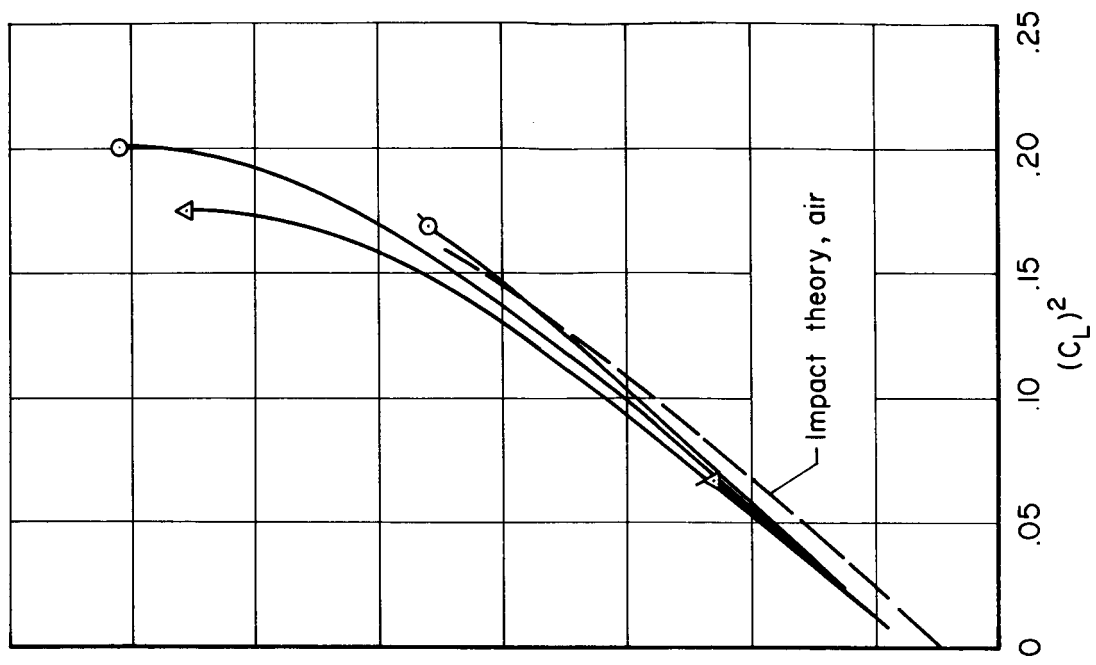
(c) Lift-drag ratio.

Figure 30.- Longitudinal aerodynamic characteristics measured in air and in helium at  $M = 10.4$ ; canopy on,  $25^\circ$  rudder flare.

~~CONFIDENTIAL~~



(d) Drag coefficient.  
Figure 30.- Continued.



(e) Drag due to lift.  
Figure 30.- Concluded.

~~CONFIDENTIAL~~

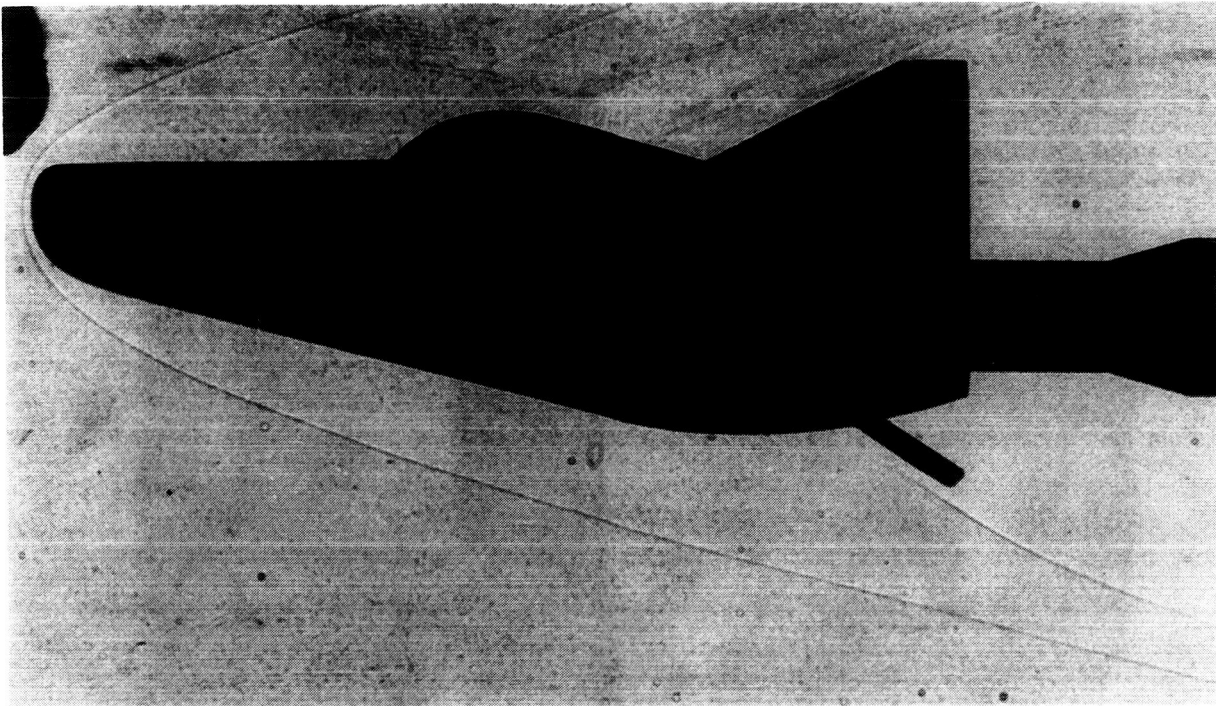


Figure 31.- Shadowgraph of the 6-inch model in air at  $M = 10.4$ ;  $\alpha = 0^\circ$ ,  
 $\delta_p = 45^\circ$ ,  $R = 0.5 \times 10^6$ .

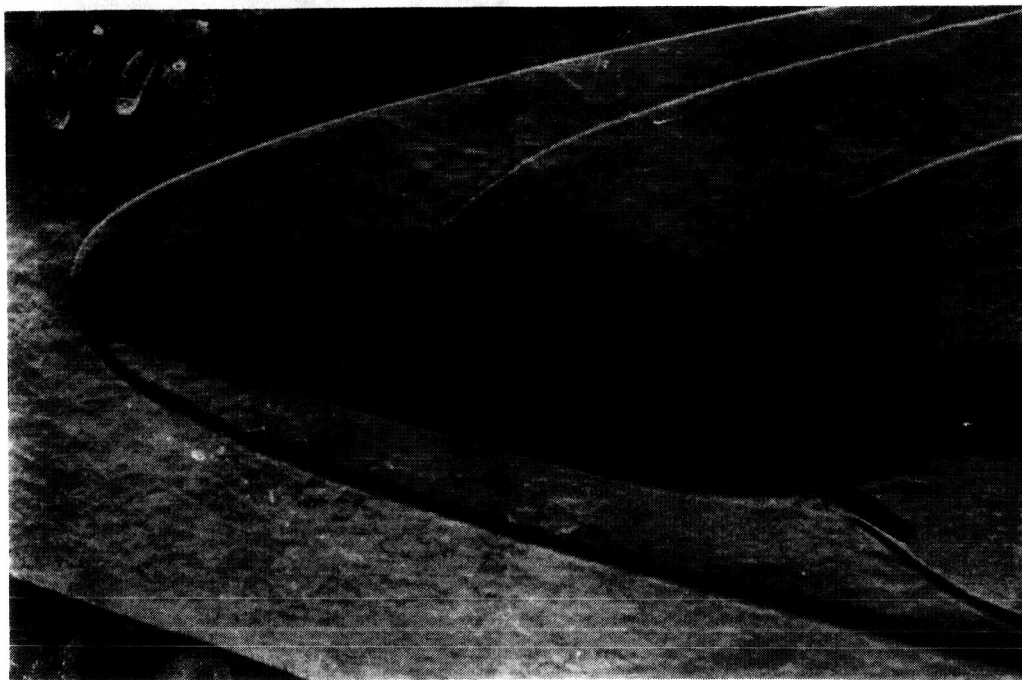
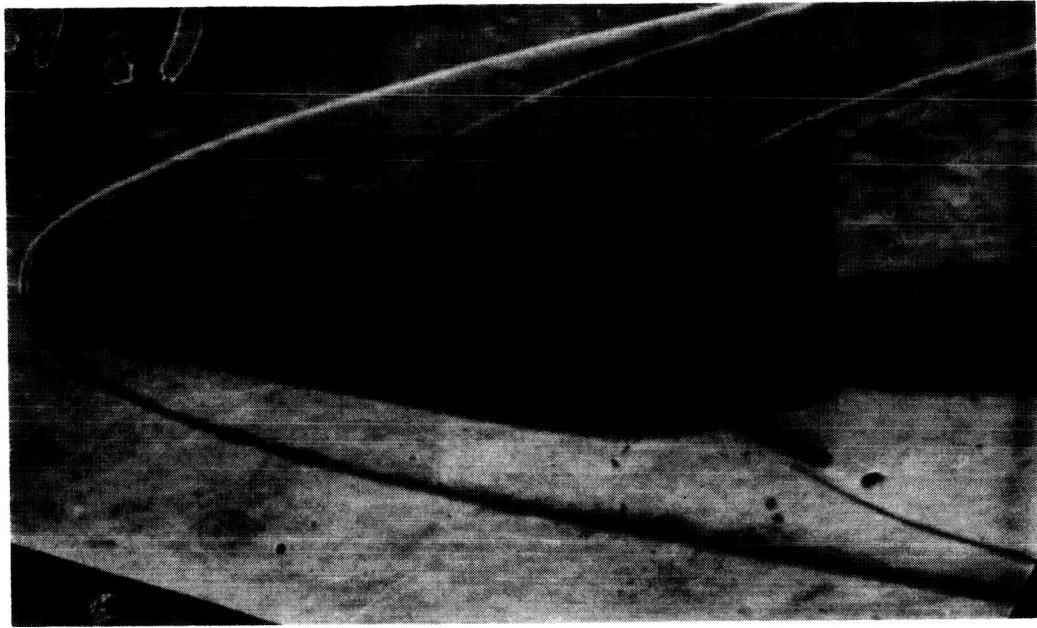


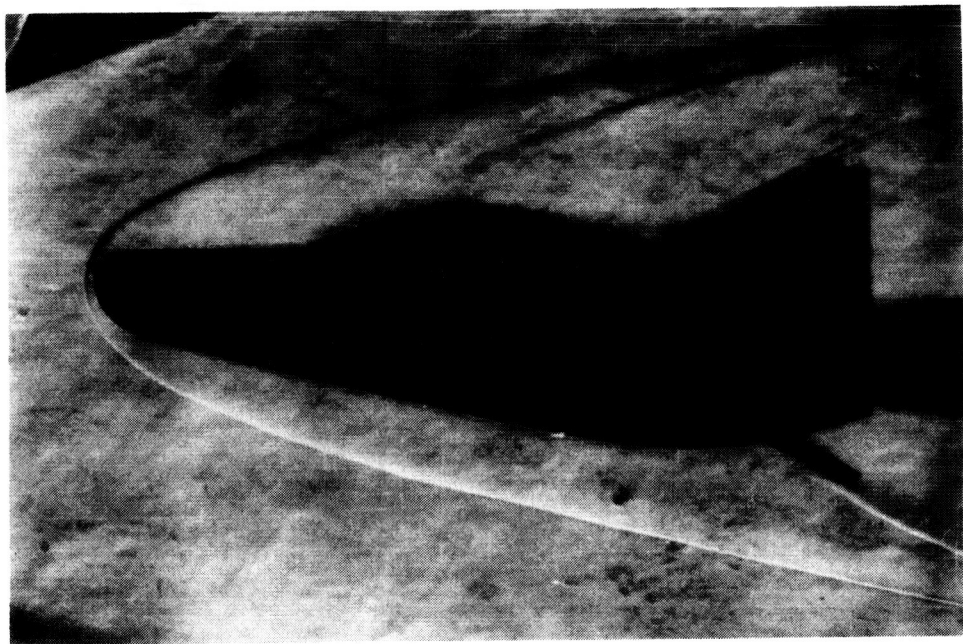
Figure 32.- Schlieren photograph of the 6-inch model in helium at  $M = 10.4$ ;  
 $\alpha = 0^\circ$ ,  $\delta_p = 45^\circ$ ,  $R = 1.7 \times 10^6$ .

~~CONFIDENTIAL~~

~~CONFIDENTIAL~~



(a) Original canopy.



(b) Modified canopy.

Figure 33.- Schlieren photographs of the 6-inch model in helium at  $M = 21.0$ ;  
 $\alpha = 0^\circ$ ,  $\delta_p = 45^\circ$ ,  $R = 4.3 \times 10^6$ .

~~CONFIDENTIAL~~

*"The aeronautical and space activities of the United States shall be conducted so as to contribute . . . to the expansion of human knowledge of phenomena in the atmosphere and space. The Administration shall provide for the widest practicable and appropriate dissemination of information concerning its activities and the results thereof."*

—NATIONAL AERONAUTICS AND SPACE ACT OF 1958

## NASA SCIENTIFIC AND TECHNICAL PUBLICATIONS

**TECHNICAL REPORTS:** Scientific and technical information considered important, complete, and a lasting contribution to existing knowledge.

**TECHNICAL NOTES:** Information less broad in scope but nevertheless of importance as a contribution to existing knowledge.

**TECHNICAL MEMORANDUMS:** Information receiving limited distribution because of preliminary data, security classification, or other reasons.

**CONTRACTOR REPORTS:** Technical information generated in connection with a NASA contract or grant and released under NASA auspices.

**TECHNICAL TRANSLATIONS:** Information published in a foreign language considered to merit NASA distribution in English.

**TECHNICAL REPRINTS:** Information derived from NASA activities and initially published in the form of journal articles.

**SPECIAL PUBLICATIONS:** Information derived from or of value to NASA activities but not necessarily reporting the results of individual NASA-programmed scientific efforts. Publications include conference proceedings, monographs, data compilations, handbooks, sourcebooks, and special bibliographies.

*Details on the availability of these publications may be obtained from:*

SCIENTIFIC AND TECHNICAL INFORMATION DIVISION  
NATIONAL AERONAUTICS AND SPACE ADMINISTRATION

Washington, D.C. 20546

~~CONFIDENTIAL~~